LINE EMISSION FROM GALAXIES AT HIGH REDSHIFT

by

James Daniel Lowenthal

A Dissertation Submitted to the Faculty of the

DEPARTMENT OF ASTRONOMY

In Partial Fulfillment of the Requirements
For the Degree of

DOCTOR OF PHILOSOPHY

In the Graduate College

THE UNIVERSITY OF ARIZONA

1 9 9 1

INFORMATION TO USERS

This manuscript has been reproduced from the microfilm master. UMI films the text directly from the original or copy submitted. Thus, some thesis and dissertation copies are in typewriter face, while others may be from any type of computer printer.

The quality of this reproduction is dependent upon the quality of the copy submitted. Broken or indistinct print, colored or poor quality illustrations and photographs, print bleedthrough, substandard margins, and improper alignment can adversely affect reproduction.

In the unlikely event that the author did not send UMI a complete manuscript and there are missing pages, these will be noted. Also, if unauthorized copyright material had to be removed, a note will indicate the deletion.

Oversize materials (e.g., maps, drawings, charts) are reproduced by sectioning the original, beginning at the upper left-hand corner and continuing from left to right in equal sections with small overlaps. Each original is also photographed in one exposure and is included in reduced form at the back of the book.

Photographs included in the original manuscript have been reproduced xerographically in this copy. Higher quality 6" x 9" black and white photographic prints are available for any photographs or illustrations appearing in this copy for an additional charge. Contact UMI directly to order.

Line emission from galaxies at high redshift

Lowenthal, James Daniel, Ph.D.

The University of Arizona, 1991

LINE EMISSION FROM GALAXIES AT HIGH REDSHIFT

by

James Daniel Lowenthal

A Dissertation Submitted to the Faculty of the

DEPARTMENT OF ASTRONOMY

In Partial Fulfillment of the Requirements
For the Degree of

DOCTOR OF PHILOSOPHY

In the Graduate College

THE UNIVERSITY OF ARIZONA

1 9 9 1

As members of the Final Examination Committee, we certify that we have read

the dissertation prepared by James Daniel Lowenthal

entitled Line Emission from Galaxies at High Redshift

_____   _____

_____   _____

_____

and recommend that it be accepted as fulfilling the dissertation requirement

for the Degree of Doctor of Philosophy   .

Marcia J. Rieke	*11 September 1991*
	Date
(C. Hogan)	*11 Septmb 1991*
	Date
Richard J. Green	*11 September 1991*
	Date
	_____
	Date
	_____
	Date

Final approval and acceptance of this dissertation is contingent upon the
candidate's submission of the final copy of the dissertation to the Graduate
College.

I hereby certify that I have read this dissertation prepared under my
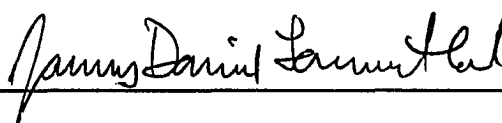direction and recommend that it be accepted as fulfilling the dissertation
requirement.

Richard J. Green   *24 September 1991*
_____   _____
Dissertation Director   Date

STATEMENT BY AUTHOR

This dissertation has been submitted in partial fulfillment of requirements for an advanced degree at The University of Arizona and is deposited in the University Library to be made available to borrowers under the rules of the Library.

Brief quotations from this dissertation are allowable without special permission, provided that accurate acknowledgment of source is made. Requests for permission for extended quotation from or reproduction of this manuscript in whole or in part may be granted by the head of the major department or the Dean of the Graduate College when in his or her judgement the proposed use of the material is in the interest of scholarship. In all other instances, however, permission must be obtained from the author.

SIGNED: *James David Farmsteel*

ACKNOWLEDGMENTS

I cannot say with certainty that this dissertation would have turned out differently had I not met my soulmate, Kelly Moore, but certainly the dissertator has. Kelly has given me an increased awareness of the social forces affecting scientific endeavors (sometimes I feel like a bug under a glass) but more importantly has been a great source of moral support, love, and inspiration during this particular endeavor.

Many people at Steward Observatory have made my five years here rich, memorable, productive, and exciting, too many to list on the one allotted page. The atmosphere among graduate students and faculty alike reflects a collegial and collaborative spirit, a characteristic I value deeply. Countless times, Hans-Walter Rix helped me through sticky problems or indulged me in rambling but productive conversation. Friendships with my long-term officemates Sally Oey and Brian McLeod will continue long past the relatively short tenure of my stay in Tucson, but I'll sorely miss their company. Rob Kennicutt has been a steady and patient source of solicited advice on issues both astronomical and political (perhaps too patient: we have yet to finish a project begun two years ago), and discussions with Jill Bechtold have always been enlightening. Thanks to Richard Elston for helping wet my feet in infrared astronomy. I'll miss long conversations with Steve Pompea over coffee, and bike rides with Tom Greene.

Many thanks are due to my advisors, Craig Hogan and Richard Green, for showing me many facets of the craft of astronomy, but also for allowing me the freedom to explore things on my own and seek help when necessary, a path that, I think, leads to the best balance of knowledge and experience. Thanks also to Marcia Rieke, the third member of my committee, both for reading this dissertation and for providing the infrared detectors used for some of the observations, and to Bruce Woodgate, my advisor at NASA/GSFC, who provided the opportunity for me to develop and use the Fabry-Perot imager, a crucial instrument for my thesis, not to mention the stipend that put food on my table for the last three years. I am grateful to Jane Charlton for a careful reading of the thesis and helpful suggestions.

I feel especially close to the other students who arrived in Tucson with me, and I am grateful for their companionship. Joe Haller and Scott Grossman were incomparable officemates for the first two years, and lasting friends since then. Many a late night was spent with Diana Foss, Todd Henry, Davy Kirkpatrick, and Dennis Zaritsky working on problem sets or even nobler causes. Thanks also to Liz Paley for her friendship and musical companionship.

Agnese Haury has been a generous and staunch supporter over the years.

Finally, I thank my parents, Anne and John Lowenthal, and my sister Annie for their undying support and love, and for the confidence that I could do whatever I wanted. I couldn't have done it without their help right from the start.

Table of Contents

List of Illustrations

List of Tables

ABSTRACT

The results of a multi-faceted search for spectral line emission from galaxies at high redshift are presented. Deep two-dimensional spectra of four blank sky fields were taken at the Multiple Mirror Telescope (MMT) at wavelengths corresponding to redshifted Lyα emission in the range $2.7 < z < 4.7$, and the resulting non-detections are used to place upper limits on the space density of randomly distributed Lyα emitters. Although the predictions of a conservative model of galaxy formation incorporating cold dark matter are not excluded in a statistical sense, the search would have detected star-forming dwarf galaxies comparable to the Magellanic Clouds at $z = 3$, given minimal extinction by dust.

The Goddard Fabry-Perot Imager, a piezo-electrically controlled tuneable narrow-band filter system with a stand-alone CCD system, was developed and tested, and used at the Kitt Peak National Observatory (KPNO) 4 m telescope to image the damped Lyα absorbing clouds towards three high-redshift QSOs in the light of redshifted Lyα. A companion galaxy to one of the damped systems was discovered and confirmed with followup spectroscopy, and its properties are presented and discussed; the companion exhibits strong Lyα and weak C IV $\lambda1549$ and He II $\lambda1640$ emission lines, and is apparently producing stars at a rate $SFR \sim 5 - 10 M_\odot$ yr^{-1}. The implications of the companion's proximity to the damped cloud are analyzed in view of the previous non-detections, and a lower limit to the spatial correlation function of the damped Lyα systems with galaxies is given. Spectroscopic limits on Lyα emission from seven damped systems, including some known to have low chemical and dust abundances, imply low levels of star formation, $SFR \lesssim 1$ M$_\odot$ yr^{-1}, but extinction by dust in some cases may cause an underestimation of these rates.

With near-infrared spectrographs at the MMT and the KPNO 4 m, eight damped

Lyα systems were searched for spectral lines characteristic of star formation regions but redshifted from the optical into the near-infrared. A possible detection of [O II] λ3727 and Hβ from one system implies a star formation rate on the order of 100 $M_\odot$ yr^{-1}, though the remainder of the observations produced non-detections compatible with the Lyα emission limits. The implications for galaxy formation and evolution at high redshift are discussed.

Chapter 1

INTRODUCTION

Normal galaxies, visible in great abundance at the current epoch, presumably formed at redshifts $1 < z < 10$, corresponding to lookback times $4 < \tau < 18$ Gyr for reasonable cosmological models. Direct observations of galaxies at high redshift can help identify the epoch and nature of galaxy formation and elucidate how galaxies evolve towards their present-day states.

Currently, the strongest observational constraints on the nature and period of galaxy formation come from the isotropy of the cosmic microwave background (CMB), cluster and field galaxies seen out to $z \sim 1$, QSO absorption line systems seen beyond $z = 3$, and from QSOs observed out to redshifts approaching 5.

In addition to the fundamental question of whether galaxies form via a buildup of previously formed stars or even small galaxies, or through the gravitational collapse of a primordial gas cloud that subsequently forms stars, pressing questions whose answers may lie at high redshift include the nature of dark matter, the origins of large scale structure, and the history of galactic heavy element enrichment through stellar processing. These questions provide the primary motivation for the observations of high-redshift galaxies described in the following chapters.

In this chapter, I will review the predictions for the appearances of normal galaxies at high redshift based on various models of galaxy formation; summarize

the observational evidence for galaxy evolution, as well as the recent detections of some luminous objects at high redshift that may be galaxies seen in the early stages of star formation; and discuss QSO absorption line systems in the context of galaxy formation and evolution.

Throughout this dissertation, I assume a Friedmann cosmology, *i.e.*, an expanding Robertson-Walker universe with cosmological constant $\Lambda = 0$. The expansion is expressed via the Hubble Law, $v = H_0 r$, with $H_0 = 100 \ h^{-1}$ km s^{-1}Mpc^{-1}. Several standard algebraic relations are used (*e.g.*, Sciama 1971; Weedman 1988; Weinberg 1972; Zel'dovich & Novikov 1983) to calculate physical quantities of the objects observed at high redshift, and I list them here for reference.

The current ratio of the universe's density to the critical density required for a closed universe is

$$\Omega_0 = \rho_0/\rho_C = \rho_0(3H_0^2/8\pi G)^{-1}, \tag{1.1}$$

while the universal expansion is slowing at the rate given by the decceleration parameter

$$q_0 = \Omega_0/2 \tag{1.2}$$

with $q_0 = 0.5$ for a "flat" universe, *i.e.*, expansion asymptotically slowing to zero, and $q_0 < 0.5$ for an infinitely expanding universe. The lookback time to a given redshift z is given by

$$\tau \equiv \tau(0) - \tau(z) = \frac{z}{H_0(1 + z)} \quad \text{(for } q_0 = 0\text{)} \tag{1.3}$$

$$= \frac{2}{3H_0}[1 - (1 + z)^{-3/2}] \quad \text{(for } q_0 = 0.5\text{)}. \tag{1.4}$$

An object of proper size a subtends an apparent angular size in radians calculated from

$$\theta = \frac{a(1 + z)^2}{D}, \tag{1.5}$$

where D is the luminosity distance to the object, *i.e.*, the distance at which the object would lie to appear equally bright if the universe were Euclidean,

$$D = \frac{c}{H_0} \frac{\{q_0 z + (q_0 - 1)[(1 + 2q_0 z)^{1/2} - 1]\}}{q_0^2} \quad \text{(for } q_0 > 0\text{).} \tag{1.6}$$

Finally, the observed flux f_o received from an object emitting radiation with luminosity L_e is

$$f_o = L_e / 4\pi d^2 (1 + z)^2, \tag{1.7}$$

where d, the proper distance to the object, is

$$d = \frac{c}{H_0} \frac{\{q_0 z + [q_0 - 1][(1 + 2q_0 z)^{1/2} - 1]\}}{q_0^2 (1 + z)} = \frac{D}{(1 + z)}. \tag{1.8}$$

1.1 The Formation of Galaxies

To predict the appearance of primeval galaxies (PGs), which I here define as galaxies seen during their highest rate of star formation, reasonable physical models are needed to describe their formation. It has generally been assumed that galaxies formed by the gravitational collapse of bound masses of gas, stars, dark matter, or a mixture of all three. However, there is no certainty about the nature of the original catalyst of the collapse, *e.g.*, slightly overdense regions superposed on the ambient medium vs. shock fronts, which bears on the fundamental question of which formed first, galaxies or stars.

Models of galaxy formation can in general be divided into three main types (see Baron & White 1987 for a review): gravitational collapse of large, slightly overdense regions from an otherwise uniform medium, followed by breakup and further collapse into galaxies and stars; condensations of cooling protogalactic material swept up in shock fronts propagating outwards from a series of explosive events; and finally, a hierarchical scenario, in which galaxies form by accumulating smaller, preexisting

particles, *e.g.*, stars, and in which the largest structures (superclusters and up) form last. The gravitational collapse and the hierarchical scenarios have been explored both with and without dissipation of energy during the formation process, and the predictions of all the models span a wide range of time, morphology, and visibility. Indeed, since stars might plausibly form before the collapse of a galaxy-sized assemblage is complete, the "highest rate of star formation" may occur before anything resembling current-day galaxies appears. As Baron & White point out, this caveat makes it unclear whether or not we would ever recognize a primeval galaxy; our pre-disposition towards expecting to see familiar objects at high redshift may tend to obscure the true nature of galaxy formation.

1.1.1   Gravitational Accretion

Let us examine the three families of galaxy formation theory outlined above. Partridge & Peebles (1967) introduced a simple instability scheme in which a slightly overdense cloud of self-gravitating gas collapsed with almost no dissipation to form a galaxy of stars in less than .2 Gyr, corresponding to redshifts from 10 to 30, depending on the cosmological model adopted. After the primordial gas cloud's initial expansion halted, turbulent heating ionized the gas, allowing cooling via spectral lines as well as the subsequent formation of the first halo stars, thus defining the maximum extent of the galaxy. Arguing that heavy-element production must have been essentially complete by the time any remaining material collapsed to form a disk, Partridge & Peebles estimated that the first epoch of star formation must have been exceptionally active, resulting in an extremely luminous object, as much as 700 times brighter than current-day values. Furthermore, the Lyα line alone, it was proposed, could contain as much as 6% of the total luminosity. Were this model's optimistic prediction borne out, PGs would have long ago been identified

in abundance.

A much less spectacular process was suggested by Larson (1976), who extended previous calculations to include more detailed descriptions of how the formation of spheroids, which in his models produced their stars early, differed from that of disks, which formed via the long-term settling of gas that dissipated energy through gas-cloud collisions before finally forming stars. The Hubble sequence was partially explained in this scenario, in which it was suggested that the differing star formation rates for halos and disks resulted either from tidal forces acting in the later stages of collapse to inhibit star formation and thus allowing disk formation, or from a two-phase initial gas, with high-density pockets forming the early spheroid stars.

The observational implications of Larson's models were explored by Meier (1976) using population synthesis to estimate the observed spectrum of the PGs given an initial mass function (IMF) and a star formation rate (SFR) predicted by the models. The brightest phase of formation of a giant elliptical galaxy, it appeared, would correspond to the development of the nucleus, as opposed to the halo-bright phase of Partridge & Peebles' model; a particular model with an initial radius of 30 kpc and a mass $M = 10^{11} M_{\odot}$, observed 2.4×10^8 yr after the collapse started, would produce 380 $M_{\odot}$ yr^{-1}, with 25% of the star formation taking place within the central 1.8 kpc. However, the most luminous phase was predicted to occur, for reasonable cosmological parameters, at redshifts close to 10 and with corresponding R magnitudes fainter than 25, spelling doom for easy detection and identification.

The effects of radiation pressure on the interstellar medium (ISM) of a collapsing proto-spiral galaxy were studied by Cox (1985) in a simple model predicting a dramatic stage of star formation similar to that proposed by Partridge & Peebles. Cox calculated the hydrostatic forces and mass transfer in different stages during the infall of the proto-galactic material, and concluded that Lyα radiation pressure

could regulate the collapse and the SFR, keeping the disk "inflated" and preventing further shrinking of the halo; the peak luminosity of a Milky Way-type spiral would be around 10^{46}erg s^{-1}, roughly 25 times brighter than at the current epoch, at $t \sim 1$ Gyr after the big bang. However, Cox chose not to include dark matter in his calculations, despite the growing evidence that it can dominate the dynamics and evolution of galaxies.

The "pancake" models of Zel'dovich (1970) and Sunyaev & Zel'dovich (1972), in which giant gas clouds at caustic regions of high density collapse with dissipation to form flattened galaxy superclusters that later fragment into individual galaxies, is also representative of this general family of models.

1.1.2 Explosive Galaxy Formation

Stars or other objects that form early in the history of the universe and explode soon thereafter will produce expanding shock fronts that sweep up large masses of the ambient medium; the cooling shells can then foster gravitational instabilities and fragment to form galaxies. In papers by Ikeuchi (1981) and Ostriker & Cowie (1981), it was proposed that early populations of QSOs or massive stars, respectively, could have provided the sources of such explosions. Alternately, the cooling shock fronts could have resulted from the nonuniform gravitational collapse of larger structures. While the collapse of individual galaxies in these scenarios may be similar to the formation processes described in the more straightforward models, there are several important distinctions. First, the explosive galaxy formation models necessarily address the issue of large scale structure, which for the most part is unexplained by the gravitational accretion models described above. In general, the intersections of hydrodynamic shock fronts resulting from primordial explosions will define the loci of galaxy clusters and superclusters, accounting qualitatively for the frothy texture

seen in galaxy redshift surveys (*e.g.*, Huchra *et al.* 1990). Second, the cavities evacuated by such explosions should be essentially swept clean (whether the "voids" in the redshift surveys are indeed empty or merely underpopulated with bright galaxies–dark matter may be present–remains to be seen; if they are real, then in fact the energy required to produce the observed voids may exclude the models). If the IGM is already significantly lumpy before the passage of shocks, however, it will resist the formation of significant voids. The strongest argument against explosive models is that the early production of massive stars should result in substantial amounts of dust at high redshift ($z \gtrsim 3$), a prediction that has not been borne out by the Cosmic Background Explorer (COBE) satellite, which failed to observe the expected sub-millimeter deviation from the CMB spectrum (Mather *et al.* 1990.) Furthermore, the explosive galaxy formation models do not provide satisfactory explanations for the processes by which the post-recombination primordial material coalesced to form the requisite stars or QSOs (although they may be similar to those described by other models); indeed, the explosions themselves would probably be brighter than the galaxies formed in their wake, but have not been observed.

1.1.3 Hierarchical Models

A final category of galaxy formation theories proposes that the process was a bottom-up hierarchical one, in which smaller units coalesce to form larger units, progressing through stars to galaxies and clusters. A version by Press & Schechter (1974), extending ideas of Peebles (1965; 1972), required isothermal seed perturbations of mass $M \sim 3 \times 10^7 M_\odot$ at the time of recombination ($z \sim 1000$) in order to form galaxies. The most popular current theories of galaxy formation, which invoke cold dark matter (CDM), are also hierarchical in nature (Blumenthal *et al.* 1984; Baron & White 1987). One of many explanations for the dark matter whose

existence is inferred from the observed dynamics of galaxies and galaxy clusters, CDM postulates an abundance of massive, non-baryonic particles that interact only gravitationally with baryons; their thermal velocity is small compared to the Hubble velocity, so primordial density fluctuations are not erased by diffusion before recombination. Other possibilities include warm and hot dark matter, with CDM currently holding a narrow lead both in predicting the dynamics, morphology, and plausible histories of individual galaxies and in describing the link of galaxy formation to larger structures; the ability to place galaxy formation in the larger context of big bang cosmology is reassuring and increasingly necessary as the cosmological importance of dark matter becomes clearer. CDM also appears to be the most successful at avoiding conflicts with the ever-tightening constraints of the microwave background isotropy, which rule out large fluctuations of matter in the universe immediately following recombination; however, there may be increasing conflict at the low-redshift end, with CDM hard pressed to account for the largest structures seen in the galaxy redshift surveys.

The accumulative nature of CDM models implies a relatively late formation of galaxies, and in general not a spectacular one. The initial spectrum of fluctuations is probably Gaussian, but depends on the exact cosmological model adopted. Because the dark matter may outweigh baryons by a factor of ten or more, much of the baryonic matter's fate is sealed by the dynamics of the dark matter. However, as Cole (1991) points out, there are additional complex factors, notably gas hydrodynamics and radiative cooling, governing the baryonic matter that must be taken into account. Specifically, he finds that gas cooling and condensation onto small galaxies in CDM halos at high redshift can be so efficient that little gas remains to form larger systems at low redshift, thus requiring some process to inhibit the cooling, perhaps star formation.

Numerical simulations by several workers (*e.g.*, Frenk *et al.* 1985) have shown that by requiring galaxy formation to occur preferentially at the densest peaks of the dark matter distribution ("biased galaxy formation") CDM can reproduce fairly accurately the foamy structure of the universe seen in deep redshift surveys (*e.g.*, Huchra *et al.* 1990); observations implying the existence of structure on scales of ~ 100 Mpc begin to challenge the limits of non-biased CDM models.

While elliptical galaxies and the haloes of spirals can form without dissipation in the CDM schemes, the collapse of disks usually requires dissipational processes, often in a protracted, relatively quiescent mode during which gas slowly settles in from the halo. In a relatively generic calculation of the collapse of PGs from a 10 to 1 mix of cold dark matter and gas, Baron and White (1987) reaffirmed earlier findings that substantial star formation could continue until $z = 2$ or even later, although 60% of the galaxies' final population of stars formed by the end of one collapse time. They stress that collapse is likely to be inhomogeneous, possibly resulting in a single gravitationally bound system with several bright knots that might be mistaken for individual galaxies; also, the PGs formed in this way are considerably fainter than the early predictions. Assuming that the current galaxy luminosity function is well-described by that of Schechter (1976), but modifying it to include only spheroidal systems, and further assuming that all elliptical galaxies and spiral bulges have the same collapse time, Baron & White show that the number counts expected from their model would easily escape detection by then-current searches: for a $q_0 = 0.5$ universe, a formation redshift $z = 1.5$, and an R magnitude of 24, only 1 source per square degree is expected. By $R \sim 30$, the model predicts about $3 \times 10^5 \mathrm{deg}^{-2}$, or almost 100 arcmin^{-2}, but this is well below the sensitivity currently attainable.

1.2 · Search Techniques

Two general techniques lend themselves to the identification of randomly distributed PGs: selection by color and magnitude followed by spectroscopic confirmation, and selection by emission lines known to accompany active star formation. In the first case, deep imaging with CCDs or other two-dimensional detectors employing broadband filters produces large numbers of faint galaxies, typically 100 arcmin^{-2} down to $R \sim 28$ (Tyson 1988). By comparing the observed colors both with nearby star formation regions, *e.g.*, Galactic and extragalactic H II regions and blue compact dwarf galaxies, and with theoretical models of the spectral energy distributions (SEDs) expected for young populations of stars, such as the evolutionary spectral synthesis calculations of Bruzual (1983) and Charlot & Bruzual (1991), one can in theory winnow out likely PG candidates from the multitude of older galaxies. In practice, this technique is hampered by uncertainties in the expected colors of PGs, which in turn are affected by the unknown redshift of formation. For example, if PGs form as recently as $z \leq 2.3$, then active star formation is likely to cause them to appear blue in $B - V$ due to the presence of large numbers of massive hot stars. However, at higher redshifts, the Lyman break, caused by absorption of ultraviolet (UV) light by neutral hydrogen either in the radiating galaxy or along the intervening line of sight, will pass into the B band, making the PG appear much redder in $B - V$. Furthermore, large infrared (IR) fluxes can be interpreted either as old *or* young stellar populations, complicating the age interpretation of broad-band colors (*e.g.*, Lilly 1988; Chambers & Charlot 1990).

While deep CCD imaging has indeed uncovered a large population of faint blue galaxies (Tyson 1988; see Section 1.3, and note that Lilly *et al.* 1991 dispute the blueness), spectroscopy, whenever brightness allows, indicates that the bulk of the population either contains no emission lines and thus cannot be assigned a redshift,

or else represents unexceptional galaxies at moderate redshifts, $z < 1$; no convincing high-redshift PG candidates have yet been discovered, though star formation is almost certainly enhanced at $z \gtrsim 0.5$ relative to local levels (Colless *et al.* 1990).

The second general method of searching for PGs capitalizes upon the strong emission lines, such as [O II] $\lambda 3727$, [O III] $\lambda 5007$, Hβ, Hα, and Lyα, known to occur in regions of rapid star formation. Using nearby H II regions and emission line galaxies, including normal spirals and dwarf irregulars, as basic starting points, we can predict the emission line spectra of PGs as a basic function of star formation rate, metallicity, dust content, and IMF. Regardless of the apparent faintness of a PG, any emission lines will stand out above the night sky background with greater contrast than continuum; thus, any method of observation that disperses the spectrum will maximize the probability of detection. Either narrow-band imaging or two-dimensional spectroscopy, especially with charge coupled devices (CCDs), is an appropriate tool for singling out the emission lines expected from PGs. This technique provides the basis for the present work, and will be discussed in further detail in later chapters.

1.3 Observational Evidence for Galaxy Formation and Evolution

What direct indications are there that galaxies do indeed evolve? Apart from the major arguments supporting the big bang model of the universe, which of course implies a time before galaxies existed at all, there are several lines of evidence that show a different universe at reasonably recent lookback times. These fall into four loose categories: field galaxy counts and colors, cluster galaxy evolution, QSO and radio galaxy luminosity function evolution, and QSO absorption line systems.

Deep images of "blank sky" made with CCDs on large telescopes show a multi-

tude of faint objects, and almost all the sources fainter than $B \sim 27$ can be safely assumed are galaxies (most are in fact extended)(Tyson 1988; Lilly *et al.* 1991). Because of their faintness, spectroscopy is difficult, so redshifts are hard to come by. However, there are several interesting features in the galaxy counts that have cosmological bearing. First, the sheer number of galaxies seen is several times the number expected if the universe were the same out to $z = 4$ as it is today. The surplus is especially difficult to reconcile with a flat universe: there are 10 times too many if $q_0 = .5$ and $H_0 = 100$ km s^{-1}Mpc^{-1}. There are several possible explanations for the excess: There were more galaxies in the past, implying that galaxy mergers were common since then, or that galaxies "turn off" and thus escape detection locally (pure number density evolution); galaxies were much brighter on average in the past (implying pure luminosity evolution); or a combination of the two. Finally, the comparison of Tyson's results with predictions is not straightforward, since his isophotal magnitude measurements are non-standard; uncertainties in the corrections may account for some of the excess.

Another result from the deep galaxy counts is that some of the fainter galaxies appear to be blue in $B - R$ (Tyson 1988, and note that Lilly *et al.* 1991 dispute the blueness). A natural explanation for this is that star formation was enhanced in the past, giving rise to a large population of massive stars that contribute strongly to the rest-frame UV continuum. Guhathakurta *et al.* (1990), studying the statistics of faint objects from Tyson (1988), estimate that if this is an accurate interpretation of the galaxies' blueness, then 93% of the sources must be at $z < 3$, or absorption of UV continuum below the Lyman break by neutral hydrogen would prevent the objects from being seen in the B-band. One caveat to this result, as pointed out by Phillipps *et al.* (1990), is that we may be misunderstanding the populations being observed at increasing redshifts; *i.e.*, we necessarily tend to sample the brightest galaxies as the

average galaxies become too faint (surface brightness goes as $[1 + z]^{-4}$), and since these tend to be galaxies with substantial star formation, selection effects may mimic evolutionary effects. Another note of caution is that we may live in a region of galaxy underdensity, which would lead us to overestimate the excess outside that region; but calculating the galaxy luminosity function is not a straightforward problem, so no dramatic progress can be expected on this front. Despite these caveats, there appears to be no way around such a large excess except via galaxy evolution of some sort. However, according to Elston (1991), deep near-IR imaging reveals a population of red galaxies, quite possibly field ellipticals at $z < 1$, whose distribution is consistent with little or no evolution models, suggesting that evolution depends on galaxy type.

Evolution of galaxies has also been observed in a statistical sense in clusters of galaxies, starting with the work of Butcher & Oemler (1978a,b; 1984), who found that there was an excess of blue galaxies in clusters seen at redshifts $z \sim$ 0.4 compared to local clusters, the "Butcher-Oemler effect." After some dispute centered on cluster membership of individual galaxies, the effect was confirmed by Dressler, Gunn, & Schneider (1985) and Newberry *et al.* (1988), although the density of elliptical galaxies is seen to remain essentially constant (Lilly 1987; also, Hamilton 1985 found the same to be true for ellipticals selected independent of environment). Of course, part of the explanation for these effects probably lies in the nature of the cluster environment; for instance, perhaps between $z = 0.5$ and $z = 0$, spiral galaxies are somewhat stripped of interstellar clouds by their motion through a high-pressure intra-cluster medium, inhibiting star formation by the present time. Field elliptical evolution is difficult to assess due to the paucity of ellipticals outside clusters or dense groups. Finally, examination of radio galaxies (Hill & Lilly 1991) and of radio-loud QSOs (Ellingson, Yee, & Green 1991) at $z \sim 0.5$ compared to lower redshifts

reveals that the high-redshift samples preferentially reside in richer galaxy cluster environments than the lower-redshift objects. An evolving intergalactic medium has been suggested to account for the observed trends, but at any rate the average population of galaxies at $z > 0.5$ was significantly different than it is today.

Further evidence for this claim comes from the observed redshift distribution of QSOs, which increase in number per comoving unit volume until $z \sim 2.2$, at which point they appear to decline rapidly (see Hartwick & Schade 1990 for a review); at $z \sim 1$, the density of QSOs was 150 times higher than it is today. Even if the apparent downturn in the QSO luminosity function at $z > 3$ is due to some obscuring matter at high redshift (*e.g.*, dust, as proposed by Heisler and Ostriker 1988), this too is presumably due to time-varying galactic processes.

Radio galaxies are clearly different at high redshift than locally, as shown by, *e.g.*, McCarthy (1988), Spinrad (1985), and Chambers *et al.* (1990). They were more luminous, on average, at $z = 2$, and produced copious amounts of line radiation usually associated with star formation regions, including large equivalent widths of Lyα (though in some cases, the Lyα flux is too large to be explained by star formation alone, and presumably is enhanced by the AGN source). The strong Lyα lines at high redshift lead to another argument supporting evolution over the last 5–10 Gyr: there must be little dust in the high-redshift radio galaxies. In nearby galaxies showing strong star formation, such as blue compact dwarfs, Lyα is never seen at levels near the Case B recombination value expected from observed Hα and Hβ fluxes (Hartmann *et al.* 1988; Deharveng, Joubert, & Kunth 1986). The general interpretation of this paucity of Lyα is that dust is present in local galaxies in sufficient concentration to quench Lyα and convert it to thermal IR radiation. If Lyα is preferentially more likely to escape star formation regions at $z > 1.5$, we can infer that dust formation, and therefore stellar processing in galaxies, has been

substantial since then.

Finally, the galaxies thought to give rise to the heavy element absorption lines seen in QSO spectra show some evidence for evolution with redshift. If indeed the identification of such systems with normal galaxies is correct, then this piece of evidence alone is perhaps the strongest argument in support of galaxy evolution. Since these objects play a major role in this work, I will discuss them in somewhat greater detail in the following section.

1.4 QSO Absorption Line Systems

1.4.1 Basic Properties

Because lines of sight to QSOs selected by any method sample random regions of intervening space, observations of QSO absorption line systems probably provide the most unbiased means of examining average galaxies at high redshift, free from luminosity-dependent selection effects. Thus, distant, bright QSOs are used to probe a large redshift range of intervening objects whose own radiation is difficult to detect.

The multitude of absorption lines seen towards high-redshift QSOs are divided into two broad classes: those attributed to ionized species of heavy elements ("metals"), such as Mg II or C IV, and those generally identified as Lyman series lines of neutral hydrogen, the "$Ly\alpha$ Forest," usually consisting only of $Ly\alpha$ but sometimes including Ly-β and higher Lyman lines as well. The identification of single, isolated lines with redshifted $Ly\alpha$ is based largely on the fact that they appear almost entirely blueward of the redshifted $Ly\alpha$ emission line of the background QSO, as well as the lack of associated lines due to any other familiar species. The metal line systems, seen out to redshifts $z > 3$, are commonly considered to represent the haloes of galaxies perhaps similar to those we observe near us today; the $Ly\alpha$ forest

clouds, by contrast, correspond to some form of galactic or intergalactic gas that we cannot confidently identify with any familiar objects at the current epoch. They have been proposed to be either pressure-confined by a hot intergalactic medium (IGM)(Ikeuchi & Ostriker 1986), or gravitationally confined by dark matter haloes (Rees 1986; Ikeuchi, Murakami, & Rees 1988), or perhaps they represent thin, dense sheets of cool gas (Hogan 1987). While they are generally assumed to be mostly ionized, even this is disputed; in a controversial result, Pettini & Hunstead (1990) report a correlation between the Doppler parameter b and neutral hydrogen column density $N(\mathrm{H})$, implying that b measures bulk motion rather than temperature and allowing a small fraction to have $T < 5000K$ and thus be predominantly neutral clouds. Rauch et $al.$ (1991) find that the apparent correlation can be explained by selection effects, and Bechtold (1991) finds that most of Pettini & Hunstead's narrow lines can in fact be assigned to heavy-element species associated with previously unknown absorbing systems. With the exception of the broad absorption troughs seen towards some QSOs, which are generally interpreted as ejecta from the QSO itself, all the absorbers show redshift distributions consistent with their being cosmological, intervening systems not physically associated with the background QSO. When examined under high spectral resolution, many metal-line systems show complex velocity structure, with as many as 10 or more individual velocity components contributing to the system.

Two additional important types of QSO absorption line systems, Lyman limit and damped Lyα systems, might bridge the gap between the two major families of absorbers mentioned above. While Lyα forest clouds are observed to have neutral hydrogen column densities $13 \leq \log N(\mathrm{H}) \leq 17$, above the upper end of that range there are sufficient neutral atoms to cause optical thickness to UV photons with energies of 13.6 eV, the ionization potential of hydrogen. Such objects, the Lyman

limit systems, cause a sharp drop in the observed QSO spectrum below the wavelength of the redshifted Lyman limit, sometimes extinguishing the QSO continuum completely. The damped Lyα clouds occupy the highest end of the column density distribution; above log$N$(H) $\sim$ 20, on the square-root portion of the curve of growth, Lyα photons encounter so many absorbing atoms that the damping wings of the Lyα line become optically thick and broaden the line profile. Here the line itself can completely black out the background QSO continuum.

Wolfe (1986) pointed out that, based on the observed statistics of the damped systems, there was approximately as much baryonic matter contained in the damped clouds at $z \sim 2$ as there is in the visible portions, *i.e.*, stars, of disk galaxies today. This estimate has been supported by the large surveys carried out by Wolfe *et al.* (1986) and Lanzetta *et al.* (1991); 20% of the sky is covered by damped Lyα systems out to a redshift of about 2.5, and the contribution to the cosmological mass density parameter is $\Omega_{DL\alpha} \sim 0.79$–$1.45 \times 10^{-3}h^{-1}$ for q_0 =0.5–0. The Lyman limit systems, which have lower column densities but are more numerous than the damped clouds, appear to contribute a similar fraction to the density of the universe: $\Omega_{LL} \sim 4 \times 10^{-3}h^{-1}$ at $z = 3$ for $q_0 = 0.5$ (Steidel 1990), assuming various photoionization parameters for the absorbing clouds (although they must be predominantly neutral due to self-shielding, regardless of the ionization source; only because the Lyman limit systems are so numerous can they approach the mass density of the damped systems).

Both the Lyman limit and damped Lyα systems commonly exhibit absorption lines of heavy elements, and likewise, the metal line systems almost always display Lyα absorption whenever it falls above the atmospheric cutoff at 3300 Å, prompting suggestions that there is a continuum of H I column density or chemical enrichment that could account for the entire range of known absorbers (Tytler 1987). However,

there are important distinctions elucidated by recent studies that argue against such an interpretation.

1.4.2 Evidence against a Common Parent Population

The Lyα Forest Clouds and the Metal-Line Systems

The most important difference among the various groups of QSO absorbers is the observed evolution with redshift. The survey by Murdoch *et al.* (1986), settling a protracted controversy, showed that there was a highly significant trend for $z \gtrsim 1.5$ of increasing comoving number density of Lyα forest clouds with redshift. If there were no evolution of the clouds over time, then in a standard Friedmann universe one would expect the number of clouds per unit redshift to be

$$N(z) \equiv \frac{dN}{dz} = N_0(1+z)(1+2q_0 z)^{-1/2}. \tag{1.9}$$

For comparison with observations, this can be rewritten as $N(z) = C(1+z)^\gamma$, where C is a constant; from equation 1.9, we see that for a flat universe ($q_0 = 0.5$), we expect $\gamma = 0.5$, while for an empty universe ($q_0 = 0$), we expect $\gamma = 1$. Murdoch *et al.* concluded that for the Lyα clouds, $\gamma = 2.17 \pm 0.36$, *i.e.*, the comoving number density of clouds increases with redshift at a rate inconsistent with a non-evolutionary scenario: there were more clouds, or larger ones, at earlier epochs. Another finding from that work was the "proximity effect," in which the Lyα clouds are observed to thin out in number near the emission redshift of high-redshift QSOs. One explanation is that the strong UV flux from the QSO completely photoionizes any hydrogen within a region analagous to Strömgren spheres, thus decreasing the neutral hydrogen atoms available for absorption; this model was explored in detail by Bajtlik, Duncan, and Ostriker (1988), who also measured the background intensity of ionizing UV radiation, $\log J_\nu = -21.0 \pm 0.5$, by deriving

the distance from QSOs at which the background and QSO UV flux balanced and Lyα clouds began to increase in number, and who confirmed that the proximity effect was stronger near more luminous QSOs. Furthermore, when the proximity effect was taken into account, the redshift index calculated by Bajtlik *et al.* rose to $\gamma = 2.36 \pm 0.40$. Both results, the number evolution of the Lyα clouds and the proximity effect, were reconfirmed by Lu, Wolfe, & Turnshek (1991), who calculated yet a higher redshift index, $\gamma = 2.75 \pm 0.29$, based on a new sample of 38 QSO spectra including 950 Lyα lines, but who also found no evidence for larger proximity effects near more luminous QSOs. The case is not closed, however: Bechtold (1991) *confirms* the luminosity dependence of the proximity effect, and Rauch *et al.* (1991) find that the Lyα forest clouds show *little* evolution with redshift.

The equivalent width distribution of the Lyα clouds appears to obey an exponential law of the form $e^{-W/W*}$, where $W* \simeq 0.3$ Å, roughly independent of redshift; taken together with the observed possible number density evolution, this implies strong evolution of the neutral hydrogen column density in the clouds, described approximately by $N_c \propto (1 + z)^{6-8}$, where N_c is the neutral hydrogen column density of individual clouds (Murdoch *et al.* 1986), although this claim is rather model dependent.

Models for the evolution of the Lyα clouds under various conditions of the background ionizing flux predict that the decrease in the $N(\mathrm{H})$ distribution over time probably levels off considerably by $z = 0$ after peaking at $z \sim 2$ (*e.g.*, Bechtold *et al.* 1987); this is because, while the clouds are perhaps expanding over time, which would tend to increase their ionization fraction, the UV background flux probably drops, allowing clouds to remain intact. This prediction has been borne out by the recent detection with the Hubble Space Telescope (HST) of at least 9 and possibly 16 Lyα forest lines at redshifts $z < 0.16$ in the spectrum of 3C 273 (Morris *et al.*

1991; Bahcall *et al.* 1991), four times more than expected by merely extrapolating to $z = 0$ the high-redshift *evolutionary* results, but more consistent with the marginal evolution results of Rauch *et al.* (1991).

In contrast to the Lyα clouds, Bechtold *et al.* (1984), Lanzetta (1988), and Sargent, Steidel, & Boksenberg (1989) all found that the redshift distribution of Lyman limit systems is consistent with a *constant* comoving number density over the range $0.4 < z < 3.6$, implying that a single parent population could not comprise both theLyα forest clouds and the Lyman limit systems. However, that result has recently been complicated by Lanzetta (1991), who finds strong evidence for evolution of the Lyman limit systems at $2.5 \leq z \leq 3.7$, with $N(z) \propto (1 + z)^{5.7\pm1.9}$, while confirming the constancy of incidence for $z < 2.5$. Different results again are obtained for both the systems identified by the Mg II $\lambda\lambda2800$ doublet and those selected by the C IV $\lambda\lambda1549$ doublet: the density of Mg II systems is seen to increase slightly with redshift with $\gamma = 1.45 \pm 0.63$ (Lanzetta, Turnshek, & Wolfe 1987; Sargent, Steidel, & Boksenberg 1988), consistent with no evolution if $q_0 = 0$ but marginally inconsistent if $q_0 = 0.5$ (although the effects may depend on equivalent width; Caulet 1989), while the comoving space density of C IV systems is observed to *decrease* with redshift, going as $(1 + z)^{-1.26\pm0.56}$ over the range $1.3 \leq z \leq 4$ (Sargent, Boksenberg, & Steidel 1988; Steidel 1990), or to increase from $z = 0$ to $z \sim 2$, then decrease (Khare, York, & Green 1989). Steidel (1990) argues that this can be explained best by an increase in actual carbon abundance over time, supporting the hypothesis that the metal-line systems represent haloes of actively star-forming galaxies, though this claim is disputed by Peng & Weisheit (1991), who explain the observed effect through an evolving metagalactic radiation field.

One final distinction between the Lyα forest clouds on the one hand and heavy-element systems on the other is the observed clustering properties. While the Lyα

clouds show no clustering except perhaps very weakly on scales < 300km s^{-1} (Webb & Barcons 1989; Barcons & Webb 1990), the Mg II and C IV systems cluster very strongly on scales $\delta v < 600$km s^{-1} (Sargent, Steidel, & Boksenberg 1988; Steidel 1990), again supporting their identification with galaxies, which are known to cluster locally on similar scales. The C IV systems also exhibit some clustering on much larger scales, $\delta v \sim 1000$–10000 km s^{-1}, perhaps implying structures too large to form via gravitational instability (Heisler, Hogan, & White 1989).

The Damped Lyα Clouds

Statistics on the damped Lyα systems, the least numerous of the QSO absorbers, are too meager to conclude anything significant about their clustering properties. They are also too rare for evolutionary effects to be claimed with confidence, although according to Lanzetta *et al.* (1991) the evidence to date is consistent with no-evolution scenarios. As those authors discuss, however, the observed number density of damped systems at $z \sim 2.5$ exceeds by at least 2–4 times the number expected by extrapolation from the local disk galaxy population. While it is plausible that the local galaxy luminosity function is seriously underestimated, perhaps allowing gas-rich dwarf galaxies to account for the surplus of damped systems, the general result to draw from these observations is that either the damped Lyα and Lyman limit systems have evolved into present-day disk or gas-rich dwarf galaxies, with substantial portions of their high-redshift gas converted into present-day stars, or the absorbers lurk unseen in local space, perhaps analagous to the huge, dark hydrogen clouds recently detected in 21-cm emission surveys (*e.g.*, Impey & Bothun 1989; Weinberg *et al.* 1991).

Motivated by the hypothesis that the damped Lyα systems represent young galaxies, either disks or gas-rich dwarfs, several recent studies have been aimed at

measuring the metallicities and/or dust content in the absorbing clouds. Based on examination of the narrow metal absorption lines, including C II, C IV, O I, Si II, Si IV, Ni II, Zn II, and Cr II, associated with several damped systems, the picture that is emerging is one of extremely low chemical enrichment, typically 10 − 100 times below solar, with dust contents on the order of 1/10th the local value in the Milky Way's ISM (Pettini & Hunstead 1990; Meyer & Roth 1990; Rauch et al. 1990). These results are corroborated by the low level of statistical reddening of QSOs observed through damped Lyα system, presumably due to dust extinction (Fall, Pei, & McMahon 1989; Pei, Fall, & Bechtold 1991), and by the weak detection of molecular hydrogen absorption towards a particular damped cloud (Foltz, Chaffe, & Black 1988).

In summary, it is clear that, if the various QSO absorption line systems share a common origin, then they have suffered very different fates to produce the variety of characteristics observed. While it seems quite plausible that the damped Lyα Lyman limit, and metal-line systems could represent different lines of sight through similar objects, thus giving rise to varying column densities of neutral hydrogen and degrees of ionization, it is difficult to incorporate the Lyα forest clouds into such a picture.

1.4.3 Searches for Emission from QSO Absorption Line Systems

Given that the heavy element QSO absorbing clouds, as well as the damped Lyα systems, are in some way related to young galaxies, and especially in view of the strong evolution inferred to have taken place since $z \sim 2$, we might expect to observe the signatures of star formation or at least stellar light associated with the absorbers. Even without star formation, the Lyα forest clouds must at some level absorb ambient UV background radiation and glow in the light of Lyα (Hogan &

Weymann 1987). This has led to numerous searches both for continuum emission using broad-band imaging and for line emission using spectroscopy and narrow-band imaging, in the hope of learning more about the morphologies, sizes, environments, and star formation characteristics of distant, probably average galaxies selected independently of their luminosities.

Similar techniques have been applied successfully to the study of radio galaxies and QSOs at redshifts approaching 4, although these objects are almost certainly not representative of normal galaxies. Most of the high-redshift 3C, 3CR, and 4C radio sources show strong, extended line emission, including large Lyα fluxes and some lines of high ionization species such as C IV, N V, and He II, as well as the blue colors (but large IR fluxes) commonly expected from young galaxies (Spinrad 1985; McCarthy *et al.* 1987a; McCarthy 1988; Chambers, Miley, & van Breugel 1990). At least some of the line emission is almost certainly due to copious star formation. Some controversy exists over the age of the stellar populations inferred in such objects; as Chambers *et al.* (1990) point out, although the spectral energy distributions (SEDs) can sometimes be fit with a combination of old ($> 10^9$ yrs) and young stars, this can lead to calculated ages greater than the age of the universe, inspiring models with non-normal IMFs (Bithell & Rees 1990) or bursts of star formation with exponential decay (Chambers & Charlot 1990). There is also some evidence that the rest-frame UV continuum light from high-redshift radio galaxies resembles the spectra of hot stars (Chambers & McCarthy 1990), lending support to their identification with young galaxies that may have just recently formed their first stars. The "alignment effect" (McCarthy *et al.* 1987b), in which the radio and optical morphologies are seen to coincide, is commonly interpreted as further evidence that stars are closely related to the radio sources.

High-redshift QSOs, especially those with strong radio emission, also show ex-

tended line emission, including Lyα (Djorgovski *et al.* 1987; Heckman *et al.* 1991; Steidel, Sargent, & Dickinson 1991), although, as with the radio galaxies, it is unclear exactly how much ionizing flux is due to star formation and how much comes from the central AGN engine.

By contrast, previous searches for Lyα emission from the Lyα forest clouds (or any other random Lyα emitters in "blank sky," including primeval galaxies) have been uniformly unsuccessful (Koo & Kron 1980; Pritchet & Hartwick 1987; Cowie 1988; Pritchet & Hartwick 1990), indicating either that at the redshifts observed there is at most very little star formation in such systems, that the background ionizing flux is too low to excite the gas to fluoresce, or that dust attenuates any Lyα emission produced in the clouds. The second possibility is consistent with measurements of J_ν using the proximity effect, while the third possibility is difficult to constrain due to the unknown metallicities in the Lyα forest clouds.

The Mg II and C IV systems have proven to be more productive hunting grounds for galaxies visible by their own light. Using broad-band images of fields with QSOs known to shine through metal-line systems (especially Mg II systems, which can be observed down to lower redshift than the C IV systems due to the relevant wavelengths and the atmospheric cutoff), Bergeron (1988) and Bergeron & Boisse (1991) report the detection of emission associated with more than 20 absorbers. The sources are almost all separated by several arcseconds from the QSO line of sight, show spectra typical of H II regions, with strong Balmer, [OII], and [OIII] emission lines, are typically bluer than $B - V \sim 0.5$, and thus as a sample are well-described by a population of galaxies with active or recent star formation and extended, ionized haloes or else dwarf companion galaxies, with typical impact parameters of 60 kpc.

These results were extended by Yanny *et al.* (1990a,b) and Yanny (1990), who

used narrow-band imaging and fiber-optic and long-slit spectroscopy to observe line-emitting sources near Mg II systems. A surplus of blue, strongly [OII]-emitting galaxies relative to the number density expected from the local galaxy luminosity function led to the conclusion that, assuming gravitational lensing is not responsible for the observed excess, significant number and/or luminosity evolution must have taken place since $z \sim 1$.

While the metal-line systems have thus been used to locate regions of strong star formation, efforts to detect emission from the damped $Ly\alpha$ systems have been much less successful. Many hours of integration time using CCDs on large telescopes with long-slit spectroscopy (Foltz, Chaffee, & Weymann 1986) or narrow-band imaging (Smith et al. 1989; Deharveng et al. 1990) produced upper limits well below the levels of emission expected for disk galaxies supporting star formation at rates similar to those observed today. A marginal detection of emission from one damped system reported by Hunstead, Pettini, & Fletcher (1990), which has sparked some controversy, was followed by a contradictory claim of detection by Wolfe et al. (1991); this line of sight will be discussed in detail in Chapter 4.

Far from convincing workers that there is little if any star formation taking place in the damped $Ly\alpha$ clouds, the lack of strong $Ly\alpha$ emission has prompted explanations based on the attenuation of $Ly\alpha$ photons by dust. As mentioned in Section 1.4.2, the presence of dust in the damped systems has been inferred indirectly. Although the estimated levels are only 0.01–0.1 times the Milky Way dust-to-gas ratio, Charlot & Fall (1991) calculate that in most cases, this is sufficient to hide substantial SFRs, possibly over 100 $M_\odot$ yr^{-1}, depending on the assumed morphology and dust characteristics in the absorbing cloud. Wolfe et al. (1986) also emphasize that due to the multiple scatterings $Ly\alpha$ photons undergo in the optically thick gas, emission might be expected to leak out not in a single narrow

line but rather in a broad double-humped form that could easily escape detection (see Section 2.1).

This thesis contains a report of a multi-faceted search for line-emitting objects at high redshift, corresponding to galaxies undergoing rapid star formation, possibly for the first time in their histories. In Chapter 2, I present the results of a deep search for Lyα emission from "blank sky." In Chapters 3–5 I discuss positive detections and upper limits on emission associated with absorption line systems seen towards eight high-redshift QSOs. Chapter 6 presents some conclusions drawn from the search results, and the Appendix describes in detail the Fabry-Perot imager developed and used for many of the observations.

Chapter 2

SPECTROSCOPIC LIMITS ON HIGH-REDSHIFT LYα EMISSION

2.1 Introduction

A natural way to probe the distribution of gas and ionizing radiation at high redshift is to look for Lyα line radiation. As mentioned in the previous chapter, such emission is expected from gas clouds ionized in the vicinity of QSO's, from collapsing primeval galaxies undergoing initial star formation, and from the hydrogen clouds thought to be responsible for the Lyα forest seen in QSO spectra, which are ionized to some degree by the ambient intergalactic ultraviolet radiation (Hogan and Weymann 1987). In this chapter I report the results of a search for "blank sky" high-redshift line radiation and use them to place constraints on the distribution of star-forming galaxies and the intensity of intergalactic ionizing radiation at redshifts $z \simeq 3$.

Low-(~ 90 Å)-resolution interference-filter imaging of QSO environments and high-redshift radio galaxies has been very successful at discovering Lyα emission (see § 1.4.3). By contrast, searches for Lyα emission in blank sky using both narrow-band imaging and spectroscopic techniques have been interpreted as producing uniformly

null results (see Koo 1986 for a review). Koo and Kron (1980) used slitless spectroscopy to survey 4000 arcmin^2, but reached only $R = 20.6$, considerably brighter than the predictions of most primeval galaxy models. Pritchet and Hartwick (1987), using a 3.6 m telescope and a CCD with $\sim$ 100 Å filters to search 7.26 arcmin^2 of sky, found no confirmed sources at $z \sim 5$ down to R$\sim$27; a later search of 360 arcmin^2 down to a 2σ surface brightness limit of 5.4×10^{-17}erg s^{-1}cm^{-2}arcsec^{-2} at $z = 1.9$ also produced no sources (Pritchet & Hartwick 1990). Cowie (1988) conducted a deep long-slit Lyα search of 0.6 arcmin^2 at 11 Å resolution and a narrow-band (60 Å) imaging search of 2.8 arcmin^2 of blank sky; visual inspection revealed no obvious primeval galaxy candidates to a flux level of a few $\times 10^{-17}$erg s^{-1}cm^{-2}. Our strategy has been to use higher spectral resolution in order to maximize the contrast of line emission over the sky background, whose noise is the limiting factor in all such searches. This leads to a better absolute flux-density sensitivity than is possible at lower spectral resolution, at the expense of lowering the volume of space searched.

Given a two-dimensional detector (in our case, an 800×800 CCD), high resolution may be obtained in two ways: narrow-band imaging, especially Fabry-Perot imaging, and long-slit two-dimensional spectroscopy (Hogan and Rees 1979). In either case, the search maps a three-dimensional spatial volume onto the chip, and can be configured to use efficiently the entire dynamic range of the chip using optimal sampling in spatial and spectral dimensions. In a sky-limited search, the absolute flux limit is determined by the spectral resolution (which should optimally match the line width), so the limiting flux density is similar in the two cases. The first technique has the advantages of giving two-dimensional sky coverage and sampling a spatial volume that resembles a cube, with sides of comoving scale of order a few Mpc; since this is a scale where the galaxy-galaxy correlation is appreciable today, such a geometry is thus ideal for probing environments of known objects.

The long-slit technique, on the other hand, samples a volume resembling a thin yard-stick seen end-on, covering a relatively small area of sky but reaching deep in redshift space; the dimensions of the search volumes described here are of the order of .02 Mpc × 3 Mpc × 150 Mpc in comoving units, so the two methods sample roughly similar volumes. However, the larger surface area of the search volume and large redshift coverage are thus well-suited for detecting diffuse and uncorrelated emission, for example from absorption clouds spread over a wide range of redshift. The long-slit technique also has the advantage of sampling regions of space not physically associated with QSO's or other objects in the field.

The transfer of resonance transition lines, including Lyα, through astrophysical media has been worked out in considerable detail by several authors over the last 25 years, but some fundamental characteristics of the emergent flux remain uncertain, depending largely on the exact nature of the medium. Lyα photons undergo multiple scattering within H clouds, working their way via random walk motion both in space and in frequency until they reach the cloud boundary or are destroyed via absorption, $e.g.$, by dust. Auer (1968), Bonilha $et\ al.$ (1979) and Urbaniak & Wolfe (1981) all predicted that in the absence of absorption, the emergent spectrum would show a double-humped form, with typical hump separations $\sim 3\sigma_v$ where σ_v is the thermal Doppler width, and, as Adams (1972) points out, if these photons then pass from an H II region in which they were formed into a thin, blanketing, cooler H I region, they will be appear to be Doppler shifted by $\sim 30\sigma_v$ from the line center in the cooler gas and thus can avoid the bulk of further resonant scattering effects, though they will be trapped if the blanket is thick enough.

Adding absorption to the transfer process can quickly destroy Lyα. Adams (1972) calculates that the mean number of scatterings of Lyα photons $\langle N \rangle \sim \tau_0$, the optical depth of the medium, which can range up to $> 10^9$ for the observed

spread of neutral hydrogen column densities in Lyα clouds. Bonhila *et al.*, using Monte Carlo techniques to explore the transfer of resonance-line radiation through a plane-parallel slab, found that the fraction of escaping photons f_e ranged from 100% for no absorption to $\sim$ 2% for an absorption optical depth $\tau_{abs} = 0.1$, a resonance scattering optical half-depth $\tau_{1/2} = 10^8$, and a ratio of mean photon path length to optical half depth $L_0/\tau_{1/2} \sim 100$, plausible parameters for the high column density end of the Lyα cloud distribution assuming dust-to-gas ratios around 1/10th the local Galactic value. An even more pessimistic prediction was expounded by Hummer & Kunasz (1980), who found that the escaping fraction could fall as low as $f_e = 2 \times 10^{-5}$ for reasonable combinations of τ, the damping parameter a, defined as the ratio of the natural line width to the Doppler width, and morphological distributions of ionizing UV sources embedded in H gas and dust.

A less discouraging possibility was put forth by Neufeld (1991), who proposed that in a two-phase medium consisting of dense, mostly neutral clumps of dust and gas embedded in a hot, rarified ambient medium, Lyα photons can bounce from clump to clump, reflecting easily off the surfaces without penetrating deep enough to be destroyed by dust, and finally escaping from the ambient gas altogether. In this scenario, the Lyα line can actually be *enhanced* over the continuum, which does not bounce off the dense clumps but rather passes through them, suffering extinction.

The empirical picture is one of mixed success. Using IUE to search for Lyα emission from nearby extragalactic H II regions, radio galaxies, and blue star-forming galaxies (redshifted only enough to avoid the strong geocoronal Lyα line), Meier & Terlevich (1981), Ferland & Osterbrock (1985), Hartmann *et al.*(1988), and Deharveng, Joubert, & Kunth (1986) have registered detections in radio galaxies approaching the expected Case B value Lyα/H$\beta \sim$ 30, although in general the levels

for the radio-quiet objects range from 0 to 1/10th the Case B prediction. There appears to be a trend of weaker Lyα emission from the more metal-rich galaxies, supporting the view that dust produced in stellar processing is responsible for quenching Lyα photons; systems with metallicites around 0.1 times solar seem to allow Lyα to escape at a level down by a factor of 10 from the Case B value.

It is therefore not clear exactly what levels of Lyα emission we should expect from randomly distributed H clouds and galaxies at high redshift. Certainly assuming little or no extinction due to dust simplifies the matter greatly; fortunately, this assumption can be at least qualitatively justified by arguing that at high redshift, chemical enrichment of star-forming regions, including dust production, was probably substantially less advanced then than now, perhaps allowing Lyα to escape relatively unimpeded.

In this chapter I report the results of a deep long-slit spectroscopic search for high-redshift Lyα emission conducted at the Multiple Mirror Telescope. The images were subjected to rigorous statistical tests to verify the sensitivity reached. The data have been analyzed with regard to the question of blank sky emission; QSO light is used only to locate Lyα absorption systems along the line of sight, and no analysis is attempted of possible gas in the environs of the QSOs themselves. The observations are discussed in §II, the statistical analysis in §III and §IV.

2.2   Observations

The observations were made at the MMT using the CCD spectrograph (Schmidt, Weymann, and Foltz 1989) on the nights of 1987 November 23 and 1988 October 16 and 17 (see Table 2.1). Two or four integrations, ranging from 3600 to 5000 seconds each, were made of each of three fields centered on bright high-redshift $(3.0 < z < 3.5)$ QSO's selected from the Hewitt and Burbidge catalog (1987). The

long exposure times were chosen to ensure that sky noise dominated, even between night sky lines. The wavelength region observed was chosen in each case to cover the QSO's Lyα emission line, except for the highest redshift pair, which covered redshifted C IV 1549Å emission from Q0301-005; these wavelengths were chosen to search for Lyα emission from redshifts both lower and higher than that of the QSO itself. Total coverage was about 600 Å per frame at 2.4 Å resolution, and the unvignetted spectrograph slit dimensions were 1.5″×160″. The CCD was binned in the spatial direction by a factor of two to reduce readout noise, yielding a spatial scale of .6 arcseconds per pixel; the spectral scale was $\approx$ .8 Å per pixel. Between the two observations of each field, the telescope was moved by 5″–10″ along the slit, so that the QSO spectrum appears slightly shifted from one image to the next. (This technique allows cosmic rays and cosmetic defects on the CCD [e.g.,"hot pixels"] to be rejected as candidate emission features.) The seeing on all three nights was better than 2 arcseconds, and sometimes as good as 1 arcsecond. Observations of spectrophotometric standard stars were made to determine the transformation from electrons detected to photons incident upon the Earth's atmosphere. (Additional data were taken at the Steward Observatory 2.3 m telescope on Kitt Peak using the Boller & Chivens spectrograph and a CCD, but the sensitivity levels reached were uninteresting, and I will henceforth discuss only the MMT data.)

Data reduction was carried out using standard IRAF routines. The raw images

Table 2.1: Summary of Observations

QSO Field	z_{QSO}	$z_{covered}$	λ(Å)	Exposure (s)	Date of Observation
0731+653...	3.035	2.7–3.2	4483 − 5135	2 × 3600	1987 November 23
0301−005...	3.205	3.1–3.6	4934 − 5573	2 × 3600	1988 October 16
0014+813...	3.41	3.1–3.6	4934 − 5573	2 × 4000	1988 October 17
0301−005...	3.205	4.2–4.7	6285 − 6918	2 × 5000	1988 October 17

were bias subtracted and flat-fielded to correct for variations in pixel sensitivity (except in the case of the Q0731+653 field, for which flat fields were inadequate and would have increased the noise fluctuations in the frame). The data from the October 1988 run showed significant spectral curvature, due to spectrograph optics; these frames were transformed to rectilinear coordinates, after first removing obvious cosmic ray hits, which otherwise are spread out by the transformation. Finally, all the data were sky-subtracted, using as high signal-to-noise templates the averaged areas of "blank sky" bordering the QSO spectra, and flux-calibrated using standard stars. The level of RMS noise fluctuation in regions of blank sky was measured to be $1 - 4 \times 10^{-18}$ergs s^{-1}cm^{-2}arcsec^{-2}, including readout noise from the CCD, Poisson noise from the night sky emission, and a minimal amount of noise introduced during bias subtraction and flat-fielding. No correction was made for variations in flux transmitted by the slit due to fluctuations in seeing during the night; however, I estimate the errors in the absolute flux transformation due to such effects to be no larger than 25%, based on the observed seeing FWHM values.

2.3   Analysis of Blank Sky

I first analyzed the data to determine limits on any possible population of unresolved Lyα emitting clouds at random locations and redshifts in each field. Any real Lyα emission in the observed fields would appear at the same position relative to the QSO spectrum, and at the same intensity, in both frames in each pair. Any real unresolved cloud would also be expected to have an image profile corresponding to the instrumental spectral resolution and to the seeing, $i.e.$ an elliptical Gaussian with a FWHM of a few pixels. As in Cowie's (1988) search, no emission features of any size or brightness are visible to the naked eye in any of the eight frames. However, to verify a null detection and to quantify its statistical significance, a

series of numerical tests with the data frames were conducted.

Each frame was searched for candidate objects by convolving the image with a Gaussian filter matching the instrumental and seeing profiles, and then searching the convolved image for local maxima that exceeded a specified threshold. This procedure enhances the detection probability of real objects, while suppressing that of cosmic rays and cosmetic defects on the CCD. (The long integrations allowed several hundred cosmic rays to contaminate each frame, but they are easy to recognize by their extreme intensity and sharpness.) The candidates found in this way were then examined in closer detail. An accurate centroid and an integrated intensity with respect to background for each candidate object were computed, and the lists of candidates from the two frames of each field were compared to identify any objects that appeared in both frames at the same relative separation from the QSO spectrum, at the same wavelength, and with approximately the same intensity.

By lowering the detection threshold, the number of candidate objects from a single frame could be increased to over 1000. Most of these were merely low-level noise events, although a few cosmic rays slipped through the Gaussian filter. Given enough candidates, a match between two features from different images of the same field is inevitable; it is then important to evaluate the significance of the detection. Here the slight shift between images of a given field was again helpful. The detection threshold was adjusted so that just enough candidate objects appeared to produce a few matches between the two frames. Features from the two candidate lists were then searched for correlations at separations different from the real shift; in no case did the number of matches at the correct separation exceed the spurious correlations, indicating that the matches were between random noise spikes, not interesting detections.

To determine the level of Lyα emission that could be excluded by our non-

detection, I tested our search method with synthetic signals. For each of a range of intensities, 100 features that matched the Gaussian seeing and instrumental profiles were added to both image frames of a given field. Running the search routine on the synthetic data then yielded a detection probability p_d for a single feature of the tested intensity. Given p_d over a range of intensities, it remained to calculate the average space density of $Ly\alpha$ emitters as a function of intensity that could produce a null detection (*i.e.*, a high average density of dim objects could entirely escape detection, while a single bright object per field could not). The probability of a null detection is

$$P_{x=0} = \sum_{N=0}^{N \gg \langle n \rangle} P_{have}(\langle n \rangle, N) \times P_{detect}(x = 0, N) \qquad (2.1)$$

where the first term is the probability of having N objects in the field of view given an average density of objects $\langle n \rangle$ per field of view, and the second term is the probability of detecting $x = 0$ objects given N objects in the field. P_{have} is given by the Poisson probability distribution, while P_{detect} is given by the binomial distribution, calibrated by our synthetic data. The probability of a null detection is then

$$P_{x=0} = \sum_{N=0}^{N \gg \langle n \rangle} \frac{\langle n \rangle^N}{N!} e^{-\langle n \rangle}(1 - p_d)^N. \qquad (2.2)$$

Setting this equal to 0.05, one can calculate the values of $\langle n \rangle$ that can be excluded with 95% confidence for a given intensity of $Ly\alpha$ emitters. Figure 2.1 shows the limits placed by our observations on the space density of $Ly\alpha$ emitters in an $\Omega = 1$ universe as a function of their observed flux. I plot our results in units of space number density rather than surface number density on the sky, since the latter requires uncertain corrections for redshift space searched compared to total redshift space occupied by $Ly\alpha$ emitters. The limits are calculated for each redshift range individually; our null result considered over the entire volume searched would lead to even stricter limits. The limits for the range $3.1 < z < 3.6$ reach the lowest
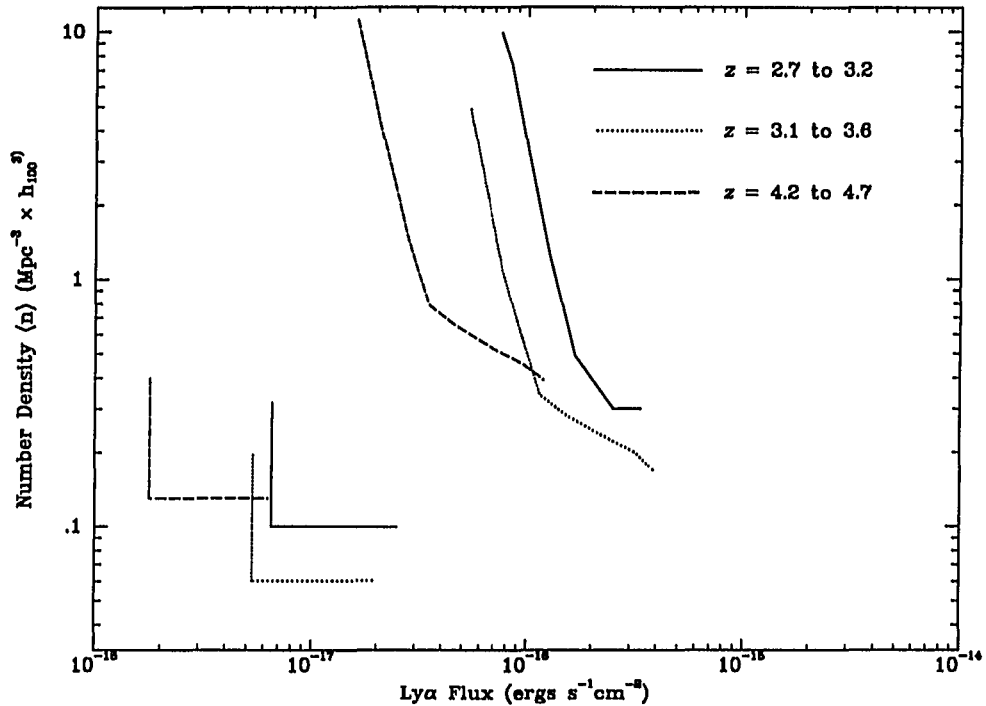
Figure 2.1: Curved lines show statistical 95%-confidence upper limits on the co-moving number density of unresolved Lyα emitters in various redshift ranges, as a function of their flux in the line. Straight lines show 2σ flux limits for 1 arcsec^2 sources. Regions to the upper right of both sets of lines are excluded.

number density, while for $4.2 < z < 4.7$ they reach the faintest flux, thanks to larger spatial coverage and better CCD quantum efficiency, respectively. Although visual inspection of the frames with synthetic features added produced a higher number of identifications than the automated procedure, it also produced many spurious candidates, indicating that our search algorithm, which returned null results, is conservative but rigorous.

Also plotted in Figure 2.1 are the limits corresponding to the 2σ noise levels in our data, for < 1 source per field measuring 1 arcsec^2. If we assume a rest equivalent width in Lyα of 70Å for Lyα clouds (Partridge and Peebles 1967; Koo 1986), we

can calculate the total flux expected in a given broad bandpass, including both line and continuum emission. Our 2σ detection limits would then correspond to brightnesses, from lowest to highest redshift, of $B \sim 28.8$, $V \sim 28.5$, and $R \sim 29.1$, making our search the most sensitive to date. It should be stressed, however, that our simulations indicate constraints at the 95% confidence level that are about one order of magnitude brighter than the nominal 2σ limits.

2.4 Limit on Diffuse Ionizing Radiation

Our data can also be analyzed from a different point of view, namely, given the fact that HI gas is known to exist at certain places in our search volumes, a lack of Lyα emission from the gas constrains the incident UV flux (Hogan and Weymann 1987). We focus on one particular absorption system in the 0731+653 field, a Lyα absorber at $z = 2.912$ known to have a Lyman continuum optical depth greater than 3 (Sargent, Steidel, and Boksenberg 1989). Assuming that a fraction β of incident ionizing radiation re-emerges as Lyα with β probably in the range 0.6–0.8, the observed Lyα flux density is just $J_{\nu\alpha0} = (1 + z)^{-3}\beta J_\nu$, where J_ν is the flux density of the ionizing background at redshift z. Based on common-absorption-line studies (*e.g.* Foltz *et al.* 1984) and on the identification of the Lyman limit systems with the extended halos of galaxies, the angular size of the absorbing cloud is likely to be larger than our spatial resolution element; $\theta = 1$ arcsec $(R/3.8h^{-1}\,\mathrm{kpc})$ at this redshift. Therefore, a limit on the Lyα emission surface brightness in the absorption line core translates directly into a limit of the diffuse ionizing flux at high redshift. Since the Lyα emitting gas lies close to the surface of the cloud (at $\tau_{UV} \lesssim 2$), quenching by dust is not a problem in this situation.

I obtain this limit somewhat differently from the previous blank-sky analysis, because we now know exactly where the emission should occur in the image in

wavelength. To begin with, we can now use co-added data from two frames to reduce the noise. Adding artificial flux matching the instrumental point-spread function to the appropriate place in the data frame then allows one to see how much is needed to be confidently detected by visual inspection such that the absorption line is significantly non-zero; this turns out to correspond to a 2σ flux in the peak pixel, and a total intensity in the line $F = 4.8 \times 10^{-17}\mathrm{erg}\ \mathrm{s}^{-1}\mathrm{cm}^{-2}\mathrm{arcsec}^{-2}$, or $J_{\nu\alpha 0} < 3.2 \times 10^{-21}\mathrm{erg}\ \mathrm{s}^{-1}\mathrm{cm}^{-2}\ \mathrm{sr}^{-1}\ \mathrm{Hz}^{-1}$. This translates directly into an upper limit on J_ν at the redshift of the system:

$$J_\nu < 19 \times 10^{-20}\beta^{-1}\mathrm{erg}\ \mathrm{s}^{-1}\mathrm{cm}^{-2}\ \mathrm{sr}^{-1}\ \mathrm{Hz}^{-1}.$$

Theoretical expectations for this quantity vary widely (Bechtold et al. 1987); however, they do not generally go as high as the present limit. This limit is also not as sensitive as measurements based on modeling the "proximity effect" (Bajtlik, Duncan and Ostriker 1988) which yield $J_\nu \simeq 10^{-21\pm0.5}$. However, it is possible that the proximity effect is entirely unrelated to photoionization by the QSO, in which case J_ν could be much higher. Therefore the present limit is not surprising, but it probably represents the most direct information about the diffuse ionizing flux at high z.

2.5 Discussion

Although the negative results of most recent searches for direct evidence of galaxy formation have been interpreted as excluding recent ($z = 1 - 3$) primeval galaxies (Koo 1986), some current models of galaxy formation have not been constrained by the observed non-detection levels. The primeval galaxy models of Baron and White (1987), for example, discussed in Chapter 1, simulate the dissipational inhomogeneous collapse of protogalaxies in a CDM scenario, predicting relatively recent

formation of the bulk of stars, possibly continuing until $z = 1 - 2$, and taking place over an extended period of time, as opposed to the spectacular bursts suggested in earlier models. The resulting objects tend to be large, dim, and diffuse, but with several peaks of emission corresponding to 28 mag arcsec^{-2} across ~ 2 arcseconds at the redshift of formation. Could we detect such an object, or the brightest peaks?

White (1988) provides scaling laws for the appearance of the primeval galaxies modelled in Baron and White (1987). Assuming a constant mass, and that the primeval galaxies are observed at the time of collapse, White shows that cosmological and evolutionary factors conspire to keep the angular diameter constant with z, while the surface brightness scales as $(1 + z)^{-1/2}$ (including $(1 + z)^{-4}$ from cosmological factors and $(1 + z)^{7/2}$ from evolutionary factors). Assuming a rest equivalent width of Lyα of 70Å (corresponding to the bulk of stellar ionizing radiation emerging as Lyα), the bright $2''$ diameter peaks would then have a total observed Lyα flux $\sim 3.4 \times 10^{-17}$ergs s^{-1}cm^{-2} for $z = 3.0$, or $\sim 3.0 \times 10^{-17}$ergs s^{-1}cm^{-2} for $z = 4.5$. From Figure 2.1 it can be seen that the low-redshift values are not exluded for any number density by our observations, but the emission peaks would escape detection only marginally. Furthermore, the high-redshift curve in Figure 2.1 excludes objects of the calculated flux with an average space density $\langle n \rangle > 1$ Mpc$^{-3}h^3$. Baron and White, however, predict $< .02$ emission peaks Mpc^{-3}, assuming an average of 5 such peaks per primeval galaxy and a uniform distribution of objects from $z = 3.9$ to $z = 6.4$, so the model is not constrained by our data, because it covers an insufficient volume.

Although I cannot exclude with any certainty the specific model proposed by Baron and White, the proximity of our sensitivity level to the predicted characteristics of a very conservative primeval galaxy model is encouraging. Our 95% confidence limits indicate that we would have detected sources at all redshifts sur-

veyed emitting $> 10^8 L_\odot h^{-2}$ in the Lyα line for $q_0 = 0.5$, or $\gtrsim 10^{10} L_\odot h^{-2}$ total luminosity (if at least 1% of the total emergent flux appears in the Lyα line), values corresponding to only moderately luminous galaxies today and more than 1000 times fainter than the predictions of the disk formation model by Cox (1985). If galaxies collapse with a greater dissipation rate than that modelled, if the initial gas fraction is higher, or if there are more massive stars in the IMF, the objects will appear brighter (White 1988). On the other hand, even a small amount of dust present in a collapsing gas cloud could reduce Lyα emission by a large factor below the 70Å assumed above. Although it is encouraging that large equivalent widths of Lyα emission are actually observed in such high-redshift objects as the Lyα companion to 3C 326.1 (McCarthy *et al.* 1987), there is no guarantee that this would hold for most galaxies.

Also interesting, and not dependent on the dust abundance, is the possibility of reaching the level at which all optically-thick absorbers would glow detectably in Lyα due to the UV background. If the UV background is only as large as inferred from the inverse effect, an increase in sensitivity by a factor of 100 would be needed to detect Lyα from all optically-thick hydrogen clouds. Such a large increase does not seem immediately practicable, although 2-D Lyα line mapping of gas distributions in the environs of QSOs, where UV fluxes are larger, has already proven fruitful (*e.g.*, Heckman *et al.* 1991).

Chapter 3

THE DAMPED LYα SYSTEM TOWARDS PHL 957

3.1 Introduction

In Chapter 2, the focus was on Lyα emission from randomly distributed H clouds, such as those giving rise to the Lyα forest, although PGs were also sought, and the Lyman limit system towards Q0731+653 was examined closely. Here, I turn to a damped Lyα absorption line system. The apparent similarities between the damped systems and current-day galaxies make the former attractive targets for a directed emission search; with reason to believe that 10^{10} M$_{\odot}$ of stars could have formed in only a few Gyr, we stand to gain knowledge about the morphology, kinematics, and evolution of a class of object constituting a significant fraction of the galactic mass of the universe.

The prediction that intense Lyα emission lines should be characteristic signatures of young, actively star-forming galaxies at high redshift (Partridge & Peebles 1967; Meier 1976; Cox 1985) has prompted searches for emission from the damped Lyα systems, including the system studied here, using both narrow-band imaging techniques (Smith *et al.* 1989; Deharveng, Buat, & Bowyer 1990; Wolfe *et al.* 1991) and spectroscopy (Foltz, Chaffee, & Weymann 1986; Hunstead, Pettini & Fletcher

1990; Pettini & Hunstead 1990), especially long-slit. Despite extensive observations by several workers, only two weak (and contradictory) detections have been reported: an unresolved spike of emission in the bottom of the Lyα absorption trough in the spectrum of QSO $0836 + 113$ ($z_{em} = 2.70, z_{abs} = 2.47$) (Hunstead et al. 1990; see Chapter 4); and an extended source around the *same* damped cloud, reported by Wolfe et al. (1991), who do not confirm the detection of Hunstead et al.. These detections, as well as the upper limits of other searches for Lyα emission from high redshift galaxies (*e.g.*, Chapter 2; Pritchet & Hartwick 1990), are at levels much fainter than expected for an actively star-forming galaxy, if much of the ionizing UV radiation appears in the Lyα line. In contrast to the faintness of the absorbers, large equivalent widths of Lyα emission have been observed from objects associated with high redshift radio galaxies and QSOs (see § 1.4.3). The lack of strong detections of Lyα emission from damped Lyα systems and other putative primeval galaxies can be interpreted in three ways: either the star formation rates (SFRs) in normal galaxies at high redshift are considerably lower than predicted (the unconfirmed detection of Hunstead et al. corresponds to SFR $\gtrsim 1$ M$_\odot$yr^{-1}, comparable to Sb galaxies today); or there is sufficient dust in the observed sources to quench Lyα radiation, which is especially susceptible to dust extinction due to multiple scattering within the optically thick gas; or the damped systems do not represent any form of normal galaxies. The presence of dust in the damped Lyα clouds has been inferred independently by the observed reddening of QSOs that shine through damped clouds (Pei, Fall & Bechtold 1991), and Charlot & Fall (1991) find that, depending on the morphology and orientation of the absorber as well as its neutral hydrogen column density, observationally allowed amounts of dust could hide the Lyα emission produced by star formation rates up to two orders of magnitude higher than in the solar neighborhood.

In this chapter, I report the discovery of line and continuum emission near the damped Lyα cloud seen at $z_{abs} = 2.309$ towards the QSO PHL 957 (=0100+13)($z_{em} = 2.681$). The damped system towards PHL 957 is an especially well-studied target, and a particularly interesting one for a Lyα emission search: with a neutral hydrogen column density $N_{HI} = 2.5 \times 10^{21} \text{cm}^{-2}$, the absorber has been shown to have a metallicity only 4% of solar, with a dust-to-gas ratio only 3% of the Galactic value, based on metal absorption line ratios (Meyer & Roth 1990; Pettini, Boksenberg & Hunstead 1990); a ratio of molecular to neutral hydrogen five orders of magnitude below Galactic, based on upper limits on H_2 absorption bands (Black, Chaffe & Foltz 1987); and a ratio of carbon monoxide to neutral hydrogen two orders of magnitude below average Galactic levels, based on upper limits on CO absorption (Levshakov et al. 1990). Taken together, these observations imply an extremely poorly-enriched absorber from which Lyα photons might be allowed to escape without substantial obstruction by dust.

3.2 Observations

3.2.1 Fabry-Perot Imaging

Deep narrow-band CCD images of the PHL 957 field were taken at the KPNO 4-meter telescope with the Goddard Fabry-Perot Imager (GFPI; see the Appendix for details on the instrument) on the nights of 24–26 January 1990 (UT) in poor seeing conditions ($2.''4 - 3.''6$ FWHM). Operating in interference order 19, the etalon was tuned to 4023 Å, the wavelength of redshifted Lyα for the damped system at $z = 2.309$; the FWHM of the transmission function was 24 ± 3 Å, corresponding to Lyα in the redshift range $2.299 - 2.319$. Off-band comparison images were taken at a wavelength of 4319 Å with a FWHM of 28 ± 4 Å. Wavelength calibration is achieved by illuminating the field of view with a Penray high-voltage spectral line

lamp and scanning the etalon in wavelength across a known spectral line. The error in the FWHM arises from the complex structure in the etalon's reflectivity; even a small wavelength step between a calibration line and the wavelength of observation can introduce a significant but unknown change in the transmission function. The transmitted wavelength shifts to the blue towards the edge of the field of view, due to the angle of incidence of the incoming collimated light beam; however, for these observations, the wavelength shift was only 0.6 Å a small fraction of a FWHM, so the images are essentially monochromatic (see Appendix A). Although the GFPI is susceptible to internal reflections from bright sources, the resulting ghost images always appear at repeatable distances and orientations with respect to the original sources, allowing discrimination from genuine detections.

The detector, KPNO's "Tek2," is a Tektronix 512×512 CCD with 8 e^- pixel^{-1} rms read noise and a scale of $0\overset{''}{.}53$ pixel^{-1}, after demagnification of the Cassegrain focus by the instrument's reimaging optics and on-chip binning by a factor of 2, giving a field of view of $2'.3$. Dark current was measured to be negligible.

Total integrations of three hours on-band and 1.3 hours off-band were obtained in variable conditions over the three nights; see Table 3.1 for a summary of the observations. The spectrophotometric standard star G191 B2B was observed in both bands for flux calibration.

The data were reduced in the usual way, using standard IRAF software routines. A coadded, median-combined bias frame was subtracted from each program

Table 3.1: Summary of Observations

Date (UT)	Telescope	Instrument	Integration (sec)	Seeing (arcsec)	Resolution (FWHM)(Å)	λ Range/ Central λ (Å)
26 Oct 1989	MMT	Red Channel	25200	1.8	2.5	3811–4864
24-26 Jan 1990	KPNO 4m	GAFPIC+Tek2	10800	2.4-3.6	18	4023
24-26 Jan 1990	KPNO 4m	GAFPIC+Tek2	4709	2.5	28	4319
8 Dec 1990	MMT	Red Channel	9000	1.5	24	3034–8142
9 Dec 1990	MMT	Red Channel	6600	2.2	2.8	3677–4333
14-15 Jan 1991	MMT	Red Channel	10800	1.9	2.4	3692–4353

frame, which was then divided by a normalized high signal-to-noise dome flat image to correct for pixel-to-pixel variations in response. Individual exposures from the two separate bands were then registered to sub-pixel agreement and coadded, weighting by the exposure times, to produce a final on- and off-band image. The transformation from electrons detected to physical units of flux incident upon the Earth's atmosphere was achieved by adopting the nominal FWHMs quoted above for each band and assuming that the integrated area under the transmission curve was $A = 1.1 \times \tau \times$ FWHM, where τ is the peak transmission. The number of electrons detected from the standard star, coupled with its known flux density over the bandwidth observed, then yields the total throughput and the flux transformation.

A significant patch of emission is clearly visible in the on-band image $48''$ to the northwest of the QSO at position angle $PA = 119.3°$ (see Figure 3.1a). The object appears to be resolved, with two main peaks of emission separated by $\sim 3''$ at $PA \simeq 71°$; however, the variable seeing over the three nights prevents an accurate estimate of the object's spatial extent. Total flux recorded was $6.5 \pm 1 \times 10^{-16}$erg s^{-1}cm^{-2}, corresponding to $\sim 10\sigma$ as measured in nearby patches of blank sky. No extended emission is visible in the immediate vicinity of the QSO line of sight. Due to the blackness and breadth of the damped Lyα absorption line, the QSO all but disappears in the on-band image; the little flux that does appear at the position of the QSO (marked Q in Figure 3.1), 1×10^{-16}erg s^{-1}cm^{-2}, is easily accounted for by leakage of QSO continuum into the broad wings of the FP's Airy transmission function, and so cannot be interpreted as unresolved emission from the damped cloud.

No corresponding emission is visible in the off-band frame (Figure 3.1b), down to the limiting sensitivity (3σ) for a point source of 2.7×10^{-17}erg s^{-1}cm^{-2}, indicating that the flux seen in the on-band image is line emission.
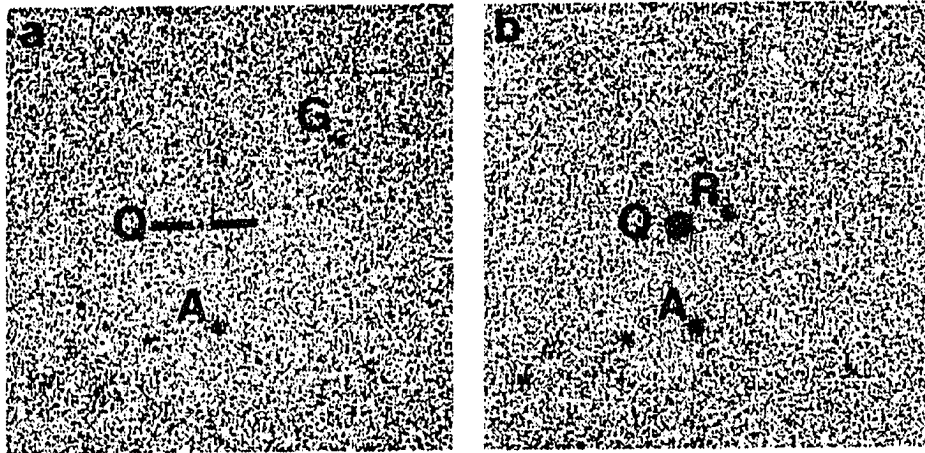
Figure 3.1: (a) On-band Fabry-Perot CCD image of the PHL 957 field. North is up and east is to the left; the field of view is 2 × 2 arcminutes. $\lambda_0 = 4023$ Å; FWHM=18 Å. The position of the QSO is labelled Q, object A is a foreground star, and the companion galaxy is labelled G. (b) As in (a), but off-band image. $\lambda_0 = 4319$ Å; FWHM=28 Å. Label R indicates a ghost reflection of the QSO.

3.2.2 Long-Slit Spectroscopy

Long-slit spectra of PHL 957 were obtained with the Red Channel CCD Spectrograph (Schmidt *et al.* 1989) at the Multiple Mirror Telescope (MMT) on 25 October 1989 UT (before the emission-line object had been discovered) and on 8-9 December 1990 and 14-15 January 1991 UT (after the object's discovery). All observations were made with a $1\rlap{.}''5\times180''$ slit and either a 1200 l mm^{-1} grating for moderate resolution (2.6 Å FWHM) or a 150 l mm^{-1} grating for low resolution (24 Å FWHM); the pixel scales after binning by a factor of two spatially were $0\rlap{.}''6 \times 0.8$ Å pixel^{-1} and $0\rlap{.}''6 \times 6.4$ Å pixel^{-1}, and spectral coverage was $\sim 3700-4300$Å and $\sim 3000-8100$Å, respectively. Seeing conditions ranged from $1\rlap{.}''5 - 2\rlap{.}''2$ (FWHM); total integration times were 7 hours in three exposures for the initial high-resolution data, 2.5 hours in three exposures for the low-resolution spectra, and 4.8 hours in five exposures for the remaining high-resolution spectra. Observations of spectrophotometric standard stars were obtained using the same setup during each run for flux calibration, and the program frames were interleaved with observations of internal helium-neon-argon spectral line lamps for wavelength calibration. For the October 1989 observing run, before the emission-line object had been discovered, the spectrograph slit was placed north-south. For all subsequent runs the slit was placed at $PA = 119.3°$, to include both the QSO and the companion galaxy; at the telescope, this setting was achieved via a rotational offset from the line connecting the QSO and star "A" in Figure 1. The absolute positions of the QSO and star "A" were also verified using the NOAO Grant Measuring Engine and the appropriate Palomar Observatory Sky Survey plate.

The data were reduced as usual, including bias subtraction, flat fielding, transformation to rectilinear coordinates, coaddition of individual frames to produce a final low- and high-resolution image, and flux calibration. Each image was scaled to

a common level based on the observed QSO continuum level before coaddition. No attempt was made to correct for variations in the flux calibration due to variable seeing and the constant slit width, but such an effect probably introduces errors in the absolute flux smaller than 20%.

A strong emission line is clearly detected in both the low- and high-resolution spectra at 4027.3 ± 0.3 Å separated by $48''$ from the QSO, with a flux of $5.6 \pm 1 \times 10^{-16}$erg $s^{-1}cm^{-2}$, consistent with the Fabry-Perot result. Also visible in the low-resolution image is continuum from the object over most of the spectral range covered, at a flux level corresponding to B$\sim$ 24.2 (excluding the strong line) and V$\sim$ 23.6; although the spectrum includes part of the R band, no order blocking filter was used during the observations, so this region of the image may be contaminated by second-order UV light. Two faint but clear emission lines are seen at 5135 ± 4 Å and 5436 ± 5 Å. I identify the one strong and two weak lines as redshifted Lyα $\lambda1216$, C IV $\lambda1549$, and He II $\lambda1640$, respectively, yielding an emission redshift $z_{em} = 2.3128 \pm 0.0004$, based on the high-resolution spectrum of the Lyα line alone, and confirming that the object is indeed a companion to the damped Lyα cloud. The difference in redshift between the emission and absorption systems, confirmed by examination of narrow metal absorption features in the high-resolution spectrum of the QSO, corresponds to a velocity difference $\Delta v = 346\pm \sim 20$ km s^{-1}. A one-dimensional spectrum of the galaxy extracted from the low-resolution image is shown in Figure 3.2, and the two-dimensional high-resolution spectrum is presented in Figure 3.3; properties of the emission are summarized in Table 3.2.

The Lyα line is clearly resolved spectrally in the high-resolution spectrum, showing a FWHM $= 9.5\pm0.5$ Å, corresponding to ~ 700 km s^{-1}. Although the emission appears to be marginally resolved spatially, the variable seeing conditions again prevented an accurate measurement; more observations are necessary to determine

Table 3.2: Properties of the Damped Lyα Absorber towards PHL 957

| Parameter	Value		
		$q_0 = 0.1$	$q_0 = 0.5$
R.A. (1950)	$01^h00^m30^s.55$	...	...
Dec. (1950)	$+13°00'33''.6$	...	...
$\lambda_{Ly\alpha}$	$4027.3\pm.3$Å	...	...
$\Delta\lambda$(FWHM).............	9.4 ± 1Å	...	...
z_{em}	2.3128 ± 0.0004	...	...
$F(Ly\alpha)^a$	5.6×10^{-16}erg s^{-1}cm^{-2}	...	...
$W_{E,rest}(Ly\alpha)$	140Å	...	...
CIV/Lyα	0.1	...	...
HeII/Lyα	0.1	...	...
V	~ 23.6	...	...
B-V	~ 0.6	...	...
L(Lyα)..................	...	$1.1 \times 10^{43}h^{-2}$	$5.3 \times 10^{42}h^{-2}$erg s^{-1}
SFR^b	...	$11\ h^{-2}$	$5\ h^{-2}$M$_\odot$ yr^{-1}
Size	...	$\leq 17h^{-1}$	$\leq 12h^{-1}$ kpc
Projected Distance from Damped Cloud ...	...	$270h^{-1}$	$190h^{-1}$ kpc
Velocity Separation from Damped Cloud...	346 ± 19km s^{-1}	...	...

^{a} Error may be $\pm30\%$.

^{b} Assuming no dust and Case B recombination.
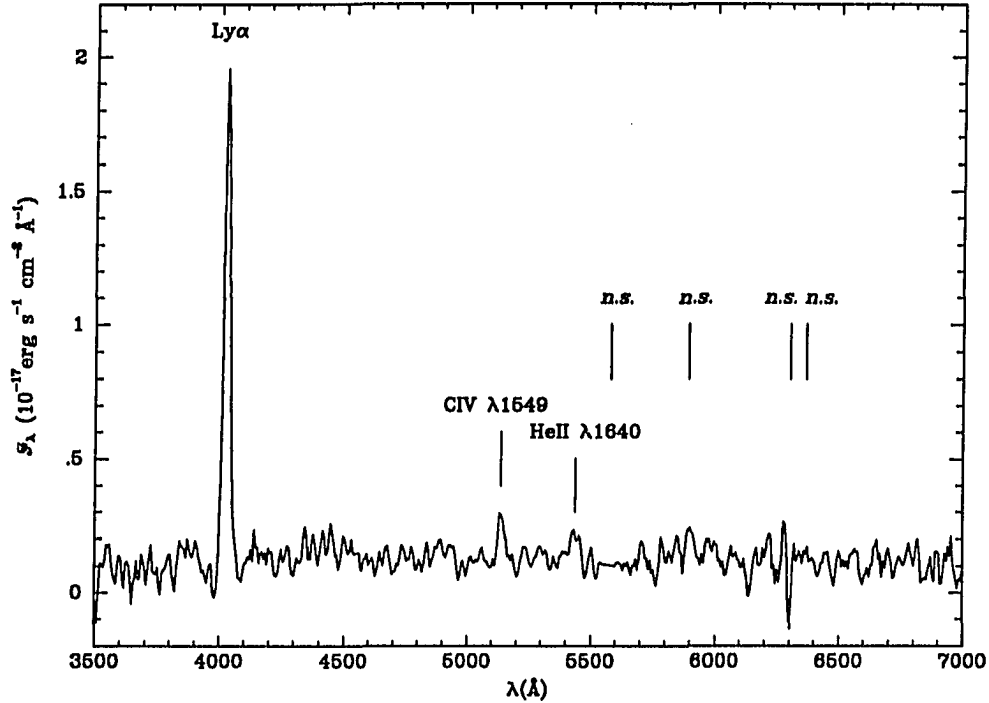
Figure 3.2: Low-resolution (24 Å FWHM) spectrum of the companion galaxy to the damped Lyα cloud towards PHL 957. Important emission features are indicated, as are the locations of residual night sky lines (marked $n.s.$). The spectrum has been smoothed by 3 pixels $\simeq$ the spectral FWHM, to suppress the noise.

the true spatial extent.

No emission is detected from the damped Lyα cloud itself at either of the two position angles, down to a limiting flux (3σ) in the high-resolution data for an unresolved source $F \leq 2 \times 10^{-17}$erg s^{-1}cm^{-2}, $\sim$ 30 times fainter than the Lyα emission observed from the companion galaxy and a factor of $\sim$ 4 lower than the previous upper limit, set by Pettini *et al.* (1990). A very slight excess of flux ($\sim 2\sigma$ as measured in circular apertures approximating the FWHM of an unresolved source) is measured in the 1989 October data at a position coincident with the QSO PSF and the centroid of the Lyα absorption trough, but confusion with cosmic ray hits
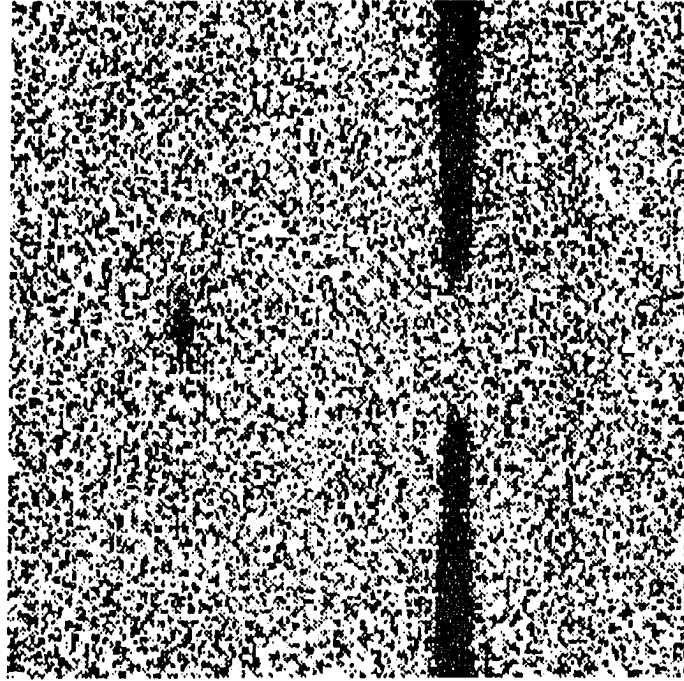
Figure 3.3: Two-dimensional high-resolution (2.6 Å FWHM) sky-subtracted spectrum of PHL 957 (right) and the Lyα companion galaxy (left), showing the core of the damped Lyα absorption line in the QSO and the Lyα emission line (FWHM~ 9.4 Å) in the galaxy. The image covers the spectral range 3946–4105 Å, with red at the top; the horizontal axis covers two arcminutes, with northwest to the left.

and the absence of emission in the later images convinced us that it was spurious.

Imaging of the companion galaxy was also attempted in broad-band B, R, and K colors, but the weather failed to cooperate, and the resulting upper limits were uninteresting.

3.3 Discussion

The emission-line object does not correspond to any previously reported X-ray, radio, or optical source in the literature. We interpret the observed continuum radiation as evidence that the source contains stars, as opposed to being a passive cloud excited by an external source of radiation; I assume it represents some form of galaxy in a group or cluster also containing the damped Lyα cloud, and compare the properties of the companion with three possible types of galaxy: 1) Seyfert 2 galaxies, 2) radio galaxies, and 3) giant extragalactic HII regions or starburst galaxies at an early stage of star formation. The width of the Lyα emission line (FWHM $\sim$ 700km s^{-1}) is comparable to the most narrow lines seen in Seyfert 2 galaxies, and extended Lyα emission has recently been observed around high-redshift QSOs (Heckman *et al.* 1991). However, despite the presence of He II and C IV, emission lines from other high-ionization species generally seen in AGN spectra, notably NV, are absent.

Our detection exhibits line ratios and a continuum slope strikingly characteristic of high-redshift radio galaxies, such as the 3CR sample studied by McCarthy (1988). Chambers & McCarthy (1990) argue that the rest-frame UV continua of such objects match well the continua of the hottest O-type stars studied with IUE, suggesting that a major portion of the light seen in such radio galaxies is starlight. However, the present galaxy is considerably fainter than most of those sources, both in continuum and line flux, and it also does not appear in any all-sky strong radio-source surveys.

Unfortunately, CIII] λ1909, which is commonly seen in high-redshift radio galaxies, falls near a strong night sky line in our spectra and cannot be measured accurately. VLA observations are planned to address the possibility that the source is a faint radio galaxy.

Finally, I consider the hypothesis that the object is an isolated region of strong star formation, without an imbedded non-thermal radiation source. While the equivalent width of Lyα emission ($W_E \sim 140$ Å in the rest frame) is substantial, it is not outside the realm of possibility for active star formation (e.g., Elston 1988; Spinrad 1988). Of greater concern is the presence of He II and C IV, which implies an abundance of photons corresponding to the peak of a black body curve at $T > 10^5$ K; only the most massive stars, such as Wolf-Rayet's, can produce such radiation in substantial amounts. However, both C IV λ1550 and He II λ1640 are seen in absorption or with P-Cygni profiles in IUE spectra of some nearby extragalactic HII regions (e.g., Rosa et al. 1984; Hartmann et al. 1988), and other lines of C IV and He II are seen in emission from the nebulae surrounding some Wolf-Rayet's (e.g., Polcaro et al. 1991; Niemela, Heathcote & Weller 1991), indicating that a non-thermal source is not necessary for such species to exist. Furthermore, the strength of the Lyα line argues strongly against the presence of large amounts of dust, a condition that should also increase the escape probability of other line radiation in the UV. Certainly, the Lyα flux resembles the early, optimistic predictions of Partridge & Peebles (1967) more than the discouragingly low equivalent widths observed by IUE in nearby star-forming regions, including those with metallicity as low as one-tenth solar (e.g., Hartmann, Huchra, and Geller 1984; Meier & Terlevich 1981), the most likely interpretation being extremely low levels of dust.

If we assume that there is in fact negligible destruction of Lyα radiation by dust, then the observed Lyα luminosity is a direct indicator of flux of ionizing UV

photons, which can in turn be used to estimate a star formation rate, under the assumption that all the UV radiation is produced by hot stars. Assuming Case B recombination, one can expect $Ly\alpha/H\alpha \sim 10$. I then follow Kennicutt (1983), who parameterized the total star formation rate (SFR) of local spiral galaxies in terms of the total observed $H\alpha$ luminosity as $SFR(M_\odot\ yr^{-1}) \sim L(H\alpha)/10^{41}erg\ s^{-1}$, assuming a modified Miler-Scalo/Salpeter initial mass function, and find that for our observed $Ly\alpha$ flux, $SFR \sim 5-11h^{-2}M_\odot\ yr^{-1}$ for $q_0 = 0.5$ and 0.1, respectively. This rate is certainly not extraordinary; indeed it corresponds to a typical Sc galaxy in Kennicutt's sample. Of course, the calculated rate depends strongly on the adopted IMF, which must be assumed. A shallow IMF (*i.e.*, more high-mass stars), for example, will produce a stellar population with more ionizing flux and therefore more $Ly\alpha$ emission than a steep IMF or one truncated at moderate masses. However, for most reasonable IMFs the estimated SFR is unlikely to change by more than a factor of a few in either direction.

The size of the emitting region, $r \lesssim 15$ kpc, is compatible with a wide range of possible star formation scenarios seen at the current epoch, including starburt galaxies, normal late-type spirals, and giant extragalactic HII regions, as well as gas-rich dwarf irregulars.

The rest-frame UV continuum emission from the galaxy, however, is ~ 500 times brighter than NGC 2903, a luminous Sc galaxy, would appear at $z = 2.3$, assuming no evolution (Coleman, Wu, & Weedman 1980). Although the continuum signal-to-noise ratio is low ($S/N < 2$), the continuum is apparently slightly redder than a source with flat F_ν, consistent with the continuum source being starlight from a relatively young population, but not inconsistent with a non-thermal contribution. I conclude that either the object represents an ultra-luminous phase of normal galaxies familiar to us at the current epoch, a true primeval galaxy, or it is an

unusual object, such as an AGN, occupying the bright end of the emission-line galaxy luminosity function. Deep broad-band imaging of the PHL 957 field may reveal additional, fainter objects associated with the emitter and the absorbing cloud.

The companion galaxy would have been easily seen in recent "blank sky" searches for randomly distributed $Ly\alpha$ emitters, such as the one described in Chapter 2. Using these as control fields, I interpret the fact that it was discovered in association with a previously known absorption system as evidence for spatial correlation of the damped $Ly\alpha$ clouds with galaxies (and indirectly with themselves). This in turn encourages an identification of the damped $Ly\alpha$ clouds with nearby galaxies, which are known to correlate strongly on scales of a few hundred kpc. The spatial correlation further supports the hypothesis that the damped clouds are a different class of object from the low column density $Ly\alpha$ forest clouds (Lanzetta *et al.* 1991), which exhibit weak or no detectable clustering in velocity space, although they may be closely related to other metal-line systems, such as Mg II and C IV absorbers, which are known to cluster in redshift and with other objects at the same redshift (Sargent, Steidel & Boksenberg 1988; Steidel 1990; Yanny, York & Williams 1990). These issues are explored in more detail in Chapter 6.

The fact that no $Ly\alpha$ emitters similar to the one discussed here have been found in "blank sky" may have implications for the size of the damped systems. If, as Hunstead *et al.* (1990) and Tyson (1988) suggest, the damped $Ly\alpha$ clouds represent dwarf galaxies, then the known sky covering fraction ($\sim 20\%$ out to $z \sim 2.5$) implies that any field the size of our FP frames should contain many such clouds; why then is it necessary to direct our search towards a *known* damped cloud to find an associated emitter? Conversely, as Wolfe *et al.* (1991) point out, if the damped $Ly\alpha$ clouds are large disk systems, then the number density can be much lower, explaining why a

directed search is necessary to find companion galaxies.

The 3σ upper limit on emission from the damped system itself, ~ 25 times below the level of Lyα flux from the companion galaxy, suggests a low level of star formation. Following Charlot & Fall (1991) and adopting a dust-to-gas ratio $k = 0.024$, 3% the Galactic value of 0.79 (here $k \equiv 10^{21}(\tau_B/N(\mathrm{H}))\mathrm{cm}^{-2}$ with τ_B the extinction optical depth in the B band), a velocity dispersion within the cloud of 10km s^{-1}, a reddening curve similar to that in the SMC, and assuming any star-forming regions to be distributed in a plane embedded in the cloud, I estimate the attenuation of Lyα photons by dust in the damped cloud to be $\sim 90\%$; this would agree with the IUE observations by Hartmann $et\ al.$ (1988) of nearby metal-poor star-forming regions. I then derive an upper limit on star formation in the damped cloud of SFR $\lesssim 2 - 4h^{-2}\mathrm{M}_\odot$ yr^{-1} for $q_0 = 0.5$ and 0.1, respectively; in the absence of attenuation by dust, these limits would be a factor of 10 lower. This result is in contrast to the detection of strong Hβ and [O II] $\lambda3727$ emission from another damped cloud (towards Q1215+333) at a level implying a SFR~ 100 M$_\odot$ yr^{-1} (Elston $et\ al.$ 1991); clearly more observations are needed to determine which of these two scenarios is more common (although Pei, Fall, & Bechtold 1991 point out that the uncertain composition of dust in the damped systems make the Zn-Cr estimates less accurate than usually recognized, implying that the upper limit quoted here is too stringent).

The significant difference between the object probed by the QSO line of sight and the emission line region may be due to several effects. Certainly, the damped cloud is enriched to some small degree, as inferred from the presence of heavy element absorption lines, presumably due to star formation. From the lack of observed strong Lyα emission, I conclude that star formation in the damped cloud is either episodic, occurs in a strong burst that quickly decays to a much lower level, or

quickly self-enriches with dust to cloak UV radiation. The last possibility seems strongly constrained by the low levels of dust and heavy elements measured in the PHL 957 system.

Chapter 4

THE LINE OF SIGHT TO Q0836+113

4.1 Background

The line of sight towards the radio-quiet QSO Q0836+113 (z_{em} = 2.696) is both complex and controversial. The spectrum shows not only a damped Lyα system at z = 2.467, but also two Mg II absorbers at z = 0.368 and z = 0.788 and a C IV system at z = 1.822 (Turnshek *et al.* 1989). A tremendous amount of interest was generated by the report of Hunstead, Pettini, & Fletcher (1990; hereafter HPF) of a spike of Lyα emission in the black absorption trough of the damped Lyα cloud. The emission appeared to be unresolved both spatially ($<$ 2″) and spectrally ($\leq$ 60km s^{-1}) and centered perfectly in the bottom of the absorption line; total flux measured was 2.9×10^{-17}erg s^{-1}cm^{-2}, corresponding to a line luminosity $L(\mathrm{Ly}\alpha)$ = 4.8×10^{42}h^{-1}erg s^{-1} for q_0 = 0.5. Although this was not the first claim of detected emission from a damped Lyα system (Foltz, Chaffe, & Weymann 1986; Smith *et al.* 1987), it was perhaps the strongest.

Emphasizing the lack of spatial extent of the emission, HPF argued that the detection was evidence against the damped systems being large disk systems and in favor of their being analogs to nearby gas-rich dwarf galaxies instead. Interpreting

the observed luminosity as a measure of ionizing flux from hot stars, HPF applied the same comparison with Kennicutt's (1983) Hα–SFR relation as described in Chapter 3 and derived SFR $\gtrsim$ 1M$_\odot$ yr^{-1}, probably less than in the Milky Way, but sufficient to build a modest galaxy of stars in the time between then and now, $\sim$ 6.5 h^{-1} Gyr.

The result did not stand up to further scrutiny, however: Wolfe *et al.* (1991) reported that, at a high level of confidence, a deep long-slit spectrum taken at the Palomar 5 m telescope failed to confirm the presence of the emission spike. Moreover, those authors claimed a detection of a different sort: *extended* emission observed using a narrow-band (25 Å FWHM) filter centered on 4214 Å, the wavelength of redshifted Lyα for the damped system. The flux reported was extremely low, with a peak surface brightness of 2.6 $\pm$ 0.4 $\times$ 10^{-18}erg s^{-1}cm^{-2}arcsec^{-2}, and distributed in an ellipse with dimensions 6.2″ ×2.9″ oriented at $PA \simeq 15°$. The new detection corresponded to a total line luminosity $L(Ly\alpha) = 2.3 \times 10^{41}h^{-1}$erg s^{-1} for $q_0 = 0.5$, more than an order of magnitude lower than the HPF result. Wolfe *et al.* conclude that the discovery is the second direct piece of evidence supporting the disk galaxy interpretation of the damped clouds, following the result of Briggs *et al.* (1989), who found that an object of at least 8h^{-1} kpc was necessary to explain the common absorption spectra towards different parts of the extended background QSO PKS 0458 − 020.

In this chapter, I present evidence that muddies the water even more, but that may clarify matters in the end. There is some chance that even the Wolfe *et al.* detection is spurious, and at any rate needs to be followed up rigorously.

Table 4.1: Summary of Observations

Date (UT)	Telescope	Intrument	Integration (hours)	Seeing (arcsec)	Resolution (FWHM in Å)	λ Range/ Central λ (Å)
24-26 Jan 1990	KPNO 4m	GFPI+Tek2	4	1.7-2.0	20	4214
24-26 Jan 1990	KPNO 4m	GFPI+Tek2	2	2.1-2.6	30	4319
23 Mar 1990	MMT	Red Channel	3.5	1.8	13.5	3971-6815
14-15 Jan 1991	MMT	Red Channel	13	2.1	2.6	3870-4525

4.2 Observations

4.2.1 Fabry-Perot Imaging

Motivated by the result of HPF and the fact that most extended emission associated with the damped Lyα absorber towards Q0836+113 would have been missed by their long-slit spectrograph, which was not rotated with the sky during their integrations, I obtained narrow-band Fabry-Perot (FP) images of the Q0836+113 field with the GFPI at the KPNO 4 m telescope on the nights of 24-26 January 1990 (UT) using the KPNO Tek2 CCD. The etalon was tuned to 4214 Å, the wavelength of redshifted Lyα for the damped system, and the bandpass was 14 ± 3 Å (FWHM); off-band comparison images were taken at 4319 Å with bandpasses of 20 ± 5 and 30 ± 5 Å. Seven hours of total integration were obtained on-band, and two hours for each of the off-band settings; however, seeing conditions were highly variable, and three hours of on-band and two hours off-band were data were essentially useless. Only those data actually used (namely, those with seeing FWHM no worse than twice that in the best image) are shown in Table 4.1.

The data were reduced in the usual way using standard IRAF routines, and coadded to produce a final on- and off-band image, shown in Figure 4.1. The spectrophotometric standard star G191 B2B was observed for transformation from digital units to flux in units of erg $s^{-1}cm^{-2}$ above the Earth's atmosphere. The standard star images also help identify ghost reflections from the FP's internal optics; the ghost images always appear at the same orientation and with the same
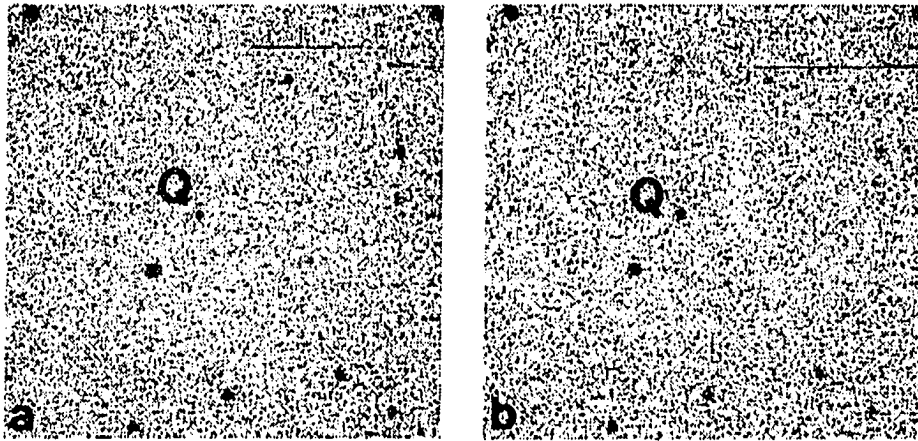
Figure 4.1: (a) Fabry-Perot CCD image of the Q0836+113 field, taken at 4214 Å, the wavelength of redshifted Lyα for the damped Lyα system at $z = 2.467$; FWHM = 20 ± 5 Å. The QSO position is labeled "Q." (b) Same as (a), but off-band; $\lambda_0 = $ 4319 Å, FWHM = 30 ± 5 Å.

intensity, usually $\sim 1\%$, relative to the source.

Comparison of the final images reveals no objects with significant excess flux in the on-band image relative to the off-band, down to the limiting flux (3σ) of $\sim 2 \times 10^{-17}$erg s^{-1}cm^{-2}. Despite the depth and breadth of the damped Lyα absorption line, some residual flux is visible at the position of the QSO in the on-band frame; however, as with PHL 957, this is easily accounted for by leakage of background QSO flux into the broad wings of the FP transmission function. The flux measured at the QSO position was $1.1 \pm 0.1 \times 10^{-16}$erg s^{-1}cm^{-2}, while convolving the etalon transmission curve with the published profile of the damped Lyα absorption line yields an expected leakage of $\sim 1 \pm 0.3 \times 10^{-16}$erg s^{-1}cm^{-2}, so any excess in our images has an associated 1σ uncertainty approximately as large as the HPF *detection*.

Additional Fabry-Perot images were obtained at 6617 Å and 6662 Å with bandpasses of 15 Å; these wavelengths correspond to redshifted C III] $\lambda1909$ for the damped Lyα system at $z = 2.467$ and redshifted [O II] $\lambda3727$ for the Mg II system at $z = 0.788$, respectively. These additional observations were intended to investigate the possibility that there is substantial star formation in the damped systems, but that Lyα is severly quenched by dust, leaving other nebular emission lines as alternatives for study; C III] is commonly seen both in planetary nebulae and in high-redshift radio galaxies. The longer wavelength integrations were planned as off-band comparisons, but the convenient placement of [O II] $\lambda3727$ from the Mg II absorber presented itself as an inviting target at the same time.

Again, no excess emission is visible in the on-band (C III]) images down to the 3σ limit for an unresolved source of $\sim 7 \times 10^{-18}$erg s^{-1}cm^{-2}. However, the off-band (for C III] from the damped Lyα system = on-band for [O II] $\lambda3727$ from the Mg II system) images revealed a patch of emission, clearly visible in each of the two

frames, separated by $3\overset{''}{.}7$ from the QSO at $PA \simeq 12°$. The emission source appears to be marginally resolved spatially, with FWHM~$2.2''$; the total flux recorded was $7 \pm 1 \times 10^{-17}$erg s^{-1}cm^{-2}. The final pair of co-added images is shown in Figure 4.2.

4.2.2 Long-Slit Spectroscopy

To confirm the hypothesis that the line emission observed with the FP in the C III] *off*-band frame was in fact redshifted [O II] λ3727 from the lower redshift Mg II system, I obtained long-slit spectra of the object with the Red Channel CCD Spectrograph at the MMT on 23 March 1990 (UT). Using a 270 1 mm^{-1} grating in first order and a blocking filter to prevent second-order light from contaminating the spectrum, I achieved a resolution with a $1\overset{''}{.}5 \times 180''$ slit of 13.5 Å over the range 3971–6815 Å. The spectral region and resolution were chosen to cover both Lyα for the damped Lyα cloud and [O II] λ3727 for the Mg II system. The slit was placed on the QSO at $PA = 15°$ for the first three 1800-sec integrations, a compromise between an early estimate of the observed positions of Wolfe *et al.*'s object and the 6661 Å emission source; but the lack of a detection immediately visible at the telescope prompted me to change to $PA = 10°$, closer to our source, for the remaining three exposures (as it turned out, the [O II] λ3727 emission was visible in all the reduced data). At a distance of $3\overset{''}{.}7$ from the QSO, the difference of 5° corresponds to $0\overset{''}{.}3$, negligible for the $1\overset{''}{.}5$ slit and the $1\overset{''}{.}8$ seeing, especially for resolved sources. The spectrophotometric standard star G191 B2B was observed through the same slit for flux transformation. The data were reduced in the usual way (as described in Chapters 3 and 4) and co-added to produce a single two-dimensional spectrum. Night sky emission was subtracted in the individual frames by fitting a low-order polynomial function to the spatial line at each wavelenght of the two-dimensional
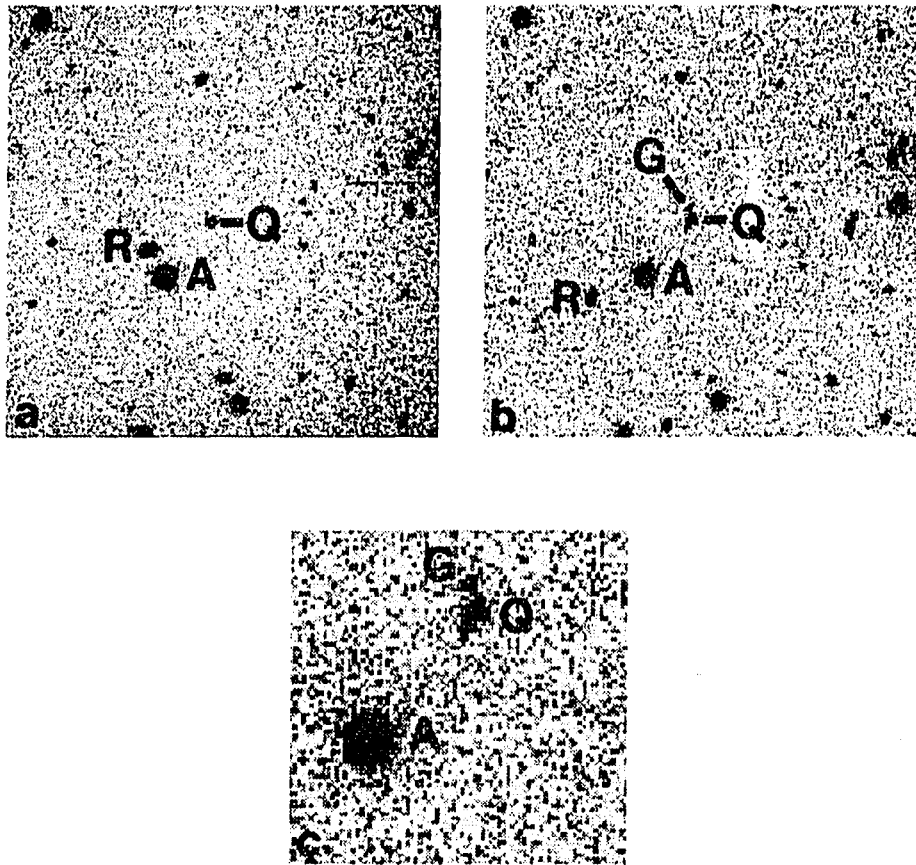
Figure 4.2: As in Figure 4.1, but for C III]λ1909. (*a*) λ_0 = 6617 Å, FWHM = 15 Å. (*b*) λ_0 = 6662Å, FWHM= 15 Å. (*c*) Expanded view of central region of (*b*). The QSO position is labeled "Q," while the [O II] λ3727 emission from the Mg II galaxy at $z_{Mg\ II}$ = 0.788 is labeled "G." Note the different pattern of reflections in the two images: the feature labelled "R" is in each case a ghost image of star A.

frame, avoiding the regions within 10 pixels of the CCD edges or the QSO spectrum, and then subtracting the fitted function from the data line.

A faint but clear source of continuum is visible at the expected separation, 4″, from the QSO spectrum. Furthermore, a strong emission line is visible at 6661 Å, the exact wavelength of redshifted [O II] $\lambda 3727$ for the Mg II system at $z = 0.788$. The continuum is visible over almost the entire spectrum (the system throughput drops rapidly towards the blue end) at an average level of $1 \pm 0.3 \times 10^{-18}$erg s^{-1}cm^{-2}Å^{-1} at 5500 Å, corresponding to $V \sim 24.0$. At the red and blue ends of the spectrum, the object's continuum brightness is estimated at $R \sim 23.4$ and $B \sim 25.4$, but due to insufficient spectral coverage, the inherent errors of slit photometry, and the low signal-to-noise ratio, these values may be in error by more than 0.5 mag. The line flux measured was $1 \pm 0.3 \times 10^{-16}$erg s^{-1}cm^{-2}, in good agreement with the value obtained from the FP observations; the observed equivalent width is then $W_{Obs} \sim 120$ Å, while in the galaxy's rest frame, $W_0 = 67$Å. A one-dimensional optimally-extracted spectrum of the object is shown in Figure 4.3.

No other emission lines are visible anywhere in the two-dimensional or the extracted spectrum, although Lyα emission at 4493Å and UV continuum from the background QSO severely contaminate the blue end. I argue that together with the perfect wavelength agreement predicted by the absorption-line redshift, this confirms the identification of the emission line as [O II] $\lambda 3727$ from the $z = 0.788$ absorber; if the emission line were Hβ at $z = 0.37$, one would expect [O II] $\lambda 3727$ at 5107 Å, or if it were [O III] $\lambda 5007$ at $z = 0.33$, one should see Hβ at 6467 Å and/or [O II] $\lambda 3727$ at 4958 Å, but none of these is seen.

The low signal-to-noise ratio near the damped Lyα line, which is due mostly to the grating blaze, precludes these image from being used to set interesting limits on emission from the damped system, or even to confirm HPF's object.
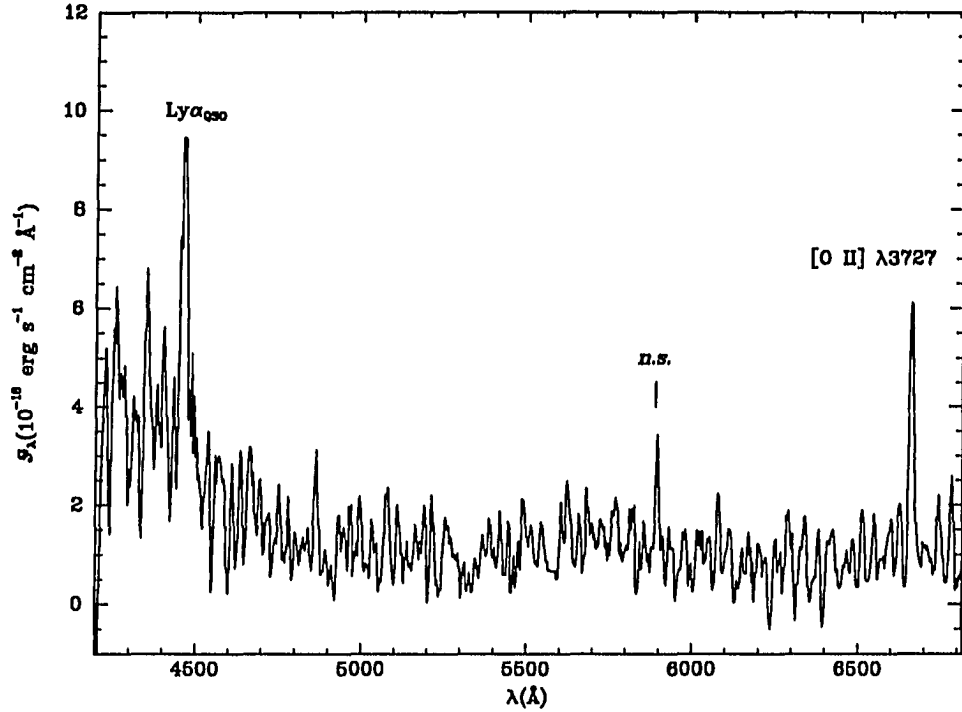
Figure 4.3: One-dimensional optimally-extracted spectrum of the Mg II absorber at $z = 0.788$ towards Q0836+113. The [O II] $\lambda 3727$ emission line is labelled; note also the background QSO's Lyα and UV emission, which contaminate the blue end of the spectrum.

Finally, on 14-15 January 1991 (UT), I obtained long-slit spectra of Q0836+113, again with the Red Channel CCD Spectrograph at the MMT, but at higher resolution: with a 1200 l mm^{-1} grating in first order with a $1\rlap.{''}5 \times 180''$ slit, the spectral FWHM near the center of the spectral range was 2.6 Å. A small amount of preflash was used before each exposure to improve the charge transfer efficiency in regions of low signal. These observations, centered spectrally on the damped Lyα absorption line at 4214 Å, were designed to test the claims both of HPF and of Wolfe *et al.* (1991).

Thirteen total hours of integration in 10 exposures were obtained over the two

nights; the seeing, as measured by the spatial FWHM of individual frames, was $2''\!.1$, and apart from some thin cirrus during the first half of the first night, clear skies prevailed. The standard star G191 B2B was observed for flux calibration, and the data were reduced, sky-subtracted, and combined as usual to form a single final frame, shown in Figure 4.4.

Due to the higher dispersion of these data, continuum emission from the Mg II galaxy was not visible above the noise.

4.3 Discussion

It is clear from Figure 4.4 that no significant emission was detected from the damped Lyα cloud towards Q0836+113. Down to what flux level is this true? A careful statistical examination of the final image, including pixel-to-pixel rms variation as well as simulated apertures containing several pixels, showed that for an unresolved source of emission with a profile matching the instrumental spatial and spectral point spread function (PSF), the 1σ flux level was $3.0 \pm 1 \times 10^{-18}$erg s^{-1}cm^{-2}; therefore the emission reported by HPF should have appeared as a 7–10σ feature in the middle of the absorption line. A portion of the one-dimensional optimally-extracted spectrum containing the damped Lyα line is shown in Figure 4.5; also shown for comparison is a simulated feature matching the flux reported by HPF.

The extended Lyα flux claimed by Wolfe *et al.* (1991) is much fainter, of course; however, faint extended sources can be easier to detect than point sources with similar surface brightness as measured in a given aperture, such as one matching the instrumental PSF. We can therefore examine the possibility that the Wolfe *et al.* flux could have been detected as follows. First let us assume that at the resolution of the January 1991 MMT data, 2.6 Å $\approx$ 200 km s^{-1} at 4214 Å, any Lyα emission line would be at most marginally resolved; this assumption is supported
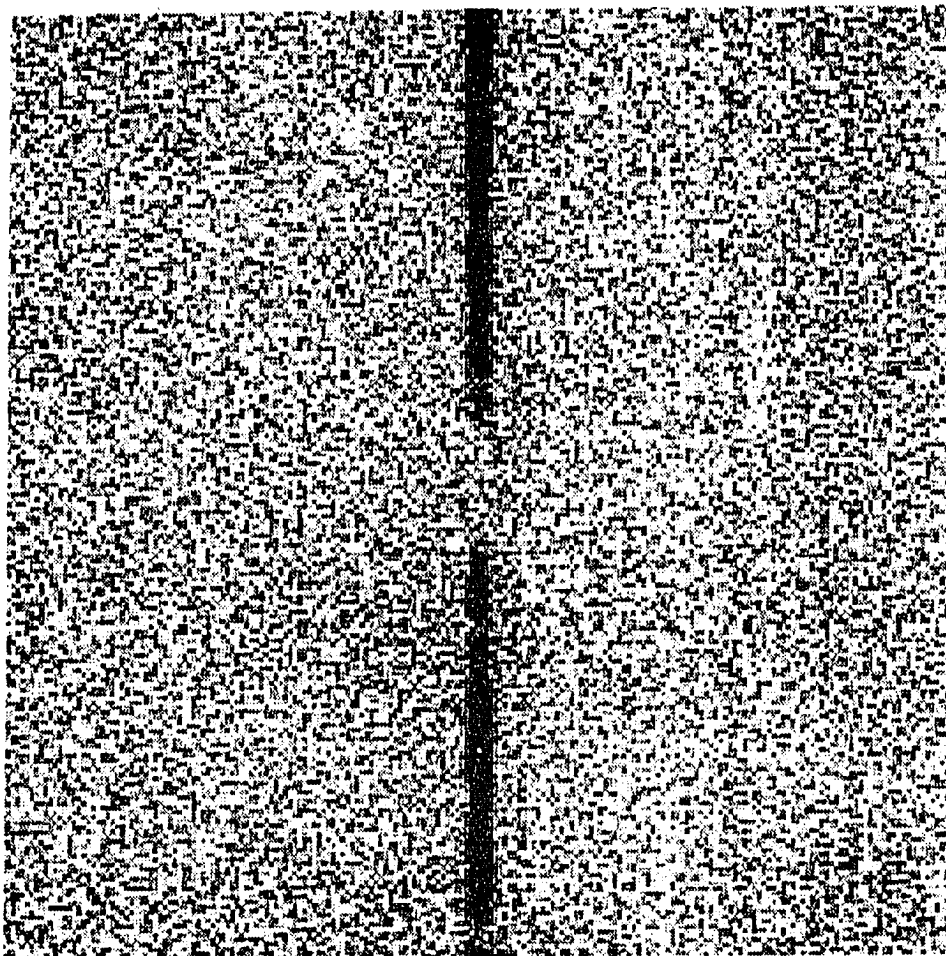
Figure 4.4: Central portion of sky-subtracted long-slit spectrum of Q0836+113, showing the damped Lyα absorption trough at $z = 2.467$. Red is up and north is approximately to the left in this image, which covers the range 4132–4296 Å at 2.6 Å resolution and shows 2$'$.0 of sky.
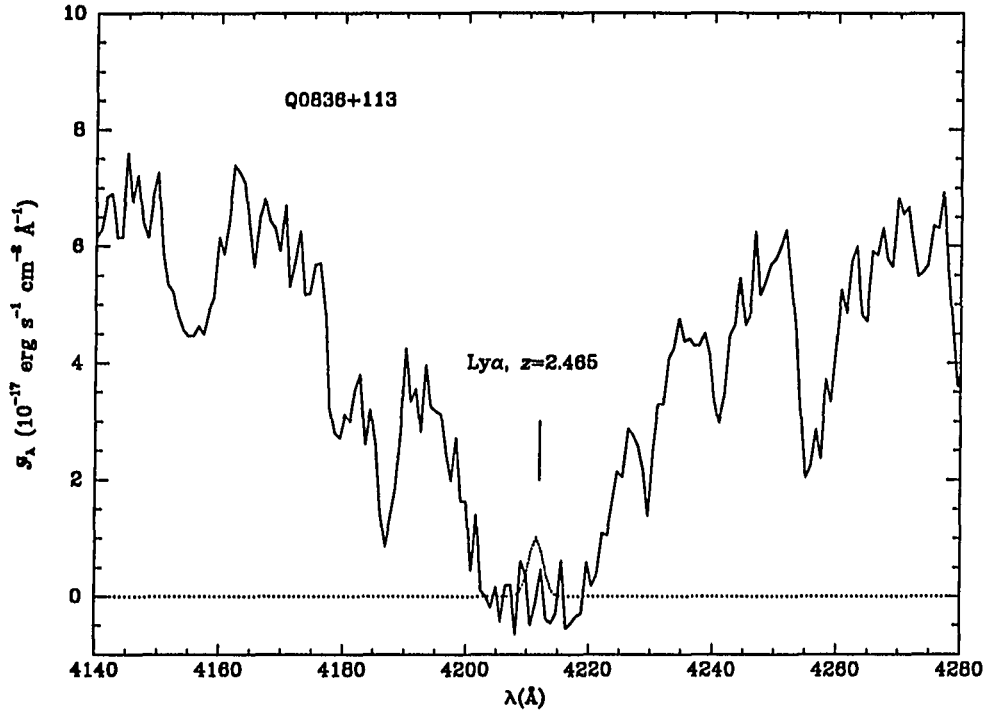
Figure 4.5: Central portion of the one-dimensional optimally-extracted spectrum of Q0836+113 showing the damped Lyα absorption line at $z = 2.467$; the dotted line represents a simulated emission line with total flux $F = 2.9 \times 10^{-17}$erg s^{-1}cm^{-2}.

by the observed widths of the metal absorption lines associated with the damped Lyα systems (although if the damped system resembles the Lyα companion galaxy described in Chapter 3, then the emission line would be considerably more dispersed). Then, assuming that approximately one half of the total emission region would be covered by the 1"5 slit, we can model the expected appearance of the source; the total flux falling on the slit would be $F = 1.4 \times 10^{-17}$erg s^{-1}cm^{-2} distributed roughly in a Gaussian of FWHM 6". Several simulated features with these parameters were placed at random positions near the damped Lyα line in the two-dimensional spectrum of Q0836; although all were detectable by blinking between the simulated and original frames, none of them would be distinguishable *a priori*

from noise fluctuations. Thus, these data are insufficiently sensitive to test Wolfe *et al.*'s claim.

Is it possible that continuum emission from the foreground Mg II system is responsible for the flux seen in Wolfe *et al.*'s narrow-band images? The continuum flux detected from the Mg II galaxy was around 1×10^{-18}erg s^{-1}cm^{-2}Å^{-1} at 5500 Å, and probably varies by no more than 25% from that level at 4200 Å. Although there is no direct evidence that the galaxy is extended in emission, it certainly contains an extended envelope of some sort; the 4″ separation at $z = 0.788$ corresponds to 16.4 h^{-1} kpc. The Mg II galaxy is thus entirely consistent with the findings of Bergeron & Boissé (1991) and Yanny, York, & Williams (1990), including its continuum and [O II] λ3727 emission as well as its minimum size.

The total flux detected by Wolfe *et al.* (1991) near the position of the Mg II galaxy in their 25 Å narrow band filter was $F = 3.9 \pm 0.5 \times 10^{-17}$erg s^{-1}cm^{-2}, over an area approximately 3″× 6″, giving an average monochromatic surface brightness $S = 9 \times 10^{-20}$erg s^{-1}cm^{-2}arcsec^{-2}Å^{-1}; they attibute $\sim 25\%$ of this to the "starlike" object C, which they identify as the Mg II system, and $\sim 75\%$ to the extended object W, supposedly the damped system. If in fact all the flux were due to continuum from the Mg II absorber, then it would need to be spread out over a patch of sky only 3″ × 4″ to match Wolfe *et al.*'s average surface brightness. I believe this is indeed the case.

The strongest argument against interpreting Wolfe *et al.*'s flux as continuum from the Mg II galaxy is that they report no extended continuum in their deep broad-band images of the Q0836+113 field, but only an unresolved feature, which they assign to the foreground system; if they had reached a spatially extended continuum level of the Mg II galaxy with their narrow-band images, they should also have reached it with their broad-band observations at about the 4σ level. Never-

theless, the position centroids relative to the QSO of Wolfe *et al.*'s Object W and the [O II] $\lambda 3727$ emission seen in the FP images agree to $0\rlap{.}''2$. The coincidental superposition of *two* emission regions from entirely unrelated absorbing galaxies along the same line of sight is improbable—one in 50 that 1 arcsec^2 sources will be superposed within a $4''$ radius circle—and all the more so that this should be the case for the *only* detection of Lyα emission from a damped system known to date. Furthermore, as mentioned above, the underlying Mg II galaxy is certainly extended on a scale of several arcseconds, so we can imagine that any emission might fall of gradually with distance from regions of intense star formation activity (Wolfe *et al.* 1991 even cite a recent image showing the Mg II galaxy to be marginally extended in continuum). However, I must conclude that I cannot rule out the identification of Wolfe *et al.*'s detection as Lyα, and moreover it is clear that confirmation will have to await 10 m-class telescopes; two entire nights of integration, or more, with 4–5 m telescopes trained on a single object begins to push the limits of current feasibility. At the very least, a spectrum showing a Lyα emission line would bring the case to a convincing close.

Finally, Wolfe *et al.* (1991) point out an additional feature in their narrow-band images, $6''$ to the southwest of the QSO line of sight, with an enhanced flux compared to the broad-band measurement; perhaps *this* is in fact the damped system! The object is too faint to appear in the FP frames, but a Lyα line could show up in a deep low-resolution spectrum.

Chapter 5

ADDITIONAL RESULTS FROM DAMPED Lyα SYSTEMS

5.1 Introduction

Few lines of sight to distant QSOs are as complicated or as well-studied as those to Q0836+113 or PHL 957; however, compelling questions about the physical nature of QSO absorption lines systems, including their sizes, ionization states, and chemical abundances, will probably be answered in a statistical way, rather than by piecemeal examination of only a few systems. Large surveys for absorbing clouds such as those carried out by Wolfe *et al.* (1986), Turnshek *et al.* (1991), Sargent, Steidel, & Boksenberg (1988; 1989), and Sargent, Boksenberg, & Steidel (1988) have contributed generously to the field not only by revealing characteristics of the absorbers such as the evolutionary effects discussed in Chapter 1, but also by providing targets for emission searches.

While the main focus of searches for emission from the damped Lyα systems has been on Lyα emission itself, the advent of arrays of sensitive IR detectors has made possible searches for other redshifted lines expected from regions of active star formation. The particular attraction of this option is that it avoids the uncertain effects that dust in the damped clouds will have on Lyα radiation; not only is the

dust content of the clouds not secure, but also the morphology of the clouds, including the distribution of any star formation regions, which would affect absorption by dust, remains unknown, making interpretation of null Lyα results difficult. Other strong emission lines normally seen in the visible, however, notably forbidden lines of O II and O III and permitted lines of the hydrogen Balmer series, suffer at most minimal reddening due to dust. Furthermore, thanks to extensive study of H II regions both in the Milky Way and in nearby galaxies, these lines are fairly well understood as diagnostics of the physical processes in star formation regions and the interstellar medium (*e.g.*, Osterbrock 1989).

In this chapter, I present the results, some of them preliminary, of a search for emission from ten damped Lyα systems. For five of these, the techniques used were similar to those discussed in the previous two chapters, including both Fabry-Perot narrow-band imaging and two-dimensional CCD spectroscopic searches for Lyα emission, but eight of the damped systems were also searched for redshifted [O II] λ3727, [O III] λ5007, Hβ, and/or Hα in the near-IR. Lyα was not detected from any of the five searched, down to levels expected for only modestly starforming, dust-free galaxies, but a tentative detection of [O II] λ3727 and Hβ from one damped cloud provides some hope for future discoveries, and the serendipitous discovery of a Mg II absorber adds to the growing body of data characterizing those absorbing clouds.

The results described below regarding Hβ and [O II] λ3727 emission from the damped cloud towards Q1215+33 have already appeared in print (Elston *et al.* 1991) and will be summarized only briefly.

5.2 Lyα Observations

5.2.1 Fabry-Perot Imaging of the Q1337+113 Field

During the same observing run at the KPNO 4 m telescope with the GFPI at which the PHL 957 and Q0836+113 (Chapters 3 and 4) fields were searched, deep images of the Q1337+113 ($z_{\rm em} = 2.92$) field were taken with the etalon tuned to 4614 Å, the wavelength of redshifted Lyα for the damped Lyα cloud at $z = 2.796$; off-band comparison images at 4319 Å were taken to verify any possible detection of line emission, and the spectrophotometric standard star G191 B2B was observed for flux transformation. The FWHM of the on-band frame was 15 ± 3Å, while for the off-band it was 28 ± 5Å. The seeing ranged from $2''.1$–$3''.6$. Six on-band integrations totalling 5.8 hours and four off-band integrations totalling 2.5 hours were obtained. As before, the pixel scale after binning 2×2 on the CCD was $0''.54$ pixel^{-1}, yielding a field of view $2'.3$ on each side.

The images were reduced in the usual way and coadded to produce two final frames, on- and off-band, shown in Figure 5.1. Visual comparison of the two images reveals no emission sources down to the 3σ limits for an unresolved source of 1.1×10^{-17}erg s^{-1}cm^{-2} in the on-band and 5.4×10^{-17}erg s^{-1}cm^{-2} in the off-band frames (as before, note that the absolute flux transformation has an associated error of around 20%, due to the uncertainty in the etalon transmission FWHM).

5.2.2 Long-Slit Spectroscopy

On two observing runs at the MMT and one at the Steward Observatory 2.3 m telescope, long-slit CCD spectra were obtained of the damped Lyα systems towards the QSOs Q1215+333 ($z_{\rm QSO} = 2.61; z_{\rm DLA} = 1.998$), Q1337+113 ($z_{\rm DLA} = 2.796$), Q1409+093 ($z_{\rm QSO} = 2.86; z_{\rm DLA} = 2.459$ and 2.670), and Q2233+131 ($z_{\rm QSO} = 3.28; z_{\rm DLA} = 3.150$). At the MMT, a 1200 l mm^{-1} grating was used in second
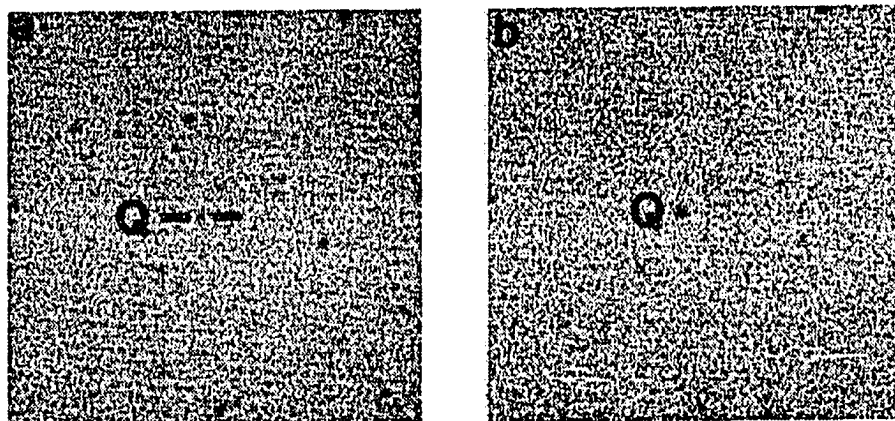
Figure 5.1: (a) Fabry-Perot CCD image of the Q1337+113 field. The QSO is labelled "Q." $\lambda_0 = 4614$ Å, the wavelength of redshifted Lyα for the damped Lyα system at $z = 2.796$; FWHM $= 15 \pm 3$ Å. North is up, east is to the left, and the field of view is $2'.3$ on each side. (b) As in (a), but off-band; $\lambda_0 = 4319$ Å and FWHM$= 28 \pm 5$ Å.

Table 5.1: Long-slit Spectroscopic Observations

QSO	Date (UT)	Tel.	z_{DLA}	Integration (sec)	θ^a	$\Delta\lambda^b$ (Å)	λ Range (Å)	PA (°)
1215+333	19 May 1991	SO	1.998	4 × 3600	2.9	1.2	3370–3944	70
1337+113	15 Jan 1991	MMT	2.796	3 × 1200	1.9	2.7	4282–4938	160
1409+093	19 May 1991	SO	2.459, 2.670 2.670	1 × 3600	2.6	1.2	4066–4639	22
2233+131	5 Jun 1991	MMT	3.150	3 × 1800	1.4	2.1	4747–5397	130

[a] Seeing FWHM in arcsec

[b] Spectral resolution FWHM in Å.

order in the Red Channel CCD Spectrograph with a $1''\!25 \times 180''$ slit for a final spectral resolution of ~ 2 Å, while at the SO 2.3 m, an 832 l mm^{-1} grating was used in first order in the Boller & Chivens Spectrograph with a $1''\!5 \times 160''$ slit to achieve a resolution of 1.15 Å; the pixel scale was $0''\!6 \times 0.82$ Å at the MMT and $1''\!6 \times 0.72$ Å at S.O. after binning the CCD twice spatially before readout (binning at the 2.3 m was due to an oversight). The 2.3 m CCD is a Texas Instruments 800×800 detector with 14 e^-pixel^{-1} rms read noise. Total integration times ranged from one hour for Q2233+13 to four hours for Q1215+33. Because the CCD in the MMT Red Channel cannot be focused uniformly along the entire spectral range, the spectrum of Q1337+113 covers only the higher redshift of the two damped systems towards that QSO. These observations are summarized in Table 5.1.

The data were reduced as usual (see Chapters 3 and 4); closeups of all four final, sky-subtracted, two-dimensional spectra in the region of the damped Lyα line are shown in Figure 5.2. The images of Q1215+33 displayed an anomalous wrinkled appearance reminiscent of fringing in the middle of the spectral range that refused to flat field properly, reducing the sensitivity somewhat. Again, no obvious emission features are seen in the final frames. A single patch of flux is faintly visible ($\sim 2\sigma$) in the trough of the damped cloud at $z = 2.459$ towards Q1409+09, but since only a single image was obtained of this object and a confirmation was impossible due to weather, I regard this as a non-detection and treat all four results as upper limits on
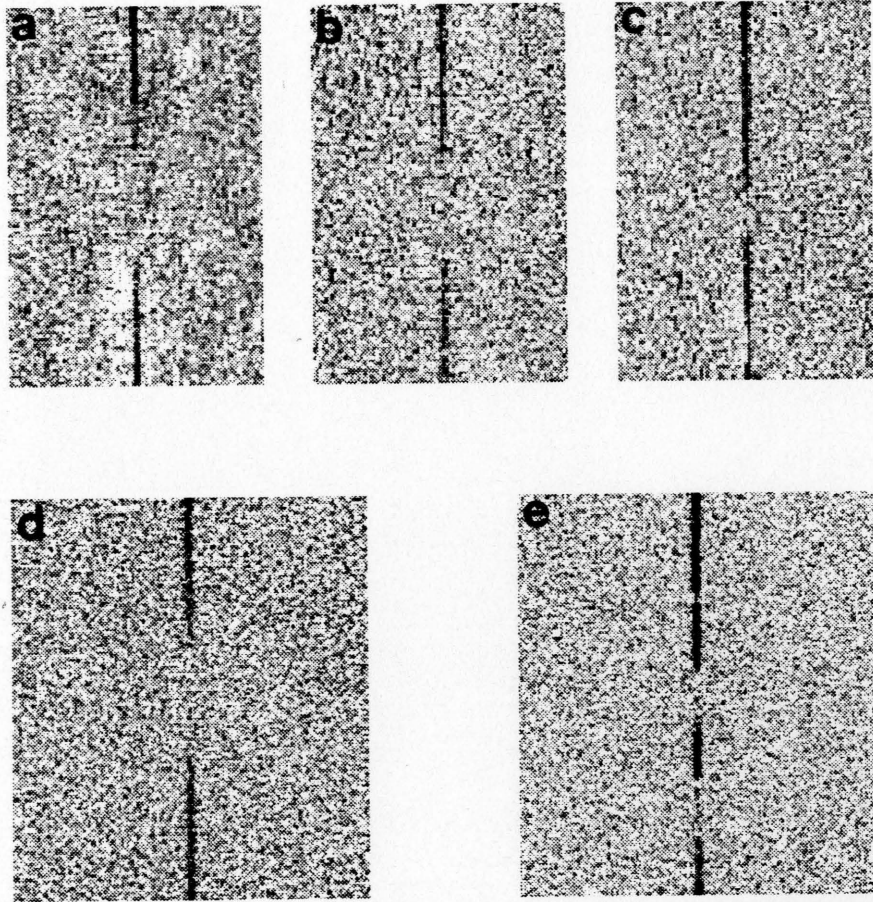
Figure 5.2: Long-slit spectra of the damped Lyα absorption clouds towards four high-redshift QSOs. Only the central region of each image is shown, centered in each case on the damped Lyα line. (*a*) Q1215+333 (*b*) Q1409+093, $z_{\text{DLA}} = 2.459$ (*c*) Q1409+093, $z_{\text{DLA}} = 2.670$ (*d*) Q1337+113 (*e*) Q2233+131. In the upper panel, the images cover $130'' \times 86$Å; the lower images show $84'' \times 131$Å.

Lyα emission from the damped clouds. These results are summarized in Table 5.3

5.3   Search for Emission Lines in the Near-Infrared

The proposed technique of this project was straightforward: obtain near-IR spectra of QSOs covering the wavelength of redshifted emission lines expected from star formation regions in known absorbing clouds. The only difference between this method and that used for spectroscopic Lyα searches, then, is the lack of a black absorption feature in which to look for emission; here, any emission line must be detectable above the underlying QSO continuum. However, this program has been plagued by problems of uncanny proportions: the MMT's building drives were disabled for one entire run by a lightning strike, the weather has ruined at least half of the observations, one of the instruments suffered a highly unusual failure, costing us the only two clear nights of another run, and a flooded river nearly swept away the other instrument, along with its principal scientist, at the start of yet another.

5.3.1   Near-IR Observations

Two IR spectrographs were used on two telescopes: the Cryogenic Spectrometer (Cryo Spec) at the KPNO 4 m telescope, and the Germanium Spectrometer (GeSpec) at the MMT. The Cryo Spec employs a two-dimensional InSb detector with 64×58 pixels and a quantum efficiency (QE) of $\sim 70\%$ at 1.5μm. At the $f/30$ Cassegrain focus of the 4 m telescope with a 300 1 mm^{-1} grating, the pixel scale is $0\overset{''}{.}97 \times 0.0018\mu$m at $\lambda = 1.2$ μm; a $2''$slit yields a resolution $R \equiv \lambda/\Delta\lambda \sim 1000$. Reading the detector elements several (e.g., 16) times non-destructively per integration limits the read noise to ~ 100 e$^-$ ADU^{-1}, which nevertheless is the dominant source of noise; dark current contributes ~ 60 e$^-$ sec^{-1}, while the thermal sky back-

ground provides $\sim 10e^-$ sec^{-1}, depending on the spectral region observed and the sky's clarity and temperature. Integrations are limited to around 600 sec by the onset of non-linearity in the detector at around 10,000 analog/digital units (ADUs). Wavelength calibration is achieved using the known wavelengths of night sky emission lines in the final image, and background sky is subtracted as with optical CCD imaging, using spatial regions flanking the object spectrum to determine the sky level as a function of wavelength.

The GeSpec consists of a pair of linear 32-pixel arrays of Germanium-doped detectors; the QE is $> 50\%$ for 0.7μm $< \lambda <1.5\mu$m. At the MMT, dual 3″ apertures separated by 22″ admit light to the spectrograph. With a 300 1 mm^{-1} grating, the pixel scale is roughly 0.0007 μm for a total coverage of ~ 0.026 μm at 1.3 μm and a resolution $R \sim 1500$. As with the Cryo Spec, the detectors are read via a non-destructive, multiple read method that reduces read noise to ~ 100 e$^-$ rms. A high-pressure Xenon lamp is used for initial wavelength calibration, while night sky emission lines are used for the final images. During each integration, the object is observed with one aperture while night sky is observed with the other; between integrations, the telescope is moved to position the object image in the alternate aperture, permitting variations in the sky emission level to be determined and subtracted. For both instrumental setups, observations of bright ($V \sim 5$) IR standard stars with spectral types close to G8 allow both flux calibration and correction for telluric absorption features.

During six observing runs in the period March 1990 – June 1991, eight damped Lyα systems were observed, including Q0836+113 and PHL 957 (=0100+130); the observations are summarized in Table 5.2. The targeted emission line in some cases depended upon the atmospheric transmission at the wavelength of interest. Given the uncertainty in the metallicities of gas in the damped systems, it is not clear

Table 5.2: Journal of Near-IR Observations

QSO	Date (UT)	Telesc.	z_{DLA}	Em. Line[a]	Integr. (sec)	λ Range (μm)
0100+130	2 Dec 1990	MMT	2.309	[O II]	$\sim$ 3600	1.22–1.24
0458−020	5 Mar 1991	MMT	2.053	Hβ	1440	1.46–1.50
0836+113	9 Mar 1990	4 m	2.467	Hβ + [O III]	—[b]	1.66–1.76
	14 Mar 1990	MMT	2.467	[O II]	—[c]	1.28–1.30
	3-4 Mar 1991	MMT	2.467	[O II]	4260	1.28–1.30
1215+333	4 Feb 1990	4 m	1.998	Hβ +[O III]	6600	1.44–1.54
	14 Mar 1990	MMT	1.998	[O II]	—[c]	1.11–1.13
	8 May 1990	MMT	1.998	[O II]	6000	1.103–1.125
	4 Dec 1990	MMT	1.998	[O II]	2700	1.110–1.131
	24 Jun 1991	4 m	1.998	Hα	6000	1.92–2.02
1337+113	5 Mar 1991	MMT	2.511	[O II]	3180	1.30–1.32
1347+112	4 Mar 1991	MMT	2.476	[O II]	4440	1.29–1.31
1409+093	3-4 Mar 1991	MMT	2.459	[O II]	4260	1.28–1.30
	24 Jun 1991	4 m	2.459	Hα	4200[d]	2.23–2.31
2233+131	24-25 Jun 1991	4 m	2.551	Hα	9000	2.29–2.37

[a]Target emission line: [O II] λ3727, [O III] λ5007, Hα, or Hβ.
[b]QSO not visible at telescope, nor detected in images.
[c]Seeing FWHM = 5''; data useless.
[d]Intermittent clouds; data useless.

which rest-frame optical line should be the strongest from a region of active star formation. In nearby spiral galaxies of low metallicity, [O III] λ5007 can be as strong as Hα, which is itself typically 3-4 times stronger than Hβ. However, in H II regions with high chemical enrichment (*e.g.*, near solar abundance), [O II] λ3727 is frequently the strongest emission line (see Dinerstein 1990 and Shields 1990 for reviews).

Due largely to the problems mentioned above, the results of this program have been for the most part inconclusive, with much of the data being too poor (*e.g.*, $F([O\ II]) < 5 \times 10^{-15}$erg s^{-1}cm^{-2}) to set useful limits on emission . However, in the case of Q1215+333, a tentative detection of [O II] λ3727 and Hβ emission from the damped Lyα cloud at $z = 1.998$ has provided some encouragement. The details are described by Elston *et al.* (1991), and here I will only summarize the results. The possible Hβ line was seen in the CryoSpec image, and GeSpec observations revealed excess flux matching the expected wavelength of redshifted [O II] λ3727. The latter detection was confirmed on two subsequent runs. If the emission lines are genuine, then they imply a star formation rate in the damped system of close to 100 M$_\odot$ yr^{-1}, far above the upper limits implied by the Lyα non-detections assuming dust-free clouds. Furthermore, the lack of an observed [O III] λ5007 line and the measured [O II]/Hβ ratio imply near-solar abundance, by analogy with local H II regions.

5.3.2 Serendipitous Discovery of a Mg II System

In order to understand better the metal abundances of the damped systems searched in the near-IR for emission lines, optical spectra of two of the QSOs, Q1215+333 and Q1409+093, were obtained at the MMT covering the spectral regions of redshifted Zn II and Cr II absorption lines expected from the damped Lyα systems towards those QSOs. These absorption lines are especially useful for determining the gas-

phase abundance of absorbing clouds, since they do not normally suffer from the effects of saturation that plague most other heavy element lines; furthermore, Cr is heavily depleted onto dust grains in the local ISM, while Zn is not, so their line ratios can be used as an indicator of dust content. The technique has been used to measure or set limits on chemical abundances in the damped Lyα clouds towards several QSOs (Meyer & York 1987; Pettini, Boksenberg, & Hunstead 1990; Meyer & Roth 1990).

The Red Channel CCD Spectrograph on the MMT was used on 5 June 1991 (UT) with a 1200 l mm^{-1} grating in first order to observe both Q1215+333 and Q1409+093. The chip was binned by a factor of two in the spatial direction to decrease read noise per unit sky area, a $1''\!.25 \times 180''$ slit was used, and the spectral regions covered were 5767–6411 Å for Q1215+333 and 6700–7341 Å for Q1409+093, with a resolution (FWHM) of 2.0 Å; three integrations of each QSO were obtained in excellent seeing (images from a single MMT mirror yielded $0''\!.5$ images; the grand total was $1''\!.2$) for totals of 120 and 100 minutes, respectively. The slit was placed at $PA = 90°$ for Q1215+333 and at $PA = 55°$ for Q1409+093.

Although analysis of the absorption line data is still underway, a surprising discovery emerged from the final, coadded image of Q1215+333: a faint line of continuum is visible displaced $6''$ to the east of the QSO spectrum, with two faint emission lines at 6045 ± 1 Å and 6234 ± 1 Å (see Figure 5.3). These lines match the wavelengths of redshifted Hβ and [O III] $\lambda5007$, respectively, for $z = 0.245$. To confirm this tentative identification, I examined the blue spectrum of Q1215+333 obtained at the SO 2.3 m telescope (§ 5.2.2) for possible absorption lines due to an extended halo around the emission line galaxy. Figure 5.4 shows expanded plots of this spectrum in the region of three absorption lines that match the expected wavelengths of redshifted Mg II $\lambda\lambda2795.528$, 2802.705 and Mg I $\lambda2852.126$. The
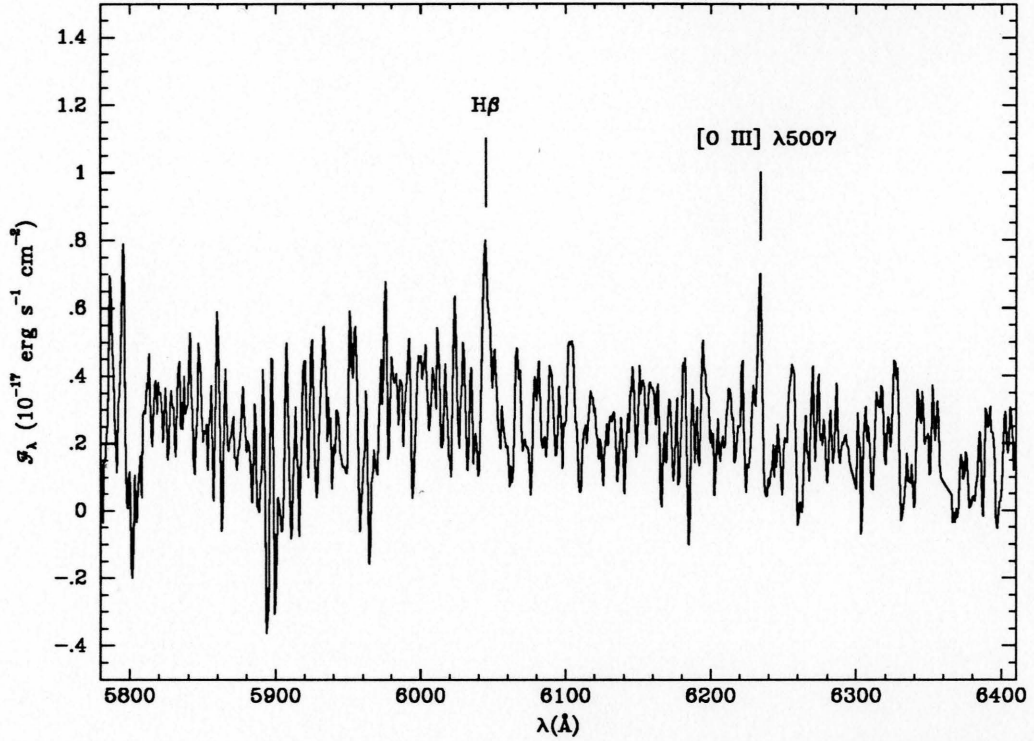
Figure 5.3: One-dimensional extracted spectrum of the probable Mg II absorbing galaxy at $z = 0.245$ towards Q1215+333. The spectrum has been boxcar-smoothed by 3 pixels to reduce the noise.

respective observed equivalent widths were 3.0, 0.8, and 2.2 Å, but the errors are probably of order 1 Å. If these lines are genuine, then this is probably the first Mg II absorber discovered serendipitously by its emission! The absorber would have escaped detection in previous searches that included Q1215+333 due to its low redshift.

The continuum level is $AB(6090\text{Å}) \sim 22.6$, and the H$\beta$ and [O III] λ5007 fluxes are $\sim 3 \times 10^{-17}$erg s^{-1}cm^{-2} and 1.7×10^{-17}erg s^{-1}cm^{-2}, respectively, making this object comparable to the Mg II galaxies observed in emission by Bergeron (1988) and Yanny *et al.* (1990). In the present case, assuming the identification is correct, we can use the observed Hβ flux in the same way Lyα was used previously to
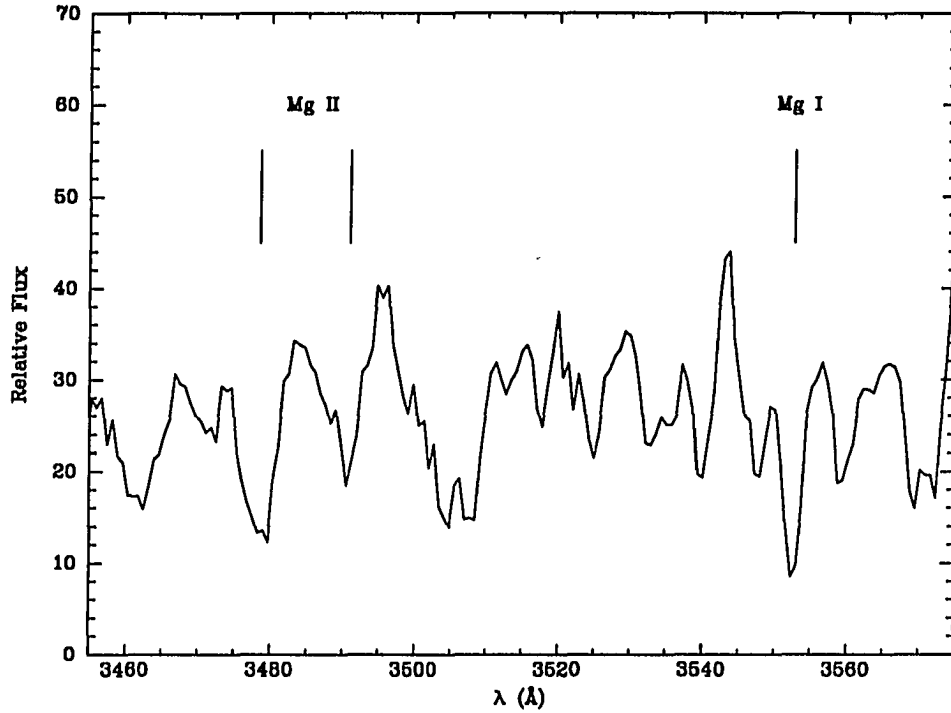
Figure 5.4: Detail of the spectrum of Q1215+333 taken at the Steward Observatory 2.3 m telescope. Absorption lines tentatively ascribed to heavy elements in an absorbing galaxy at $z = 0.245$ are indicated. The spectrum has been boxcar-smoothed by 3 pixels to reduce the noise.

measure the ionizing flux and therefore a star formation rate, assuming an IMF. The measured $H\beta$ flux corresponds at $z = 0.245$ to a luminosity $L(H\beta) = 2.2 \times 10^{39} h^{-1} \text{erg s}^{-1}$ for $q_0 = 0.5$. As before, if we assume a nominal Case B recombination value of $H\alpha/H\beta \sim 3$, and then modify Kennicutt's (1983) $H\alpha$-SFR relation to read $\text{SFR}(M_\odot \text{ yr}^{-1}) \approx L(H\beta)/3 \times 10^{30} \text{erg s}^{-1}$ for Kennicutt's IMF, then we obtain for the Mg II galaxy SFR $\sim 0.7 \ M_\odot \text{ yr}^{-1}$, a modest amount compared to the SFRs observed in nearby spiral galaxies today. This value is also lower than in the bulk of the objects observed by Yanny *et al.* (1990); perhaps this should not surprise us, considering the galaxy's low redshift, if the trend of increased star formation activity

at $z > 0.5$ is genuine. Indeed, some Mg II systems have completely undetectable levels of emission.

5.4   Discussion

Apart from the possible near-IR emission from the damped system towards Q1215+333 (and the serendipitous Mg II galaxy), none of the observations described above has resulted in positive detections. The best limits on [O II] λ3727 are for the PHL 957 absorber, which must have an [O II] flux $F < 4 \times 10^{-16}$erg s^{-1}cm^{-2}. Limits on [O II] emission from the Q0836+113, Q1337+113, Q1347+112, and Q1409+093 damped clouds are less strong, but all on the order of $F < 1 \times 10^{-15}$erg s^{-1}cm^{-2}; these results may improve somewhat in the near future. Furthermore, there is a hint of emission at the wavelength of redshifted Hα for the damped system towards Q2233+131, offset from the QSO position by 2″, but confirmation is needed. The results for all the damped systems studied for which usable data were obtained, including Q0836+113 and PHL 957, are summarized in Table 5.3.

The non-detection of Lyα from the damped cloud at $z = 2.796$ towards Q1337+113 implies $SFR < 1$–$4h^{-2}$M$_\odot$ yr^{-1} for the imaging and spectroscopic results, respectively, assuming no dust. However, dust may indeed be present; although Lanzetta, Wolfe, & Turnshek (1989) set limits on the dust abundance of about one third the Galactic value, based on the observed lack of H$_2$ absorption, and there is no evidence for selective dust absorption bands, those authors nevertheless conclude that the overall metallicity in the damped system is consistent with values ranging from 1/100 to 1 times the solar value. It is difficult to contrive a scenario in which chemical enrichment advances unaccompanied by the formation of dust; therefore we must treat the upper limit on Lyα emission with some care, since it may be heavily extinguished.

Table 5.3: Summary of 3σ Upper Limits and Detections[a]

QSO	z_{DLA}	Lyα Spect.[b]	FP[c]	[O II]	Hβ	[O III]	Hα
0100+130	2.309	2.0	7.5	40	...	...	...
0836+113	2.467	0.9	1.8	50	...	...	...
1215+333	1.998	6.3	...	$(160)^d$	$(76)^d$	60	500
1337+113	2.511	...	...	50	...	...	...
	2.796	4.4	1.1	...	...	...	...
1347+112	2.476	...	...	50	...	...	...
1409+093	2.459	5	...	60	...	...	500
	2.670	5	...	...	...	...	...
2233+131	2.551	...	...	...	...	...	100
	3.150	2.4	...	...	...	...	...

[a]All fluxes in units of 10^{-17}erg s^{-1}cm^{-2}.
[b]Limit on unresolved Lyα emission from two-dimensional spectroscopy.
[c]Limit on unresolved Lyα emission from Fabry-Perot imaging.
[d]Level of detected flux.

If we assume that the detection of [O II] $\lambda3727$ and Hβ from the Q1215+333 damped cloud is real, then we should ask whether it is an anomalously bright, active object. The upper limits on redshifted optical nebular lines from the remainder of the sample are in general consistent with the flux expected from several tens of $M_\odot$ yr^{-1}; if [O II]/H$\beta\sim$ 5, as observed in local H II regions with near solar metallicity, then an observed [O II] $\lambda3727$ flux of 5×10^{-16}erg s^{-1}cm^{-2} from an absorber at $z \approx 2$ implies $SFR \approx 50$ $M_\odot$ yr^{-1}, assuming as before the Kennicutt (1983) IMF. It then appears plausible that the Q1215+333 system occupies the high end of the emission-line galaxy luminosity function, but that substantial star formation rates at $z = 2 - 3$ are permitted in the damped Lyα clouds, consistent with a wide variety of scenarios for the origin of the absorption lines, including dwarf irregular galaxies (e.g., York et al. 1986).

Do the Lyα limits severely constrain this scenario in a statistical way? The answer depends critically on the dust content of the damped systems. Several

lines of evidence seem to favor an average ratio of dust to gas on the order of one tenth the local Galactic value. As mentioned above, no selective absorption due to Galactic-type dust is seen by Lanzetta *et al.* in the spectrum of Q1337+113 (1989), a result supported by Pei, Fall, & Bechtold (1991; hereafter PFB), who find no sign of extinction at 2175 Å, a strong Galactic dust feature, in the rest frames of several damped systems. However, other kinds of dust are not excluded, *e.g.*, similar to that seen in the Magellanic Clouds, and PFB do present convincing evidence for consistent reddening of background QSOs by foreground damped Lyα clouds; their best estimates of the typical dust-to-gas ratios in the damped systems range from 5–20%. Several authors (Meyer & Roth 1990; Pettini, Boksenberg, & Hunstead 1990) have adopted a different method, studying absorption lines of Ni II, Cr II, and Zn II, as mentioned above, to determine if Cr and Ni have been depleted onto dust grains as they have in the Milky Way. Furthermore, in one case (the absorber at $z = 2.076$ towards Q2206$-$199), examination of additional metal lines, including O I, Si II, and Si IV, yields an extremely low metallicity, [Si/H]$\sim$ -2.8 *i.e.*, less than 1/100th solar (Rauch *et al.* 1990). While measuring the gas-phase abundances of heavy elements has yielded metallicities and dust abundances consistent with the statistical reddening method, PFB caution that the unknown dust composition and, perhaps, different abundance ratios from those seen in the Galaxy make the Ni-Cr-Zn measurements less dependable than they are when applied locally, and they argue that the observed gas-phase abundances are in fact compatible with somewhat higher *total* metallicities and dust levels than usually quoted.

In summary, then, strong evidence has accrued that the average abundance and dust content in the damped systems is on the order of 1/10th the Galactic value, though large deviations are possible. As discussed in Chapter 2, such levels of dust can attenuate Lyα radiation by more than a factor of 100, depending on

the distribution of the stars producing the ionizing radiation, the column density of neutral hydrogen, and the angle of inclination to the observer, if the cloud is disk-shaped. On the other hand, a more empirical comparison with local metal-poor galaxies indicates that this may be a pessimistic view: Lyα emission is seen at about 1/10th the Case B recombination level, judging from observed Hα and Hβ fluxes, from galaxies with metal abundances about 0.1 times the solar value (Deharveng, Joubert, & Kunth 1986; Meier & Terlevich 1981; Hartmann et $al.$ 1988). It therefore seems unlikely that there is sufficient dust to quench Lyα by more than a factor of 10 in all the damped systems searched for Lyα emission to date; the more likely explanation for the non-detections is a general lack of strong star formation. Taking a nominal 3σ upper limit of $F(\text{Ly}\alpha) = 4 \times 10^{-17} \text{erg s}^{-1}\text{cm}^{-2}$ and assuming an average dust extinction of 10 times at $z = 2$, the implied Lyα luminosity is $L(\text{Ly}\alpha) = 2.8 \times 10^{42} h^{-2}\text{erg s}^{-1}$, corresponding to an upper limit on star formation in the average damped Lyα cloud assuming the Kennicutt IMF of $SFR \lesssim 3$ M$_\odot$ yr^{-1}. This level is roughly consistent with the possible detection of Wolfe et $al.$ (1991) for the absorber towards Q0836+113 if that cloud has average dust levels, but is ~ 30 times lower than for the Q1215+333 system; the latter must indeed be anomalous. Furthermore, it seems unlikely that while Mg II systems are seen to redshifts $z > 1.5$ with $SFR < 10$ M$_\odot$ yr^{-1}, there would be otherwise comparable objects, the damped Lyα systems, at $z \approx 2$ with average star formation rates ten times higher.

As mentioned in Chapter 3, the conversion from Lyα flux to star formation rate depends heavily on the assumed IMF. Our interpretations of the SFRs in high-redshift galaxies are generally cast in the paradigm of local galaxies and star-forming regions, but these may be misleading assumptions. A top-heavy or a truncated IMF can produce widely varying amounts of ionizing UV flux, and metallicity also comes

into play in the form of line-blanketing, so the limits on Lyα emission must be taken with a grain of salt. In general, however, the various factors conspire to make the present limits conservative rather than unreasonable.

One final explanation for the observed lack of strong Lyα emission hinges on the possibility of clumpiness in the damped clouds, perhaps analogous to the Milky Way, where $N(H)$ varies by over an order of magnitude (Burstein & Heiles 1982) and where star formation is presumed to originate in dense molecular clouds, rather than uniformly across the entire disk. Such sites of star formation may pollute themselves quickly with metals and dust, even if the original abundances are primordial, possibly reaching 0.5 times solar metallicity by 5×10^6 yrs after the onset of star formation (Lequeux et $al.$ 1981), while mixing with other regions in the same galaxy may take place on timescales long compared to the lifetimes of massive stars (Kunth & Sargent 1986), producing an inhomogeneous ISM in the short term. While dust production is frequently thought to occur in the asymptotic giant branch (AGB) phase of post-main sequence stellar evolution, it is also observed to form in supernova explosions, which could have a large effect on the ISM in sites of recent massive star formation. The sight lines to background QSOs therefore may preferentially sample the thinner, less enriched medium rather than the dense clouds supporting massive star formation, possibly resulting in underestimates of the chemical abundances in the dense clouds; meanwhile, if self-enrichment with dust in these clouds progresses at a reasonable rate, then any Lyα-bright phase may last only a fraction of the lifetime of massive stars, thus escaping detection unless the absorber is observed just at the onset of star formation.

This scenario may help explain why at high redshift, most searches for Lyα emission have resulted either in strong detections, such as radio galaxies (which are probably more complicated, of course) and the companion to the damped system

towards PHL 957, or no detections, such as the blank sky searches and the bulk of the damped Lyα systems. If the extended Lyα emission from the Q0836+113 absorber is genuine, then it may represent a later, post-Lyα-bright stage of enrichment; perhaps all the damped clouds glow in Lyα at a similar level.

The damped Lyα systems, while certainly much less evolved than any normal disk or dwarf galaxies familiar to us today, are therefore not true primeval galaxies; they are chemically enriched to some albeit small degree, and they do not seem as a class of object to display the high star formation rates once thought to be the signature of PGs. However, as they may in fact harbor regions of star formation processing a few solar masses per year of gas into stars, it is possible that their current SFRs are similar to their lifetime averages: 5 $M_\odot$ yr^{-1} is sufficient to process a galaxy-sized mass of gas into stars between $z = 2.5$ and $z = 1$.

Chapter 6

CONCLUDING REMARKS ON GALAXIES AT HIGH REDSHIFT

Based on the upper limits of the blank sky search presented in Chapter 2 and the meager positive results from the damped Lyα systems, we can see that galaxy formation in general is probably not accurately described by the more spectacular models discussed in Chapter 1, such as the early non-dissipational "top down" collapse model of Partridge & Peebles (1967) or the Lyα-inflation picture of Cox (1985). Even the more recent, conservative scenarios incorporating cold dark matter (*e.g.*, Baron & White 1987) predict typical L$_*$ galaxies to appear at detectable luminosities at the redshift of greatest star formation rate, although the predicted number density of such objects is too low for the blank sky Lyα search to rule out. For the latter technique, Lyα extinction by dust remains a possible problem that only the deep broad-band galaxy count surveys or additional near-IR observations can circumvent.

Nevertheless, evidence for evolution of galaxies between z =1–4 and the present continues to accrue. The galaxy counts indicate an excess of faint galaxies compared to extrapolations of the local luminosity function, requiring number evolution, lumi-

nosity evolution, or a combination of the two; however, the bulk of the faint galaxy population lies at unknown redshift, complicating their interpretation. Assuming a galactic origin for the QSO heavy-element absorption line clouds, time evolution is apparent in the form of changing number density, ionization, and/or chemical enrichment, and the damped Lyα systems, with 5–10 times higher total absorption cross section at $z \sim 2.5$ than galaxies today, must have evaporated or condensed, or else converted large fractions of their gas to stars in disk galaxies, an explanation championed by Wolfe *et al.* (1986).

In Chapters 3 and 4, I verified that Fabry-Perot imaging is a valuable tool for identifying galaxies at high redshift. While the upper limits on Lyα emission from the damped Lyα systems themselves are complicated by the dust issue, the detection of [O II] $\lambda 3727$ from the Mg II system at $z = 2.788$ towards Q0836+113 remains unambiguous (although the line of sight is more complex than ever), and the Lyα companion to the PHL 957 damped cloud is perhaps the most promising candidate for a PG yet found.

The Lyα companion galaxy at $z = 2.3$ also demonstrates a fundamental property of the damped clouds not yet realized from the sparse absorption line statistics: the damped Lyα absorbers, unlike the Lyα forest clouds, are probably spatially correlated at high redshift with objects resembling galaxies. The comoving volume searched by each FP frame is calculated from the standard equation (*e.g.*, Weedman 1988)

$$dV = 3.3 \times 10^{13}(1 + z)^{-3.5}[(1 + z) - (1 + z)^{1/2}]^2 dz \ h^{-3}\text{Mpc}^3\text{deg}^{-2} \qquad (6.1)$$

($q_0 = 0.5$ used throughout), which yields a total volume searched for Lyα emission at the absorber redshift (on-band) $V_{\text{on}} = 78 \ h^{-3}\text{Mpc}^3$; the volume searched at redshifts different from known damped systems (off-band) is $V_{\text{off}} = 106 \ h^{-3}\text{Mpc}^3$, giving a total volume observed $V_{\text{tot}} = 184 \ h^{-3}\text{Mpc}^3$. In theory, the long-slit blank sky search

could also be included, but since the different redshifts covered require assumptions about the evolution of sources and the volumes searched are small compared to the FP "control fields," I choose not to use them here.

Given the velocity proximity of the companion galaxy to the absorber, let us assume for the moment that the projected separation of 0.63 h^{-1}comoving Mpc is the true separation; the minimum volume containing the companion is then $1.04h^{-3}$Mpc^3, so the probability of finding the companion in the volume observed if similar Lyα emitters were distributed randomly would be 1 in 179. However, since we have only one detection, small number statistics dominate, and so this estimate can be misleading.

A more interesting result is obtained if we consider the tremendous volume of blank sky ($V \approx 9000h^{-3}$ comoving Mpc^3 for $q_0 = 0.5$) searched by Pritchett & Hartwick (1990), who would have detected the Lyα companion galaxy had it fallen in any of their 24 fields. We can then estimate a more formal spatial cross-correlation function $\xi(r)$ for the damped clouds with Lyα emission galaxies, defined by

$$\rho_{em}(r)dV = \rho_{ran}[1 + \xi(r)]dV. \tag{6.2}$$

Here, $\rho_{em}(r)dV$ is the number of Lyα emitters (one, in this case) comparable to the companion galaxy observed at distance r from the absorber within a search volume element dV, and ρ_{ran} is the density of randomly distributed Lyα galaxies, on which the Pritchett & Hartwick search sets an upper limit; for significant clustering on a scale r, we expect $\xi(r) > 0$, so $\xi(r)$ represents the overdensity of emitters near absorbers averaged out to the extent of our images. The average space density of emitters associated with damped systems is then $\rho_{em}(r) = 1/V_{on} = 1.28 \times 10^{-2}h^3$Mpc^{-3}; if we assume a Poisson distribution, then the 95% confidence interval is $6.4 \times 10^{-4} < \rho_{em} < 5.8 \times 10^{-2}$. The 95% confidence upper limit on the mean density of *randomly* distributed Lyα emitters comparable to our
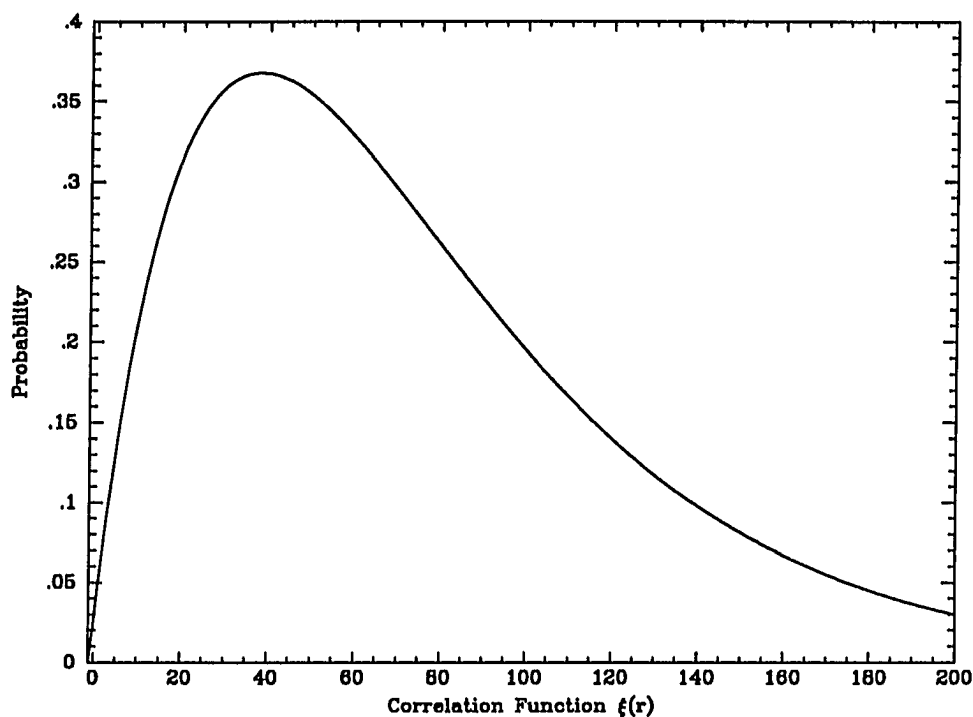
Figure 6.1: The likelihood function for the strength of the damped $Ly\alpha$ cloud—galaxy correlation function ξ is shown as a function of ξ. Note that the probability drops below 5% for $\xi > 0$, indicating a positive detection of clustering.

detection, meanwhile, again assuming a Poisson distribution, is 3.00 objects per random volume searched, or $\rho_{ran} < 3.3 \times 10^{-4}$ $h^3\text{Mpc}^{-3}$. The best estimate of the lower limit to the damped $Ly\alpha$ absorber to $Ly\alpha$ emitter cross-correlation function, then, is $\xi(.2\text{Mpc}) \geq 37.9$, while the 95% confidence interval for $\rho_{em}(r)$ yields $0.95 < \xi(.2\text{Mpc}) < 174.6$, a clear detection of clustering. The likelihood function for the lower limit to ξ is shown in Figure 6.1.

To compare the estimate of the damped $Ly\alpha$ cloud—galaxy correlation strength with the degree of clustering measured for more local objects, I will follow the convential formalism (*e.g.*, Ellingson, Yee, & Green 1991) by normalizing the QSO—galaxy spatial covariance function such that $\xi(r) = Br^{-\gamma}$, with $\gamma = 1.77$ as cali-

brated from previous studies of local galaxy—galaxy clustering, and where B is the spatial covariance amplitude (*e.g.*, values of B_{gg} for Abell richness class 0 and 1 are found to be 360 and 645, respectively [Prestage & Peacock 1988]). As Ellingson *et al.* point out, such a parameterization makes several assumptions about the distribution and luminosity function of sources, but lacking further information we must accept those assumptions for the purpose of comparison. The 95% confidence lower limit on B for the damped cloud—Lyα emitter correlation, then, is $B_{min} = 16.7$, while folding in the additional 95% confidence envelope from the estimate of $\rho_{em}(r)$ yields $0.42 < B_{min} < 76.9$. By comparison, Yee & Green (1984) find $\langle B_{gq}\rangle = 186.3 \pm 38.6$ for galaxies near QSOs between redshifts 0.05 and 2.05, while based on the results of Davis & Peebles (1983) they find $\langle B_{gg}\rangle = 67.5 \pm 6.8$ for galaxies correlated with other galaxies in the more local CfA redshift survey. Therefore the most likely lower limit on the strength of clustering of Lyα emitters with damped Lyα clouds corresponds to only weak clustering by local standards, but clearly, additional detections (such as the possible Lyα galaxy reported by Turnshek *et al.* 1991) will refine this estimate. Nevertheless, the significance of even this one object is that it demonstrates a prediliction of the damped clouds to lie near other galaxies. Additional FP observations are planned to increase the number of damped Lyα system fields surveyed.

The metallicities and dust content of high-redshift galaxies remains an important question. Only an unambiguous detection of an unreddened spectral line, such as those sought in the near-IR (Chapter 5), coupled with a detection or very stringent upper limit on Lyα emission, can resolve the issue. Curiously, preliminary results from a similar program to study high-redshift radio galaxies (Elston 1991) reveal nearly Case B recombination Lyα/Hα line ratios, indicating little or no extinction by dust. Of course, these represent unusual objects whose star formation properties,

ages, and dynamics remain poorly understand, so comparison to QSO absorption clouds and PGs may be risky.

In conclusion, it is obvious that the universe of galaxies at $1 < z < 3$ was significantly different than it is at the present. There are several reasons to believe that that epoch was one of enhanced star formation and the early stages of chemical enrichment, as well perhaps as the gravitational collapse of gas and dark matter that produced objects familiar to us as galaxies today. Much exciting work lies ahead to fill in the gaps between absorbers and emitters, between AGNs and normal galaxies, and between the redshift of galaxy formation and $z = 0$.

Appendix A

The Goddard Fabry-Perot Imager

The Goddard Fabry-Perot Imager (GFPI or FP), developed at NASA/Goddard Space Flight Center, is a tuneable narrow-band CCD imaging system designed for use at a variety of astronomical telescopes. Spectral coverage is complete from 4000–8000 Å, spectral resolution (FWHM) is variable from $\sim$ 200–1500 km s^{-1} and total throughput (atmosphere + telescope + instrument + detector) varies from $\sim$ 3% to 16% depending on λ and resolution. There are three etalons available, called blue, red, and visible. The blue etalon covers the spectral range 4000–6000 Å with a resolution (FWHM) at Hβ of 3–6 Å; the red covers 5400–7500 Å with a resolution at Hα of 7-12 Å; and the visible covers 4000-7800 Å with a resolution at Hα of 15–30 Å. The relatively low resolution was designed with faint emission line searches in mind, rather than velocity mapping of bright objects, although of course sources with a large velocity spread, e.g., supernova remnants, can be mapped in velocity space. Unlike other FP's, this instrument images only the central interference order onto the CCD, so the field is usually monochromatic, i.e., it varies typically by only a fraction of a spectral FWHM from corner to corner.

The optical train consists of a field lens and collimator that accepts up to an $f/6$ beam from the telescope (see Table A.1 and Figure A.1), followed by the etalon, blocking filters (conventional narrow band) that select a single interference order

Demagnification from focal plane to CCD: 1.5

Focal Length of camera lens: 200 mm

Fastest acceptable beam for no vignetting: $f/6$

| Telescope	FOV (arcmin)	Scale (arcsec/pixel)
KPNO 4 m	2.3	.26
KPNO 2.1 m	4.3	.51
Steward 2.3 m	3.5	.41
Steward 1.5 m	3.5	.41
MDM 1.3 m	7.3	.86
MDM 2.4 m	4.0	.47

Table A.1: Field of view and pixel scale for Tektronix 512×512 CCD

from the many orders transmitted by the etalon, re-imaging optics (a telephoto camera lens), and finally the CCD. Blocking filters are spaced every 100 Å, have a typical FWHM of 120 Å, and cover the entire range of the etalons.

The etalons of the FP, manufactured by Queensgate Ltd., are held parallel to $\sim \lambda/200$ by a feedback system of capacitors that sense the separation of the two reflective plates and piezo-electric drivers that maintain their position. Wavelength calibration is achieved with the use of "penray" He, Ne, Ar, Kr, or Hg high pressure lamps; wavelength stability is held to a fraction of a FWHM by thermal control of the instrument to within 0.5° C.

The CCD, which is used on all telescopes except those at KPNO, in which case a KPNO CCD is used, is a Tektronix 512 × 512, thinned, ion-implanted device with 80% quantum efficiency (QE) at 7000 Å and 55% at 4000 Å. Read noise is 6 electrons pixel^{-1} rms, and on-chip binning can be used to reduce the read noise per unit sky area. The CCD resides in a liquid nitrogen-cooled Photometrics dewar and is controlled by Photometrics electronics.

The entire instrument, including etalons, CCD, and the filter wheel, is controlled
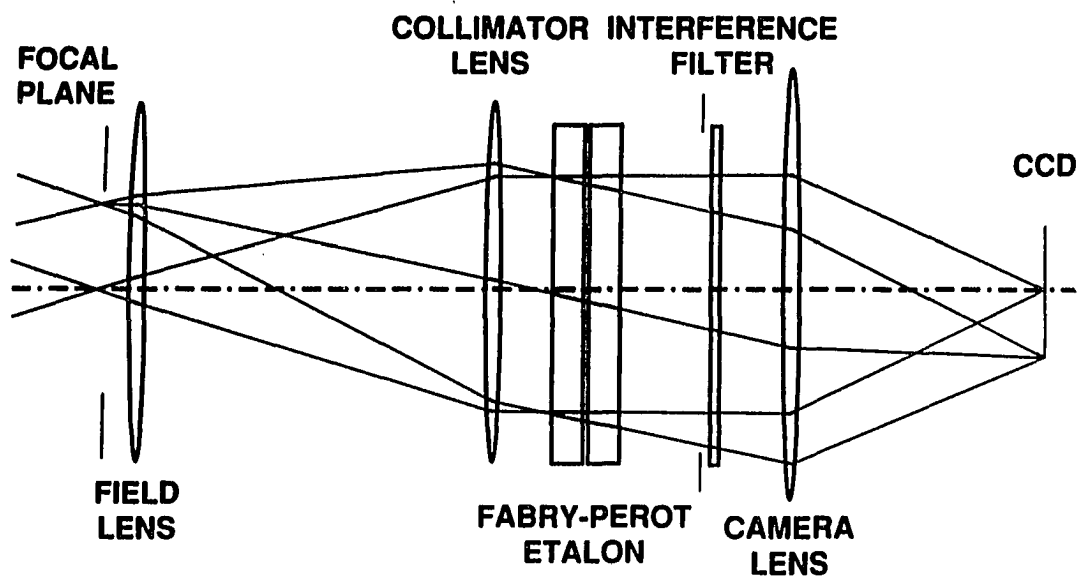
Figure A.1: Optical layout of the Fabry-Perot

by a MicroVax II computer, which also stores the images (except when using a KPNO CCD). Data can be archived on hard disks, TK50 magnetic tapes, and/or an eraseable optical disk.

Rough parallelism of the etalon plates is achieved by eye before installation. Spectral line radiation from neon lamps is examined through the etalon, and the piezo-electric driver voltages are adjusted until the neon interference rings are observed to be stable and symmetrical. Alignment with the instrument's optical axis is achieved via autocollimation with the help of an LED mounted at the optical axis on a removable slide at the focal plane; the collimator sends a parallel light beam from the LED to the etalon, which reflects the light back through the collimator to the focal plane slide. The etalon is tilted using spring-mounted adjusting screws until the focussed image of the LED is coincident with the LED itself. Finally, with the etalon mounted and under computer control, fine adjustment of the etalon's parallelism is adjusted by scanning repeatedly across a spectral line, wedging the plates slightly between scans, and searching for the plate orientation that minimizes the FWHM transmission function.

The variable resolution at any given wavelength is controlled by changing the base etalon spacing, which in turn selects a different interference order (larger gap = higher order = higher resolution, $i.e.$, smaller FWHM; see Figures A.2 and A.3). The desired wavelength of transmission is selected with smaller adjustments of the etalon spacing. Although the spacing is measured in microns (typically 4-11μm), the FP controller electronics and the control software in the computer think in the dimensionless unit Z. Z_{Coarse}, the base setting, is adjusted via the Z dial on the FP controller; Z_{Offset}, or Z_{Off}, is adjusted via the computer control program. Z_{Off} runs from -2048 to +2048; at the extrema of this range, the etalon spacing overlaps with the middle ($i.e.$, Z_{Off} =0) of the adjacent Z_{Coarse}. A single Z_{Coarse} setting will
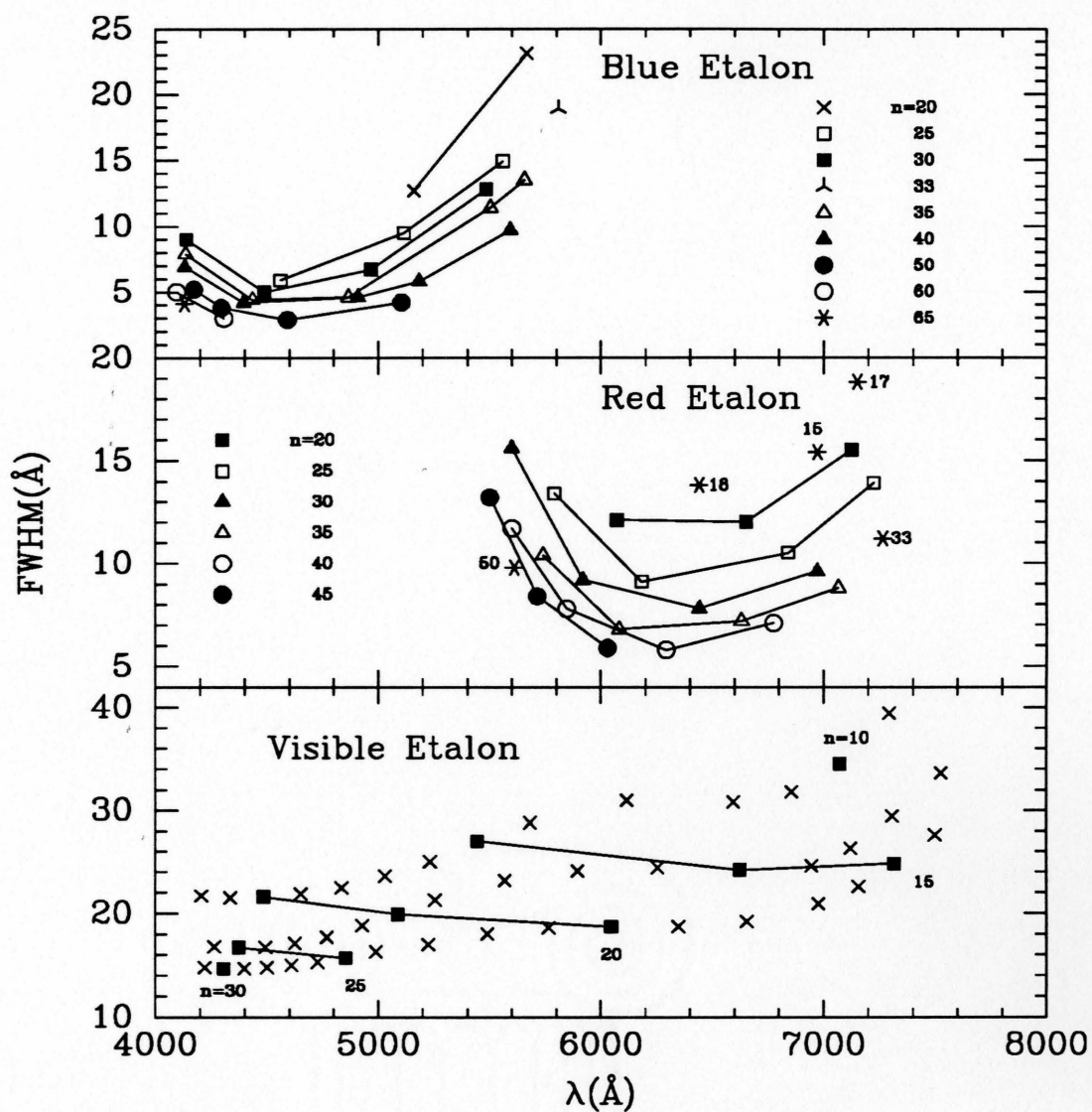
Figure A.2: Transmission FWHM as a function of wavelength λ and interference order n for the three etalons.
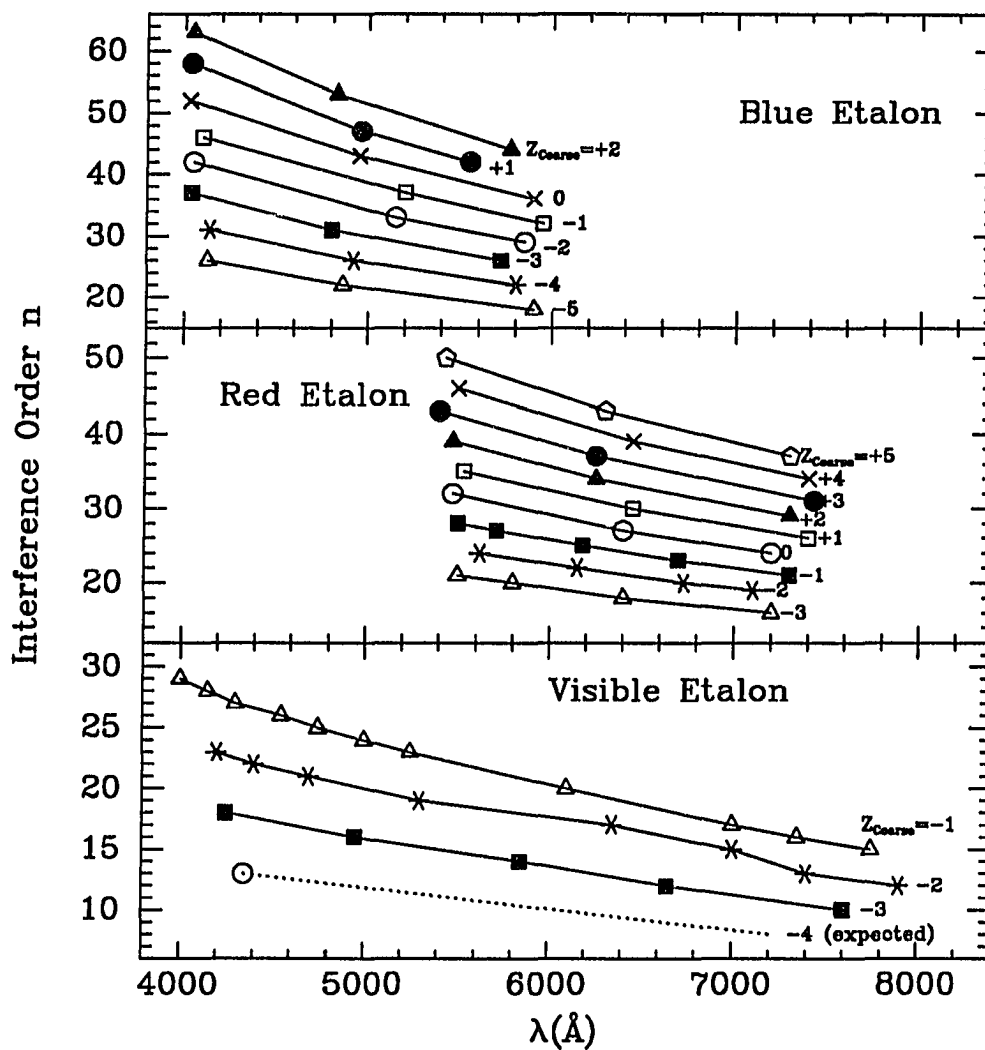
Figure A.3: Interference orders as a function of Z_{Coarse} and wavelength λ; lines show the interference order transmitted when Z_{Coarse} is set to the value shown at the right end of the line, for $Z_{off} = 0$.

cover several interference orders. Although the FP controller Z_{Coarse} dial runs from -5 to +5, only a limited subset of this range is available to each of the etalons, due to the finite range of the piezo-electric drivers. Higher Z_{Coarse} corresponds to larger etalon spacing (= higher resolution); successive values of Z_{Coarse} vary the spacing by ~ 1 μm. The entire range of wavelength, Z, interference order, and FWHM of the transmission curve have been mapped for each etalon and fit with polynomial functions stored in the computer, allowing users to enter only the desired wavelength.

The etalon transmission function is generally an Airy function, but at wavelengths near the edge of a blocking filter, the convolution of the various transmission curves can produce an asymmetrical and complex function. Furthermore, since the wavelength and shape of the transmission can be measured only at wavelengths for which there exists an isolated calibration lamp line, the FWHM and dispersion of the transmission must be interpolated for many spectral regions. For the blue and red etalons, this is a dependable technique, but for the visible etalon, whose broad-band coatings introduce non-linear and unpredictable wavelength effects, this introduces large uncertainties in the FWHM (up to 25%), especially near the ends of the accessible wavelength range. This in turn translates into a large error in the throughput, which has been measured using photometric standard stars (Figure A.4).

Flat field images varying by only a small wavelength shift but identical in blocking filter, intensity, and exposure time, tend to be virtually indistinguishable. This means that frames at slightly different wavelengths can be flattened using flat fields taken at only a few intermediate FP settings. It is generally desireable to match the illumination level in individual flat fields to the background sky level in the data frames, to avoid different degrees of streaking in columns of the CCD containing charge traps.
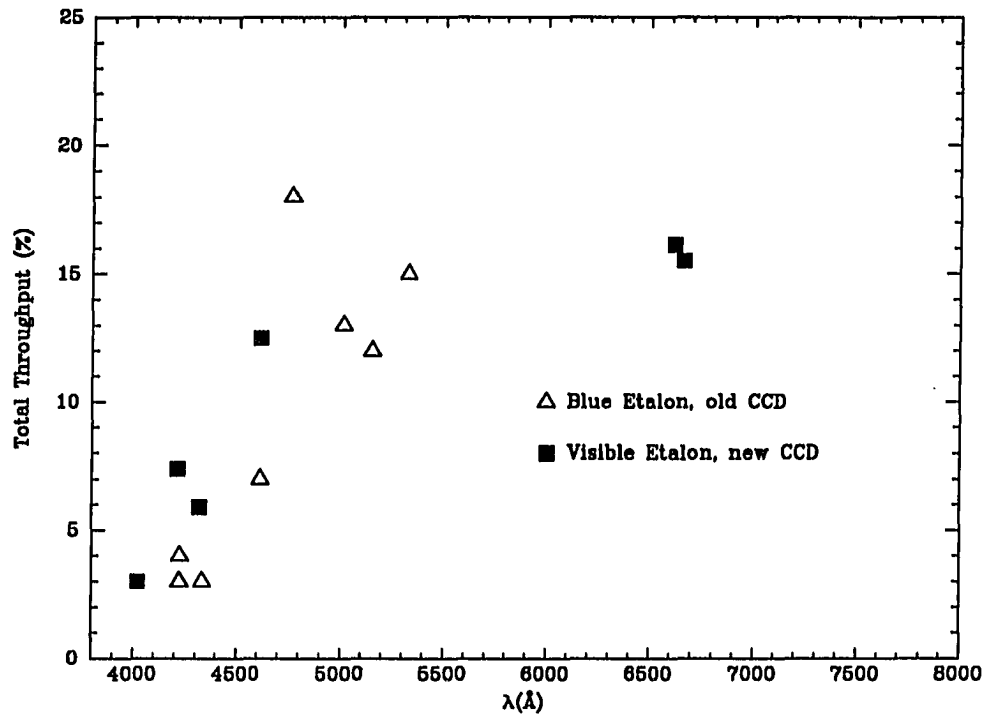
Figure A.4: Total throughput of the Fabry-Perot, including atmosphere, telescope, instrument, and detector. The throughput is defined as the ratio of photons incident upon the top of the Earth's atmosphere to photoelectrons detected.

The behavior of the etalon transmission is governed by the "etalon equation"; narrow bands of light are transmitted when

$$(n + e)\lambda = 2t\mu \cos \theta \qquad \text{(A.1)}$$

(or just $n\lambda = 2t$, when $e = 0$, $\theta = 0$, and $\mu = \mu_{air}$),

where n = (integral part of) interference order,

$\qquad e$ = non-integral phase shift,

$\qquad \lambda$ = wavelength in Å,

$\qquad t$ = etalon spacing in Å,

$\qquad \mu$ = index of refraction within the etalon cavity,

and $\quad \theta =$ angle of incidence of light.

The phase shift, e, is due to the finite thickness of the etalon's reflective coatings. This phase shift is essentially constant for the blue and red etalons, but not the visible.

The Queensgate etalon controller and the computer control program, furthermore, express the etalon spacing as

$$t = K_1 + K_2(Z_{\text{Off}} + K_3) \tag{A.2}$$

where $K_1 =$ base etalon spacing (Å) for the Z_{Coarse} being used,

$\quad K_2 = \lambda/2(z_n - z_{n-1})$ for any given wavelength λ (Å) and the Z_{Off}

$\qquad$ settings for that wavelength in two adjacent interference orders,

$\quad Z_{\text{Off}} =$ fine etalon spacing adjustment,

and $\quad K_3 =$ additive drift correction, in units of Z_{Off}, to be updated by

$\qquad$ the observer after calibration.

Combining equations A.1 and A.2,

$$\lambda = \frac{2}{n+e}[K_1 + K_2(Z_{\text{Off}} + K_3)] \tag{A.3}$$

or

$$Z_{\text{Off}} = (\frac{1}{K_2})[(n + e)\frac{\lambda}{2} - K_1] - K_3. \tag{A.4}$$

The free spectral range (FSR), defined as the separation in Å between adjacent interference orders, is given by

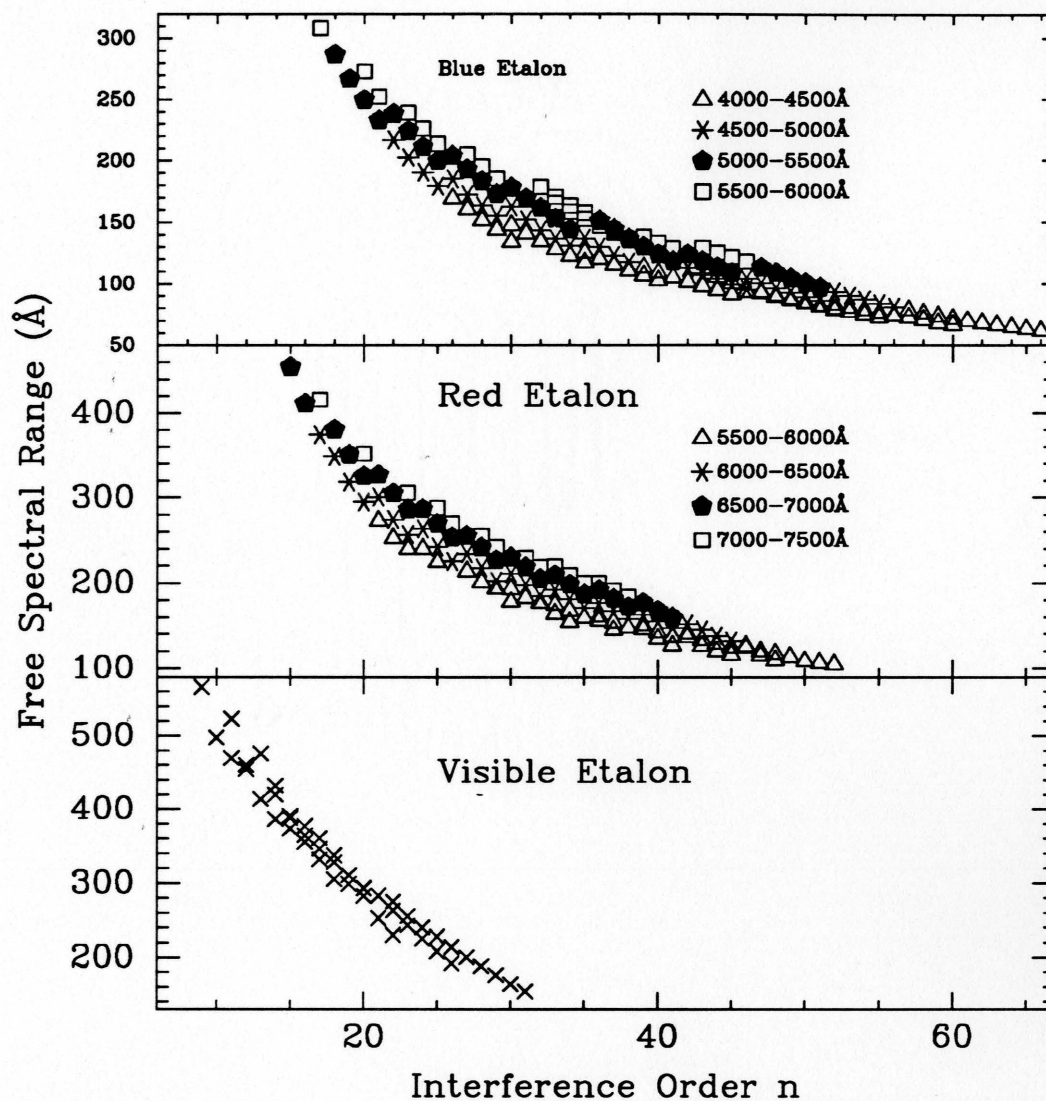$$FSR = \frac{\lambda}{n+e} \tag{A.5}$$

Figure A.5: FSR as a function of intereference order n and wavelength λ.

and is plotted in Figure A.5 for the three etalons.

Because of the dependence of transmitted wavelength on the angle of incidence, there is a slight wavelength shift toward the blue for parts of the image away from the center of the field of view. This shift is given by

$$\Delta\lambda \equiv \lambda_0 - \lambda = \lambda_0(1 - \cos\theta) \tag{A.6}$$

with

$$\theta = \arctan(r \times \frac{p}{f}) = \arctan(r \times 1.35 \times 10^{-4}) \tag{A.7}$$

where r is the distance in CCD pixels from the center of the image, $p = 0.027$ is the unbinned pixel size in mm, and $f = 200$ is the camera lens focal length in mm. This function is shown in Figure A.6 for a few representative wavelengths.

The etalons can be calibrated essentially from scratch, provided a single emission line can be located and identified as a starting point. The procedure is as follows:

1. Find a spectral line λ_1 in two adjacent interference orders n and $n_{\pm 1}$.

2. Find a different spectral line λ_2 in order n.

3. Calculate interorder spacing K_2 in units of $\text{Å}/Z_{\text{Off}}$:

$$K_2 = \frac{\lambda}{2(Z_n - Z_{n\pm 1})} \tag{A.8}$$

4. Calculate local dispersion D in units of $Z_{\text{Off}}/\text{Å}$:

$$D = \frac{Z_{\lambda_1} - Z_{\lambda_2}}{\lambda_1 - \lambda_2} \tag{A.9}$$

(See Figure A.7.)

5. Calculate effective order n (not necessarily the same as nominal order, due to variable dispersion, especially with visible etalon) and non-integral phase shift e:

$$n + e = 2K_2D \tag{A.10}$$
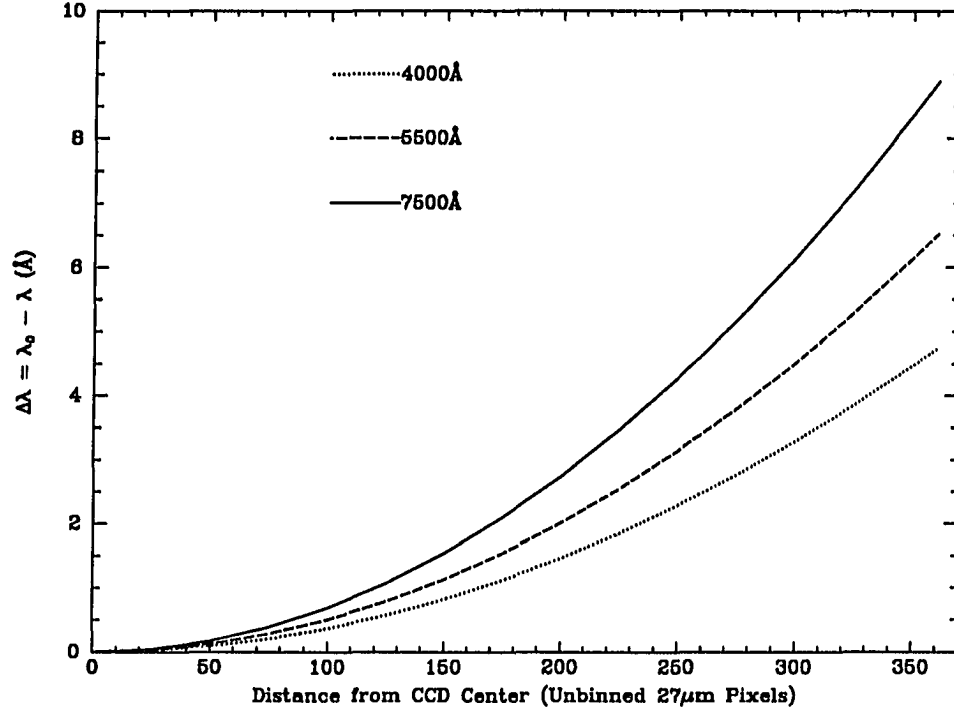
Figure A.6: Wavelength shift as a function of distance from the center of the field of view.

6. Calculate K_1, the base etalon spacing in Å:

$$K_1 = \frac{\lambda}{2}(n + e) - K_2(Z_\lambda + K_3) = \frac{\lambda}{2}(n + e) - K_2(Z_\lambda) \qquad (A.11)$$

assuming $K_3 = 0$. Either of the two spectral lines can be used.
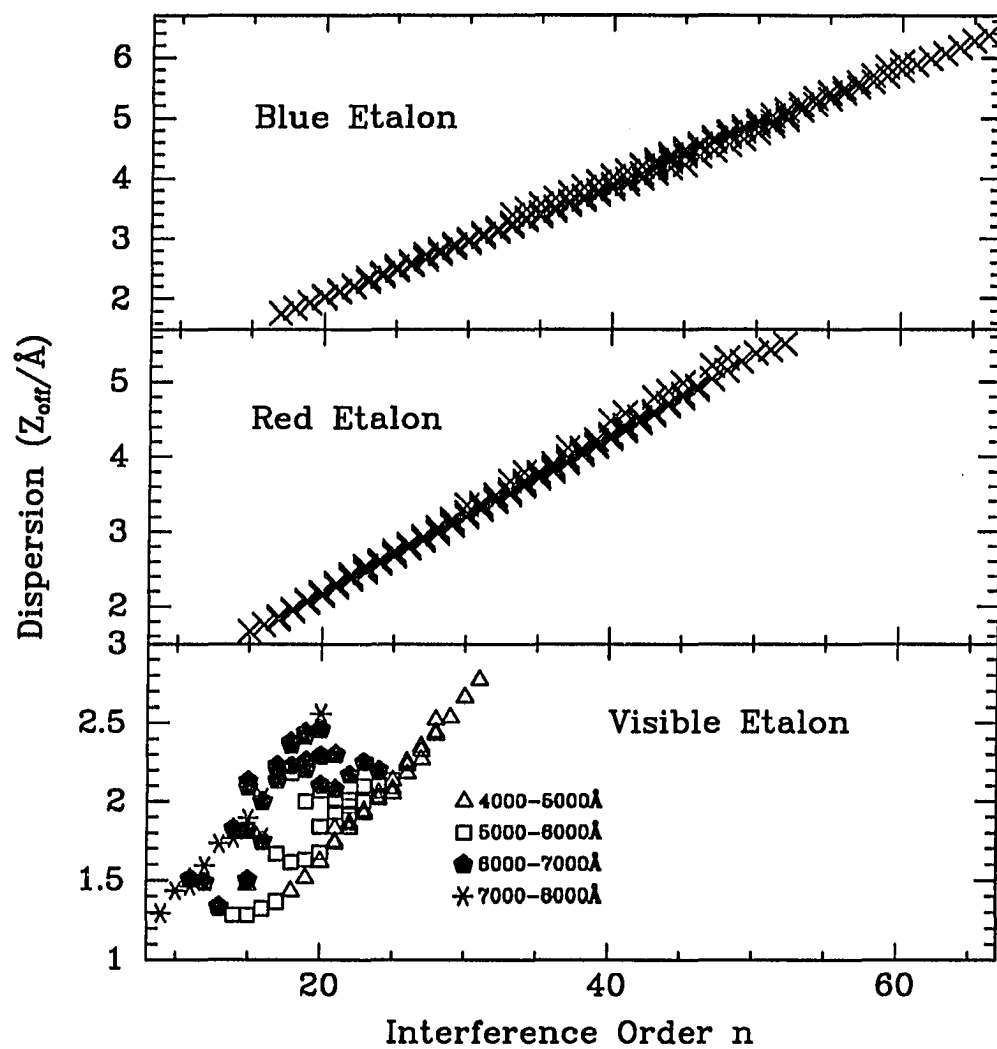
Figure A.7: Dispersion as a function of interference order n.

REFERENCES

Adams, T.F. 1972, ApJ, 174, 439

Auer, L.H. 1968, ApJ, 153, 783

Bahcall, J.N., Jannuzi, B.T., Schneider, D.P., Hartig, G.F., Bohlin, R., & Junkkari-
nen, V. 1991, ApJL, 377, L5

Bajtlik, S., Duncan, R. C., & Ostriker, J. P. 1988, ApJ, 327, 570

Barcons, X., & Webb, J.K. 1990, Short Comm. MNRAS, 244, 30p.

Baron, E., & White, S. D. M. 1987, ApJ, 322, 585

Bechtold, J. 1991, private communication

Bechtold, J., Green, R.F., Weymann, R.J., Schmidt, M., Estabrook, F.B., Sherman,
R.D., Wahlquist, H.D., & Heckman, T.M. 1984, ApJ, 281, 76

Bechtold, J., Weymann, R. J., Lin, Z., & Malkan, M. A. 1987, ApJ, 315, 180

Bergeron, J. 1988, in Large Scale Structures of the Universe, eds. J. Audouze *et al.*
(Dordrecht: Reidel), p. 454

Bergeron, J. & Boisse 1991, A&A, 243, 344

Bithell, M. & Rees, M.J. 1990, MNRAS, 242, 570

Black, J.H., Chaffe, F.H., & Foltz, C.B. 1987, ApJ, 317, 442

Blumenthal, G.R., Faber, S.M., Primack, J.R., & Rees, M.J. 1984, Nature, 311, 517

Bonhila, J.R.M., Ferch, R., Salpeter, E.E., Slater, G., and Noerdlinger, P.D. 1979,
ApJ, 233, 649

Burstein, D., & Heiles, C. 1982, AJ, 87, 1165

Butcher, H. & Oemler, A., Jr. 1978a, ApJ, 219, 18

———. 1978b, ApJ, 226, 559

———. 1984, ApJ, 285, 426

Briggs, F.H., Wolfe, A.M., Liszt, H.S., Davis, M.M., & Turner, K.L. 1989, ApJ,
341, 650

Bruzual, G. 1983, ApJ273, 105

Caulet, A, Woodgate, B.E., Brown, L.W., Gull, T.R., Hintzen, P., Lowenthal, J.D., Oliversen, R.J., & Ziegler, M.M. 1991, ApJ, submitted.

Chambers, K.C., & Charlot, S. 1990, ApJL, 348, L1

Chambers, K.C., & McCarthy, P.J. 1990, ApJL, 354, L9

Chambers, K.C., Miley, G.K., & van Breugel, W.J.M., 1988, ApJL, 327, L47

————. 1990, ApJ, 363, 21

Charlot, S., & Bruzual A., G. 1991, ApJ, 367, 126

Charlot, S., & Fall, S.M. 1991, ApJ, in press

Cole, S. 1991, ApJ, 367, 45

Coleman, G.D., Wu, C.-C., & Weedman, D.W. 1980, ApJS, 43, 393

Colless, M., Ellis, R.S., Taylor, K., & Hoo, R.N. 1990, MNRAS, 244, 408

Cowie, L. L. 1988 in The Post-Recombination Universe, eds. N. Kaiser, and A. N. Lasenby (Dordrecht: Kluwer Academic Publishers), p. 1

Cox, D.P. 1985, ApJ, 288, 465

Davis, M., & Peebles, P.J.E. 1983, ApJ, 267, 465

Deharveng, J.M., Joubert, M., & Kunth, D. 1986 in Star-Forming Dwarf Galaxies and related Objects, p. 431

Deharveng, J.M., Buat, V., & Bowyer, S. 1990, A&A, 236, 351

Dinerstein, H.L. 1990, in The Interstellar Medium of External Galaxies, eds. H.A. Thronson, J.M. Shull (Dordrecht: Kluwer Academic Publishers), p. ??

Djorgovski, S., Spinrad, H., McCarthy, P. J., Dickinson, M., van Bruegel, W., & Strom, R. 1988, AJ, 96, 836

Djorgovski, S., Strauss, M. A., Spinrad, H., Perley, R., and McCarthy, P. J. 1987, AJ, 93 1318

Dressler, A., Gunn, J.E., & Schneider, D.P. 1985, ApJ, 294, 70

Ellingson, E., Yee, H.K.C., & Green, R.F. 1991, ApJ, 371, 49

Elston, R. E. 1988, Ph.D. thesis, University of Arizona

Elston, R.J., Bechtold, J., Lowenthal, J.D., & Rieke, M. 1991, ApJL, 373, L39

Elston, R.J. 1991, private communication

Fall, S.M., Pei, Y.C., & McMahon, R.G. 1989, ApJL, 341, L5

Ferland, G.J., & Osterbrock, D.E. 1985, ApJ, 289, 105

Foltz, C.B., Chaffee, F.H., & Weymann, R.J. 1986, AJ, 92, 247

Foltz, C. B., Weymann, R. J., Röser, H.-J., & Chaffee, F. H. 1984, ApJL, 281, L1

Foltz, C.B, Chaffee, F.H., Jr., & Black, J.H. 1988, 324, 267

Frenk, C.S., White, S.D.M., Efstathiou, G., & Davis, M. 1985, Nature, 317, 595

Guhathakurta, P., Tyson, J.A., & Majewski, S.R. 1990, ApJL, 357, L9

Hamilton, D. 1985, ApJ, 297, 371

Hartmann, L.W., Huchra, J.P., & Geller, M.J. 1984, ApJ, 287, 487

Hartmann, L.W., Huchra, J.P., Geller, M.J., O'Brien, P., and Wilson, R., 1988,
    ApJ, 326, 101

Heckman, T.M., Lehnert, M.D., van Breugel, W., & Miley, G.K1991, ApJ, 370, 78.

Heisler, J., Hogan, C.J., & White, S.D.M. 1989, ApJ, 347, 52

Hummer, D.G., & Kunasz, P.B. 1980, ApJ, 236, 609

Kennicutt, R.C., 1983, ApJ, 272, 54

Khare, P., York, D.G., & Green, R.F. 1989, ApJ, 347, 626

Hewitt, A., & Burbidge, G. 1987, ApJS, 63, 1

Hogan, C.J. 1987, ApJL, 316, L59

Hogan, C. J., & Rees, M. J. 1979, MNRAS, 188, 791

Hogan, C. J., & Weymann, R. J. 1987, MNRAS, 225, 1

Hu, E. M., & Cowie, L. L. 1987, ApJL, 317, L7

Huchra, J.P., Geller, M.J., deLapparent, V., & Corwin, H.G., Jr. 1990, ApJS, 72,

433

Hunstead, R.W., Pettini, M., & Fletcher, A.B. 1990, ApJ, 356, 23

Ikeuchi, S. 1981, PASJap, 33, 211

Ikeuchi, S. & Ostriker, J.P. 1986, ApJ, 301, 522

Ikeuchi, S., Murakami, I., & Rees, M.J. 1988, Short Comm. MNRAS, 236, 21P

Impey, C. & Bothun, G. 1989, ApJ, 341, 89

Koo, D. C. 1986, in Spectral Evolution of Galaxies, eds. C. Chiosi and A. Renzini
    (Dordrecht: Reidel), p. 419

Koo, D. C., & Kron, R. G. 1980, PASP, 92 537

Lanzetta, K.M. 1988, ApJ, 332, 96

Lanzetta, K.M., Turnshek, D.A., & Wolfe, A.M. 1987, ApJ, 322, 739

Lanzetta, K.M. 1991, ApJ, 375, 1

Lanzetta, K.M., Wolfe, A.M., Turnshek, D.A., Lu, L., McMahon, R.G., & Hazard,
    C. 1991, preprint

Larson, R.B. 1976, MNRAS, 176, 31

Lequeux, J., Mauchera-Joubert, M., Deharveng, J.M., and Kunth, D. 1981, A&A,
    103, 305

Levshakov, S.A., Foltz, C.B., Chaffee, F.H., & Black, J.H

Lilly, S.J., 1987, MNRAS, 229, 573

Lilly, S. J. 1988, ApJ, 333, 161

Lilly, S.J., Cowie, L.L, & Gardner, J.P., 1991, ApJ, 369, 79

Lu, L., Wolfe, A.M., & Turnshek, D.A. 1991, ApJ, 367, 19

Mather, J.C., Cheng, E.S., Eplee, R.E., Jr., Isaacman, R.B., Meyer, S.S., Shafer,
    R.A., Weiss, R., Wright, E.L, Bennett, C.L., Boggess, N.W., Dwek, E., Gulkis,
    S., Hauser, M.G., Janssen, M., Kelsall, T., Lubin, P.M., Moseley, S.H., Jr.,
    Murdock, T.L., Silverberg, R.F., Smoot, G.F., & Wilkinson, D.T. 1990, ApJL,

, 354, L37

McCarthy, P. J., Spinrad, H., Djorgovski, S., Strauss, M. A., 1987a, ApJ, 320, 464

McCarthy, P.J., van Breugel, W., Spinrad, H., & Djorgovski, S. 1987b, ApJL, 321, L29

Meier, D.L. 1976, ApJ, 207, 343

Meier, D.L., & Terlevich, R. 1981, ApJL, 246, L109

Meyer, D.M., & Roth, K.C. 1990, ApJ, 363, 57

Meyer, D.M. & York, D.G. 1987, ApJL, 319, L45

Morris, S.L., Weymann, R.J., Savage, B.D., & Gilliland, R.L. 1991, ApJL, 377, L21

Murdoch, H.S., Hunstead, R.W., Pettini, M., & Blades, J.C. 1986, ApJ, 309, 19

Neufeld, D.A. 1991, ApJL, 370, L85

Newberry, M.V., Kirshner, R.P., & Boroson, T.A. 1988, ApJ, 335, 629

Niemela, V.S., Heathcote, S.R., & Wellere, W.G. 1991, in "Wolf-Rayet Stars and Interrelations with Other Massive Stars in Galaxies," eds. K.A. van der Hucht & B. Hidayat (Dordrecht: Kluwer), p. 425

Osterbrock, D.E. 1989, Astrophysics of Gaseous Nebulae and Active Galactic Nuclei (Mill Valley: University Science Books)

Ostriker, J.P. & Cowie, L.L. 1981, ApJL, 243, L127

Partridge, R.B., & Peebles, P.J.E. 1967, ApJ, 147, 868

Peebles, P.J.E. 1965, ApJ, 142, 1317

————. 1972, Comm. Ap. Sp. Phys., 4, 53

Pei, Y.C., Fall, S.M., & Bechtold, J. 1991, ApJ, in press

Peng, W. & Weisheit, J.C. 1991, ApJ, 373, 471

Pettini, M., Boksenberg, A., & Hunstead, R.W. 1990, ApJ, 348, 48

Pettini, M., & Hunstead, R.W. 1990, AJP, 43, 227

Pettini, M., Hunstead, R.W., Smith, L.J., & Mar, D.P. 1990, MNRAS, 246, 545

Phillipps, S., Davies, J.I, & Disney, M.J. 1990, MNRAS, 242, 235

Polcaro, V.F., Giovannelli, F., Manchanda, R.K., Pollock, A., Norci, L., & Rossi, C. 1991, in "Wolf-Rayet Stars and Interrelations with Other Massive Stars in Galaxies," eds. K.A. van der Hucht & B. Hidayat (Dordrecht: Kluwer), p. 103

Press, W.H., & Schechter, P. 1974, ApJ, 187, 425

Prestage, R.M., & Peacock, J.A. 1988, MNRAS, 184, 769

Pritchet, C.J., & Hartwick, F.D.A. 1987, ApJ, 320, 464

Rauch, M., Carswell, R.F., Robertson, J.G., Shaver, P.A., and Webb, J.K. 1990, MNRAS, 242, 698

Rauch, M., Carswell, R.F., Chaffee, F.H., Foltz, C.B., Webb, J.K., Weymann, R.J., Bechtold, J., & Green, R.F. 1991, in prep.

Sargent, W.L.W., Steidel, C.C., & Boksenberg, A. 1988, ApJ, 334, 22

Sargent, W. L. W., Steidel, C. C., & Boksenberg, A. 1989, ApJS, 69, 703

Schechter, P. 1976, ApJ, 203, 297

Schmidt, G. D., Weymann, R. J., & Foltz, C. B. 1989, PASP, 101, 713

Sciama, D.W. 1971, Modern Cosmology (Cambridge: Cambridge University Press)

Shields, G.A. 1990, Ann. Rev. Astron. Astrophys., 28, 525

Smith, H.E., Cohen, R.D., & Bradley, S.E. 1986, ApJ, 310, 583

Smith, H.E., Cohen, R.D., Burns, J.E., Moore, D.J., & Uchida, B.A. 1989, ApJ, 347, 87

Smith, H.E., Cohen, R.D., Moore, D.J., & Uchida, B. 1987, BAAS, 19, 1106

Spinrad, H. 1985, PASP, 98, 601

Spinrad, H. 1989, in "The Epoch of Galaxy Formation," ed. C.S. Frenk *et al.* (Dordrecht: Kluwer), p. 39

Steidel, C.C. 1990, ApJS, 72, 1

Steidel, C.C., Sargent, W.L.W., & Dickinson, M. 1991, AJ, in press.

Sunyaev, R.A. & Zel'dovich, Ya.B. 1972, A&A, 20, 189

Tinsley, B.M. 1980, in Fundamentals of Cosmic Physics, 5, 287

Tyson, J.A. 1988, AJ, 96, 1

Turnshek, D.A., Bencke, M., Hazard, C., Macchetto, F., Sparks, W., & McMahon, R., 1991, BAAS, 23, 840

Turnshek, D.A., Macchetto, F., Bencke, M.V., Hazard, C., Sparks, W.B., & McMahon, R.G 1991, ApJ, in press

Urbaniak, J.J., & Wolfe, A.M., 1981, ApJ, 244, 406

Webb, J.K. & Barcons, X. 1990, MNRAS,

Weedman, D.W. 1988, Quasar Astronomy (Cambridge: Cambridge University Press)

Weinberg, D.H., Szomoru, A., Guhathakurta, P., & van Gorkom, J.H., 1991, ApJL, 372, L13

Weinberg, S. 1972, Gravitation & Cosmology (New York: Wiley)

White, S. D. M. 1988, in Epoch of Galaxy Formation, NATO Advanced Research Workshop, Durham, England, ed. C. Frenk, R.Ellis, T. shanks, A. Heavens, & J. Peacock (Dordrecht: Kluwer Academic), p.15

Wolfe, A.M., 1986, Phil. Trans. Roy. Soc. Lond., 321, 503

Wolfe, A.M., Turnshek, D.A., Smith, H.E., & Cohen, R.E., 1986, ApJS, 61, 249

Wolfe, A., Turnshek, D.A., Lanzetta, K.M, & Oke, J.B. 1991, ApJ, in press

Yanny, B. 1990, ApJ, 351, 396

Yanny, B., York, D.G., & Williams, T.B. 1990, ApJ, 351, 377

Yanny, B., Barden, S., Gallacher, J.S., III, & York, D.G. 1990, ApJ352, 413

Yee, H.K.C., & Green, R.F. 1984, ApJ, 280, 79

York, D.G., Dopita, M., Green, R., & Bechtold, J. 1986, ApJ, 311, 610

Zel'dovich, Ya. B. 1970, A&A, 5, 85

Zel'dovich, Ya. B. & Novikov, I.D. 1983, Relativistic Astrophysics, Vol. 2 (Chicago: University of Chicago Press)
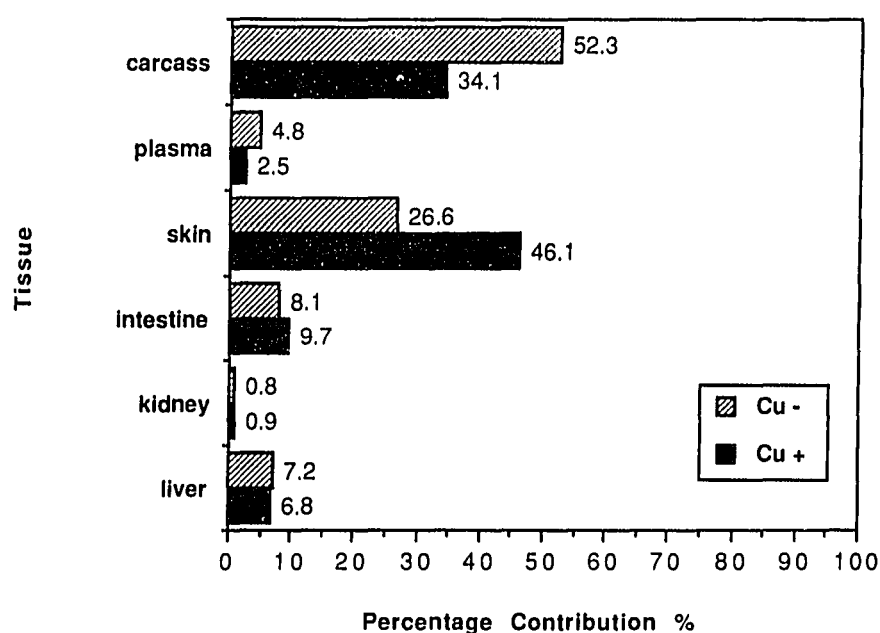
Figure 3: Tissue [³H]DPS Content (% Total Body Contribution). These values represent the data presented in Figure 2 ([³H]DPS nmol/hr-100g body wt.) expressed as a percentage of total body [³H]DPS content (22.1± 5.0 µmol/h copper-adequate; 24.1 ± 4.1 µmol/h copper-deficient). Carcass values represent all tissues not indicated separately. n=6 animals per group and data represent the mean for each group.

Table III. Tissue Cholesterol Levels

	Tissue Cholesterol (mg/g)		
Tissue	Cu-Adequate	Cu-Deficient	P-value
Liver	1.57 ± 0.07	1.46 ± 0.07	<0.05
Kidney	4.01 ± 0.21	5.09 ± 0.26	<0.005
Intestine	2.37 ± 0.37	2.65 ±0.17	n.s.
Skin	2.70 ± 0.40	2.31 ± 0.38	n.s.
Muscle	0.66 ± 0.03	0.71 ± 0.09	n.s.
Carcass	1.49 ± 0.16	1.78 ± 0.17	<0.01

Tissue cholesterol levels were determined by dissolving dried extracted DPS in 1.0 ml of EtOH. Aliquots were removed for cholesterol determination by enzymatic assay (Allain et al. 1974). The DPS-EtOH-solution was then evaporated to dryness under N_2 and scintillation fluor was added. [^{14}C]cholesterol recoveries were used to correct for recovery and the mg cholesterol/g tissue was determined. The data are presented as mean ± S.D. for n=6 (n.s. = not significantly different).

DISCUSSION

Copper deficiency frequently induces hypercholesterolemia (Klevay 1973; Allen and Klevay 1978; Lefevere et al. 1985; Lei 1977; Lei 1983), cardiac hypertrophy (Goodman et al. 1970; Kelly et al. 1974), decreased hematocrit, increased plasma volume (Lei 1983; Carr and Lei 1990) and a reduced liver copper concentration (Allen and Klevay 1978; Lei 1977). We observed an increased plasma cholesterol level, plasma volume and heart weight, a decreased hematocrit, and reduced hepatic copper levels in copper-deficient animals. Based on these parameters it was evident that the animals in this study exhibited the characteristics of copper deficiency.

Tritiated water was used to measure absolute rates of cholesterol synthesis in the rat for several reasons. Firstly, tritiated water is currently regarded as one of the most accurate measures of cholesterol synthesis, in that it avoids problems associated with variable substrate uptake and dilution associated with using labeled octanoate, acetate or pyruvate (Spady and Dietschy 1983). Secondly, tritiated water directly measures the quantity of DPS synthesized within a given time period within specific organs; whereas other in vivo measures such as sterol balance only summarize sterol synthesis for the entire organism and do not provide data relative to specific organ synthesis rates.

When tritiated water incorporation rates into sterols were calculated on a per gram tissue basis, the intestine was the most active synthetic organ of the tissues sampled (Figure 1). Previous studies conducted in the rat fed commercial non-purified diets reported similar findings, with intestinal synthesis per gram second only to adrenal and hepatic sterol synthesis rates (Spady and Dietschy 1983). Hepatic sterol synthesis rates, whether measured per gram or per organ, were markedly lower than in other reported studies of rats fed non-purified diets and sacrificed during the mid-dark portion of the light cycle (Jeske and Dietschy 1980; Spady and Dietschy 1983). HMG-CoA reductase has previously been

shown to be maximal at the mid-dark portion of the diurnal cycle (Shapiro and Rodwell 1969; Shefer et al. 1972) and varies approximately 2 to 3-fold between the peak and nadir of this cycle (Jeske and Dietschy 1980; Shefer et al. 1972). If these studies had been conducted at the peak of the diurnal expression of HMG-CoA reductase it is probable that the liver would have had higher rates of sterol synthesis relative to the other organs studied. Probably a more important factor which contributes to low rates of hepatic sterol synthesis is that casein was the protein source in the semi-purified diet used. Previous studies have demonstrated that intake of a casein based diet reduces HMG-CoA reductase activity from 60-75% when compared to plant protein based diets (McNamara et al. 1982). Thus, under the experimental conditions used here, the measured values for hepatic sterol synthesis probably accurately represent the in vivo rates.

Sterol synthesis rates in other tissues are generally less affected by diurnal rhythm and dietary factors. For example, the sterol synthetic rate for skin was 104 nmol/h-g as compared to 196 nmol/h-g reported in a previous study, in which animals fed non-purified diets were sacrificed at the peak of the diurnal rhythm (Spady and Dietschy 1983). Similarly, sterol synthetic rates for muscle were 25 nmol/h-g versus 12 nmol/h-g from the same previous study.

Copper deficiency produced a trend towards increased rates of sterol synthesis in most of the tissues examined; however, on a per gram tissue basis, only newly synthesized sterol appearing in the plasma was significant. In contrast, sterol synthesis rates in the skin of copper-deficient rats were much lower than that observed in copper-adequate animals. A recent study conducted by Carr and Lei (1990) provides evidence that skin takes up HDL particles, as measured by HDL protein, at a rate 2.4-fold greater in copper-deficient than copper-adequate rats. Therefore, it is possible that the skin of copper-deficient rats is obtaining increased amounts of cholesterol from the plasma pool and thus has a reduced

need for de novo cholesterol synthesis. This would result in decreased rates of sterol synthesis in this tissue as seen in these studies.

Because previous studies have indicated that hepatic HMG-CoA reductase activity is elevated in copper-deficient rats it was surprising to find that, although hepatic sterol synthesis was elevated with copper deficiency, it was not increased significantly. One explanation for this finding is the observation that newly synthesized sterol exported to the plasma was increased in copper-deficient animals. When expressed as nmol/h per g or nmol/h per 100 g body weight, radiolabeled DPS in the plasma was elevated 1.6 and 2.1-fold respectively in copper-deficient rats. Thus, although hepatic sterol synthesis rates may not be significantly elevated when expressed either per gram or per organ, hepatic sterol synthesis may be markedly elevated as reflected by the appearance of increased levels of newly synthesized sterol in the plasma. It is probable that radiolabeled sterol appearing in the plasma is primarily of hepatic origin for several reasons. Previous studies have shown a strong correlation between [^{3}H]DPS levels in the liver and blood of rats and other species (Spady and Dietschy 1983; Belknap and Dietschy 1988). When animals are fed increasing amounts of cholesterol, which reduces hepatic cholesterol synthesis to a minimal level, there was a reciprocal decline in the [^{3}H]DPS found in the blood. Although this relationship exists for the liver, other organs tested (intestine, skin and carcass) showed little correlation between organ and blood [^{3}H]DPS content (Spady and Dietschy 1983). Further support for the probability that plasma [^{3}H]DPS are derived from the liver stems from studies which have shown that copper deficiency results in an increased rate of export of newly synthesized cholesterol from the liver to the plasma (Shao and Lei 1980).

Previous studies have demonstrated that many organs in the copper-deficient rat take up labeled HDL protein and cholesteryl ester at a significantly increased rate over copper-adequate rats (Carr and Lei 1990). The kidney, however, does not follow this

generalized pattern, and actually takes up less cholesteryl ester with copper deficiency. This finding may be related to the observation that in the present studies the kidney was one of the few organs in which the net cholesterol content was increased with copper deficiency. In the kidney, cholesterol is primarily synthesized from circulating mevalonate (Edmond et al. 1976); however, with copper deficiency kidney uptake of mevalonate, as well as cholesteryl ester derived from HDL, is reduced. It has also been demonstrated that the kidney has a delayed release of newly synthesized cholesterol with copper deficiency (Shao and Lei 1980). Therefore, it may be that with copper deficiency the kidney has an increased need to retain cholesterol, which may account for the elevated levels of cholesterol found in the kidney.

One other item of note is that hepatic tissue cholesterol levels were reduced in the copper-deficient rat as has been demonstrated previously (Appendix A). This reduction in hepatic cholesterol with copper deficiency may elevate HMG-CoA reductase activity and thus contribute to the observed increase in newly synthesized sterol appearing in the plasma.

In this study absolute rates of sterol synthesis were determined in copper-deficient and adequate rats. Results demonstrate that copper deficiency leads to increased levels of sterol synthesis in the carcass, indicating that there is a net increase in carcass cholesterol synthesis in the rat induced by copper deficiency. Newly synthesized sterol appearing in the plasma was also increased with copper deficiency. Taken together these data support the hypothesis that copper deficiency results in an increased flux of sterol from the liver to the plasma. These findings may account in part for the hypercholesterolemia observed in copper deficient rats.

REFERENCES

Allain, C.C., Poon, L.C., Chan, C.S.G., Richmond, W. & Fu, P.C. (1974). Enzymatic determination of total serum cholesterol. Clin. Chem. 20, 470-475.

Allen, K.G.D. & Klevay, L.M. (1978). Copper deficiency and cholesterol metabolism in the rat. Atherosclerosis 31: 259-271.

Allen, K.G.D. & Klevay, L.M. (1978). Cholesterolemia and cardiovascular abnormalities in rats caused by copper deficiency. Atherosclerosis 29: 81-93.

Allen, K.G.D. & Klevay, L.M. (1980). Hyperlipoproteinemia in rats due to copper deficiency. Nutr. Rep. Internal. 22: 295-299.

Andersen, J.M. & Dietschy, J.M. (1979). Absolute rates of cholesterol synthesis in extrahepatic tissues measured with ^{3}H-labeled water and ^{14}C-labeled substrates. J. Lipid Res. 20: 740-752.

Anon: Recommended Dietary Allowances (ed 9). Food and Nutrition Board, National Research Council. Washington DC, National Academy of Sciences, 1980: 151-154.

Auwerx, J.H., Chait, A., & Deeb, S.S. (1989) Regulation of the low density lipoprotein receptor and hydroxymethylglutaryl coenzyme A reductase genes by protein kinase C and a putative negative regulatory protein. Proc. Natl. Acad. Sci. 86: 1133-1137.

Barkin, Miles and Taylor (1986) Chloroplast gene expression in nuclear, photosynthetic mutants of maize. EMBO J. 5: 1421-1427.

Basson, M.E., Thorsness, M., Finer-Moore, J., Stroud, R.M. & Rine, J. (1988) Structural and functional conservation between yeast and human 3-hydroxy-3-methylglutaryl coenzyme A reductases, the rate limiting enzyme of sterol biosynthesis. Mol. Cell. Biol. 8: 3797-3808.

Beg, S. H., Reznikov, D.C. & Avigan, J. (1986). Regulation of 3-hydroxy-3-methylglutaryl coenzyme A reductase activity in human fibroblasts by reversible phosphorylation: modulation of enzymatic activity by low density lipoprotein, sterols, and mevalonolactone. Arch. Biochem. Biophys. 24: 310-322.

Beisiegel, U., Weber, W., Ihrke, G., Herz, J. & Stanley, K.K. (1989) The LDL-receptor-related protein, LRP, is an apolipoprotein E-binding protein. Nature, 341: 162-164.

Belknap, W.M. & Dietschy, J.M. (1988) Sterol synthesis and low density lipoprotein clearance in vivo in the pregnant rat, placenta, and fetus. J. Clin. Invest. 82: 2077-2085.

Bell, G.I., Karam, J.H., Rutter, W.J. (1981) Polymorphic DNA region adjacent to the 5' end of the human insulin gene. Proc. Natl. Acad. Sci. USA 78: 5759-5763.

Bieri, J.G., Stoewstand, G.S., Briggs, G.M., Philips, R.W., Woodward, J.C. & Knapke, J.J. (1977). Report on the American Institute of Nutrition ad hoc committee on standards for nutritional studies. J. Nutr. 107: 1340-1348.

Bilheimer, D.W., Grundy, S.M., Brown, M.S. & Goldstein, J.L. (1983) Mevinolin and cholestipol stimulate receptor-mediated clearance of low density lipoprotein from plasma in familial hypercholesterolemic heterozygotes. Proc. Natl. Acad. Sci. U.S.A. 80: 4124-4128.

Boyd, E.M. & Wilson, K.M. (1935) The exchange of lipids in the umbilical cord at birth. J. Clin. Invest. 14: 7-15.

Brown, M.S., Dana, S.E. & Goldstein, J.L. (1974) Regulation of 3-hydroxy-3-methylglutaryl coenzyme A reductase in cultured human fibroblasts. J. Biol. Chem. 253: 1121-1128.

Brown, M.S., Goldstein, J.L. & Dietschy, J.M. (1979) Active and inactive forms of 3-hydroxy-3-methylglutaryl coenzyme A reductase in the liver of the rat. J. Biol. Chem. 254: 5144-5149.

Bucolo, G. & David, H. (1973) Quantitative determination of serum triglycerides by the use of enzymes. Clin Chem. 19: 476-482.

Carlson, S.E., Mitchell, A.D. & Goldfarb, S. (1978) Sex related differences in diurnal activities of hepatic microsomal 3-hydroxy-3-methylglutaryl coenzyme A reductase and cholesterol 7α-hydroxylase. Biochim. Biophys. Acta. 531: 115-124.

Carr, B.R. & Simpson, E.R. (1981a) De novo synthesis of cholesterol by the human fetal adrenal gland. Endocrinology 108: 2154-2162.

Carr, B.R. & Simpson, E.R. (1981b) Synthesis of cholesterol in the human fetus: 3-hydroxy-3-methylglutaryl coenzyme A reductase activity of liver microsomes. J. Clin. Endocrinol. Metab. 53: 810-812.

Carr, B.R. & Simpson, E.R. (1982) Cholesterol synthesis in human fetal tissues. J. Clin. Endocrinol. Metab. 55: 447-451.

Carr, B.R. & Simpson, E.R. (1984) Cholesterol synthesis by human fetal hepatocytes: effects of hormones. J. Clin. Endocrinol. Metab. 58: 1111-1116.

Carr, B.R., Rainey, W.E. & Mason, J.I. (1985) 3-hydroxy-3-methylglutaryl coenzyme A reductase in anencephalic and normal human fetal liver. J. Clin. Invest. 76: 1946-1949.

Carr, T.P. & Lei, K.Y. (1989). HDL cholesteryl ester and protein metabolism in copper-deficient, hypercholesterolemic rats. FASEB J. 3: A1062.

Carr, T.P. & Lei, K.Y. (1990) High density lipoprotien cholesteryl ester and protein catabolism in hypercholesterolemic rats induced by copper deficiency. Metabolism 39: 518-524..

Chin, D.J., Gil, G., Russel, D.W., Liscum, L., Luskey, K.L., Basu, S.K., Okayama, H., Berg, P., Goldstein, J.L. and Brown, M.S. (1984) Nucleotide sequence of 3-hydroxy-3-methylglutaryl coenzyme A reductase, a glycoprotein of the endoplasmic reticulum. Nature 308: 613-617.

Chin, D.J., Luskey, K.L., Faust, J.R., MacDonald, R.J., Brown, M.S. & Goldstein, J.L. (1982) Molecular cloning of 3-hydroxy-3-methylglutaryl coenzyme A reductase and evidence for regulation of its mRNA. Proc. Natl. Acad. Sci. 79: 7704-7708.

Chirgwin, J.M., Przybyla, A.E., MacDonald, R.J. & Rutter, W.J. (1979) Isolation of biologically active ribonucelic acid from sources enriched in ribonuclease. Biochem. 18: 5294-5299

Christian, J.C. & Kang K.W. (1977) Maternal influences on plasma cholesterol variation. Am. J. Hum. Genet. 20: 462-467.

Chu, U.M., Oishi, K.K. and Tewari, K.K. (1981) Physical mapping of the pea chloroplast DNA and localization of the ribosomal RNA genes. Plasmid 6: 279-292.

Clarke, C.F., Fogelman, A.M. and Edwards, P.A. (1984) Diurnal rhythm of rat liver mRNA's encoding 3-hydroxy-3-methylglutaryl coenzyme A reductase. J. Biol. Chem. 259: 10439-10447.

Clarke, P.R. & Hardie, D.G. (1990) Regulation of HMG-CoA reductase: identification of the site phosphorylated by the AMP-activated protein kinase in vitro and in intact rat liver. EMBO 9: 2439-2446.

Conner, W.E. & Lin, D.S. (1967) Placental transfer of cholesterol-4-^{14}C into rabbit and guinea pig fetus. J. Lipid Res. 8: 558-564.

Corey, L.A., Kang, K.W., Christian, J.C., Norton, J.A., Harris, R.E. & Nance W.E. (1976) Effects of chorion type on variation in cord blood cholesterol of monozygotic twins. Am. J. Hum. Genet. 20: 462-467.

Dawson, P.A., Ridgway N.D., Slaughter, C.A., Brown, M.S. & Goldstein, J.L. (1989b) cDNA cloning and expression of oxysterol-binding protein, an oligomer with a potential leucine zipper. J. Biol. Chem. 264: 16798-16803.

Dawson, P.A., Van Der Westhuyzen, D., Goldstein, J.L. & Brown, M.S. (1989a) Purification of oxysterol binding protein from hamster liver cytosol. J. Biol. Chem. 264: 9046-9052.

Dietschy, J.M. & Spady, D.K. (1984) Measurement of rates of cholesterol synthesis using tritiated water. J. Lipid Res. 25: 1469-1476.

Dowdy, S. & Wearden, S. (1983) *Statistics for Research* John Wiley & Sons, New York.

Edwards, P.A. & Fogelman, A.M. (1990) Cellular enzymes of cholesterol metabolism. Curr. Opin. Lipid. 1: 136-139.

Edwards, P.A., Lan , S.F. & Fogelman, A.M. (1983) Alterations in the rates of synthesis and degradation of rat liver 3-hydroxy-3-methylglutaryl coenzyme A reductase produced by cholestyramine and mevinolin. J. Biol. Chem. 258: 10219-10222.

Evans, G.W. (1973) Copper homeostasis in the mammalian system. Physiol. Rev. 53: 535-570.

Feinberg, A.P. and Vogelstein, B. (1983) A technique for radiolabeling DNA restriction endonuclease fragments to a high specific activity. Anal. Biochem. 132: 6-13.

Feingold, K.R., Hughes-Wiley, M., Moser, A.H., Lear, S.R. & Siperstein, M.D. (1983) Activation of HMG-CoA reductase by microsomal phosphatase. J. Lipid Res. 24: 290-296.

Feingold, K.R., Wiley, T., Moser, A.H., Lear, S.R. & Hughes-Wiley, M.H. (1983) De novo cholesterogenesis in pregnancy. J. Lab. Clin. Med. 101: 256-263.

Folch, J., Lees, M. & Sloane-Stanley, G.A. (1957). A simple method for the isolation and purification of total lipids from animal tissues. J. Biol. Chem. 226, 497-509.

Gertler, F.B., Chiu, C.Y., Richter-Mann, L. & Chin, D.J. (1988) Developmental and metabolic regulation of the *Drosophila melanogaster* 3-hydroxy-3-methylglutaryl coenzyme A reductase. Mol. Cell. Biol. 8: 2713-2721.

Gil, G. & Hegardt, F.G. (1982) Some properties of purified 3-hydroxy-3-methylglutaryl coenzyme A reductase phosphatases from rat liver. Arch. Biochem. Biophys. 214: 192-198.

Gil, G., Faust, J.R., Chin, D.J., Goldstein, J.L. & Brown, M.S. (1985) Membrane bound domain of HMG-CoA reductase is required for sterol-enhanced degradation of the enzyme. Cell 41: 249-258.

Gil, G., Osborne, T.F., Goldstein, J.L. & Brown, M.S. (1988a) Purification of a protein doublet that binds to six TGG-containing sequences in the promoter for hamster 3-hydroxy-3-methylglutaryl coenzyme A reductase. J. Biol. Chem. 263: 19009-19019.

Gil, G., Smith, J.R., Goldstein, J.L., Slaughter, C.L., Orth, K., Brown, M.S. & Osborne, T.F. (1988b) Multiple genes encode nuclear factor 1-like

proteins that bind to the promoter for 3-hydroxy-3-methylglutaryl coenzyme A reductase. Proc. Natl. Acad. Sci. 85: 8963-8967.

Goldstein, J.L. & Brown, M.S. (1990) Regulation of the mevalonate pathway. Nature 343: 425-430.

Goldwater, W.H. & Stetten D. Jr. (1947) Studies in fetal metabolism. J. Biol. Chem. 169: 723-738.

Goodman, J.R., Warshaw, J.B. & Dallman, P.R. (1970) Cardiac hypertrophy in rats with iron and copper deficiency: Quantitative contribution of mitochondrial enlargement. Pediatr. Res. 4: 244-256.

Goodwin, C.D. & Margolis, S. (1973) Specific activation of in vitro cholesterol biosynthesis by preincubation of rat liver homogenates. J. Biol. Chem. 248: 7610-7613.

Gould, R.G. (1951) Lipid metabolism and atherosclerosis. Am. J. Med. 11: 209-227.

Gray, L.F. & Daniel, L.J. (1964) Effect of the copper status of the rat on the copper-molybdenum-sulfate interaction. J. Nutr. 84: 31-37.

Hamprect, B., Nussler, C. & Lynen, F. (1969) Rhythmic changes of hydroxymethylgutaryl coenzyme A reductase activity in livers of fed and fasted rats. FEBS Lett 4: 117-121.

Hancock, J.F., Magee, A.I., Childs, J.E. & Marshall, C.J. (1989) All ras proteins are polyisoprenylated but only some are palmitoylated. Cell 57: 1167-1177.

Hart, E.B., Steenbock, H., Waddel, J. & Elvehjem, C.A. (1928) Iron in nutrition. VII. Copper as a supplement to iron for hemoglobin building in the rat. J. Biol. Chem. 77: 797-812.

Harvey, P.W. & Allen, K.D.G. (1985). Lipoproteins and liver lipids in copper-deficient rats. Nutr. Res. 5: 511- 525.

Hassan, A.S., Yunker, R.L. & Subbiah, M.T.R. (1981) Decreased bile acid pool in neonates of guinea pigs fed cholesterol during pregnancy. J. Nutr. 111: 2030-2033.

Fernandez, M.L., Yount, N.Y. & McNamara, D.J. 1990. Whole body and hepatic cholesterol synthesis rates in the guinea pig: effect of dietary fat quality. Biochim. Biophys. Acta. 1044:340-348..

Hershfeld, M.S. & Nemeth, A.M. (1968) Placental transport of free palmitic and linoleic acids in the guinea pig. J. Lipid Res. 9: 460-468.

Herz, J., Hamann, U., Rogne, S., Myklebost, O., Gausepohl, H. & Stanley, K.K. (1988) Surface location and high affinity for calcium of a 500-kD liver membrane protein closely related to the LDL-receptor suggest a physiological role as lipoprotein receptor. EMBO 7: 4119-4127.

Herz, J., Hamann, U., Rogne, S., Myklebost, O., Gausepohl, H. & Stanley, K.K. (1988) Surface location and high affinity for calcium of a 500-kD liver membrane protein closely related to the LDL-receptor suggest a physiological role as lipoprotein receptor. EMBO 7: 4119-4127.

Higgins, M. & Rudney, H. (1973) Regulation of rat liver 3-hydroxy-3-methylglutaryl coenzyme A reductase activity by cholesterol. Nature New Biology) 246: 60-61.

Holden, J.M., Wolf, W.R. & Mertz, W. (1979) Zinc and copper in self-selected diets. J. Am. Dietet. Assoc. 75: 23-28.

Huff, J.W., Filfillan, J.L. & Hunt, V.M. (1963) Effect of cholestyramine, a bile acid binding polymer on plasma cholesterol and fecal bile acid excretion in the rat. Proc. Soc. Exp. Biol. Med. 114: 352-355.

Hunter, C.F. & Rodwell, V.W. (1980) Regulation of vertebrate liver HMG-CoA reductase via reversible modulation of its catalytic activity. J. Lipid Res. 21: 399-405.

Ingebritsen, T.S., Geelen, M.J.H., Parker, R.A., Evenson, K.J. & Gibson, D.M. (1979). Modulation of hydroxymethylglutaryl-CoA reductase activity, and cholesterol synthesis in rat hepatocytes in response to insulin and glucagon. J. Biol. Chem. 254: 9986-9989.

Innis, S.M. & Hahn, P. (1982) Influence of litter size on the development of 7α-hydroxylase (7HL). Proc. Can. Fed. Biol. Sci. 67: 260A.

Innis, S.M. (1983a) Influence of maternal cholestyramine on cholesterol and bile acid metabolism in adult offspring. J. Nutr. 113: 2464-2470.

Innis, S.M. (1983b) Effect of cholestyramine administration during pregnancy in the rat. Am J. Obstet. Gynecol. 146: 13-16.

Innis, S.M. (1985) Effect of diet during development on the regulation of adult cholesterol homeostasis. Can. J. Physiol. Pharmacol. 63: 557-564.

Innis, S.M. (1986) The activity of 3-hydroxy-3-methylglutaryl coenzyme A reductase and acyl-CoA:cholesterol acyltransferase in hepatic microsomes from male, female and pregnant rats. The effect of cholestyramine treatment and the relationship of enzyme activity to microsomal lipid composition. Biochim. Biophys. Acta. 875: 355-361.

Innis, S.M. (1988) Effect of diet during pregnancy and lactation on HMG-CoA reductase activity in the developing rat. J. Nutr. 118: 1177-1183.

Jeske, D.J. & Dietschy, J.M. (1980) Regulation of rates of cholesterol synthesis in vivo in the liver and carcass of the rat measured using [^{3}H]water. J. Lipid Res. 21: 364-376.

Kannel, W.B., Castelli, W.P. & Gordon, T. (1979) Cholesterol in the prediction of atherosclerotic disease. Ann. Intern. Med. 90: 85-91.

Keller, G.A., Pazirandeh, M. & Krisans, S. (1986) 3-Hydroxy-3-methylglutaryl coenzyme A reductase localization in rat liver peroxisomes and microsomes of control and cholestyramine-treated animals: quantitative biochemical and immunoelectron microscopical analyses. J. Cell Biol. 103: 875-886.

Kelly, W.A., Kesterson, J.W. & Carlton, W.W. (1974) Myocardial lesions in the offspring of female rats fed a copper deficient diet. Exp. Mol. Pathol. 20: 40-56.

Kern, F., Everson, G.T., DeMark, B., McKinley, C., Showalter, R., Erfling, W., Braverman, D.Z., Szczepanik-van Leeuwen, P. & Klein, P.D. (1981) Biliary lipids, bile acids, and gallbladder function in the human female. Effects of pregnancy and the ovulatory cycle. J. Clin. Invest. 68: 1229-1242.

Klevay, L.M. (1973). Hypercholesterolemia in rats produced by an increase in the ratio of zinc to copper ingested. Am. J. Clin. Nutr. 26: 1060-1068.

Knopp, R.H., Herrera, E, & Freinkel, N. (1970) Carbohydrate metabolism in pregnancy J. Clin. Invest. 49: 1438-1446.

Knopp, R.H., Warth, M.R. & Carrol, C.J. (1973) Lipid metabolism in pregnancy. I. changes in lipoprotein triglyceride and cholesterol in normal pregnancy and the effects of diabetes mellitus. J. Reprod. Med. 10: 95-101.

Koo, S.I., Lee, C.C. & Norvell, J.E. (1988). Effect of copper deficiency on the lymphatic absorption of cholesterol, plasma chylomicron clearance, and postheparin lipase activities. Proc. Soc. Exp. Biol. Med. 188: 410-419.

Kowal, R.C., Herz, J., Goldstein, J.L., Esser, V., & Brown, M.S. (1989) Low density lipoprotein receptor-related protein mediates uptake of cholesteryl esters derived from apoprotein E-enriched lipoproteins. Proc. Natl. Acad. Sci. 86: 5810-5814.

Lefevere, M., Keen, C.M., Lonnerdal, B., Hurley, L.S. & Schneeman, B.O. (1985). Different effects of zinc and copper deficiency on composition of plasma high density lipoproteins in rats. J. Nutr. 115: 359-368.

Lei, K.Y. (1977). Cholesterol metabolism in copper-deficient rats. Nutr. Rep. Internal. 15: 597-605.

Lei, K.Y. (1978). Oxidation, excretion, and tissue distribution of [26-C] cholesterol in copper deficient rats. J. Nutr. 108: 232-237.

Lei, K.Y. (1983). Alterations in plasma lipid, lipoprotein and apolipoprotein concentrations in copper deficient rats. J. Nutr. 113: 2178-2183.

Leoni, S., Mangiantini, M.T., Spagnuolo, S., Valbonesi, M., Conti-Devirgiliis, L. & Trentalance, A. (1986) Regulation of HMG-CoA reductase by mevalonate and

cholesterol in isolated rat hepatocytes during perinatal development. Cell Molec. Biol. 32: 243-246.

Leoni, S., Spagnuolo, S., Conti-Devirgiliis, L., Dini, L., Mangiantini, M.T. & Trentalance, A. (1984) Cholesterogenesis and related enzymes in isolated rat hepatocytes during pre- and postnatal life. J. Cell Physiol. 118: 62-66.

Levin, M.S., Pitt, A.J.A., Schwartz, A.L., Edwards, P.A. & Gordon, J.I. (1989) Developmental changes in the expression of genes involved in cholesterol biosynthesis and lipid transport in human and rat fetal and neonatal livers. Biochim. Biophys. Acta. 1003: 293-300.

Li, A.C., Tanaka, R.D., Callaway, K., Fogelman, A.M. & Edwards, P.A. (1988) Localization of 3-hydroxy-3-methylglutaryl coenzyme A reductase and 3-hydroxy-3-methylglutaryl coenzyme A synthase in the rat liver and intestine is affected by cholestyramine and mevinolin. J. Lipid Res. 29: 781-796.

Liscum, L., Finer-Moore, J., Stroud, R.M., Luskey, K.L., Brown, M.S. & Goldstein, J.L. (1985) Domain structure of 3-hydroxy-3-methylglutaryl coenzyme.A reductase, a glycoprotein of the endoplasmic reticulum. J. Biol. Chem. 260: 522-530.

Liscum, L., Luskey, K.L., Chin, D.J., Ho, Y.K., Goldstein, J.L. & Brown, M.S. (1983) Regulation of 3-hydroxy-3-methylglutaryl coenzyme A reductase and its mRNA in rat liver as studied with a monoclonal antibody and a cDNA probe. J. Biol. Chem. 258: 8450-8455.

Luskey, K.L. (1987) Conservation of promoter sequence but not complex intron splicing pattern in human and hamster genes for 3-hydroxy-3-methylglutaryl coenzyme A. Mol. Cell. Biol. 7: 1881-1893.

Luskey, K.L. and Stevens, B. (1985) Human 3-hydroxy-3-methylglutaryl coenzyme A reductase. Conserved domains responsible for catalytic activity and sterol-regulated degradation. J. Biol. Chem. 260: 10271.

Luskey, K.L., Faust, J.R., Chin, D.J., Brown, M.S. and Goldstein, J.L. (1983) Amplification of the gene for 3-hydroxy-3-methylglutaryl coenzyme A reductase, but not for the 53-kDa protein, in UT-1 cells. J. Biol. Chem. 258: 8462-8469.

Maniatis, T., Fritsch, E.F. and Sambrook, J. (1989) Molecular Cloning: A laboratory Manual. Cold Spring Harbor Laboratory, Cold Spring Harbor, N.Y.

Marco, C., Ramirez, H., Gonzalez-Pacanowska, D. & Garcia-Peregrin, E. (1984) Synthesis of sterols by chick brain and liver during embryonic development. Neurochem. Int. 7: 131-135.

Markwell, M.A.K., Haas, S.M., Bieber, L.L. & Tolbert, N.E. (1978) A modification of the Lowry procedure to simplify protein determination in membrane and lipoprotein samples. Anal. Biochem. 87: 206-210.

Markwell, M.A.K., Haas, S.M., Bieber, L.L. & Tolbert, N.E. (1978) A modification of the Lowry procedure to simplify protein determination in membrane and lipoprotein samples. Anal. Biochem. 87: 206-210.

Mason, K.E. (1979) A conspectus of research on copper metabolism and requirements in man. J. Nutr. 109: 1979-2066.

McNamara, D.J., Proia, A. & Edwards, K.D.G. (1982) Cholesterol homeostasis in rats fed a purified diet. Biochim. Biophys. Acta 711: 252-260.

McNamara, D.J., Quackenbush, F.W. & Rodwell, V.W. (1972) Regulation of hepatic 3-hydroxy-3-methylglutaryl coenzyme A reductase: the developmental pattern. J. Biol . Chem. 247: 5805-5810.

Metherall, J.E., Goldstein, J.L., Luskey, K.L. & Brown, M.S. (1989) Loss of transcriptional repression of three sterol-regulated genes in mutant hamster cells. J. Biol. Chem. 264: 15634-15641.

Miguel, S.G. & Abraham, S. (1976) Effect of maternal diet on fetal hepatic lipogenesis. Biochim. Biophys. Acta. 424: 213-234.

Mitropoulos, K.A., Balasubramaniam, S., Venkatesan, S. & Reeves, B.E.A. (1978) On the mechanism for the regulation of 3-hydroxy-3-methylglutaryl-coenzyme A reductase, of cholesterol 7 α-hydroxylase and of acyl-coenzyme A:cholesterol acyltransferase by free cholesterol. Biochim. Biophys. Acta 530: 99-111.

Montes, A., Humphrey, J., Knopp, R.H. & Childs, M.T. (1978) Lipid metabolism in pregnancy. VI. Lipoprotein composition and hepatic lipids in the fed pregnant rat. Endocrinol. 103: 1031-1038.

Murray, M.G. and Thompson, W.F. (1980) Rapid isolation of high molecular weight plant DNA. Nuc. Acids Res. 8: 4321-4362.

Murthy, L. & Petering, H.G. (1976) Effect of dietary zinc and copper interrelationships on blood parameters of the rat. J. Agric. Food Chem.24: 808-811.

Naseem, S.M., Khan, M.A., Heald, F.P. & Nair, P.P. (1980) The influence of cholesterol and fat in maternal diet of rats on the development of hepatic cholesterol metabolism in the offspring. Atherosclerosis 36: 1-8.

Narita, J.O. & Gruissem, W. (1989) Tomato hydroxymethylglutaryl-CoA reductase is required early in fruit development but not during ripening. Plant Cell 1: 181-190.

Ness, G.C., Miller, J.P., Moffler, M.H., Woods, L.B. & Harris, H.B. (1978) Perinatal development of HMG-CoA reductase activity in rat lung, liver and brain. Lipids 14: 447-450.

hydroxy-3-methylglutaryl coenzyme A reductase gene. Proc. Natl. Acad. Sci. 84: 3614-3618.

Osborne, T.F., Gil, G., Goldstein, J.L. & Brown, M.S. (1988) Operator constitutive mutation of 3-hydroxy-3-methylglutaryl coenzyme A reductase promoter abolishes protein binding to sterol regulatory element. J. Biol. Chem. 263: 3380-3387.

Petering, H.G., Murthy, L. & O'Flaherty, E. (1977) Influence of dietary copper and zinc on rat lipid metabolism. J. Agric. Food Chem. 25: 1105-1109.

Rajavashisth, T.B., Taylor, A.K., Andalibi, A., Svenson, K.L. & Lusis, A.J.. (1989) Identification of a zinc finger protein that binds to the sterol regulatory element. Science 245: 640-643.

Reichen, J., Karlaganis, G. & Kern, F. (1987) Cholesterol synthesis in the perfused liver of pregnant hamsters. J. Lipid Res. 28: 1046-1052.

Reiser, R. & Sidelman, Z. (1972) Control of serum cholesterol homeostasis by cholesterol in the milk of the suckling rat. J. Nutr. 102: 1009-1016.

Reynolds, G.A., Basu, S.K., Osborne, T.F., Chin, D.J., Gil, G.G., Brown, M.S., Goldstein, J.L. & Luskey, K.L. (1984) HMG CoA reductase: a negatively regulated gene with unusual promoter and 5' untranslated regions. Cell 38: 275-285.

Reynolds, G.A., Goldstein, J.L. & Brown, M.S. (1985) Multiple mRNAs for 3-hydroxy-3-methylglutaryl coenzyme A reductase determined by multiple transcription initiation sites and intron splicing sites in the 5'-untranslated region. J. Biol. Chem. 260: 10369-10377.

Rodwell, V.W., Nordstrom, J.L. & Mitschelen, J.J. (1976) Regulation of HMG-CoA reductase. Adv. Lipid Res. 14: 1-74.

Rosser, D.S.E., Ashby, M.N., Ellis, J.L., & Edwards, P.E. (1989) Coordinate regulation of 3-hydroxy-3-methylglutaryl-coenzyme A synthase, 3-hydroxy-3-methylglutaryl-coenzyme A reductase, and prenyltransferase synthesis but not degradation in HepG2 cells. J. Biol. Chem. 264: 12653-12656.

Sale, F.O., Marchesini, S., Fishman, P.H. & Berra, B. (1984) A sensitive assay for determination of cholesterol in lipid extracts. Anal. Biochem. 142: 347-350.

Saucier, S.E., Kandutsch, A.A., Gayen, A.K., Swahn, D.K. & Spencer, T.A. (1989) Oxysterol regulators of 3-hydroxy-3-methylglutaryl-CoA reductase in liver. J. Biol. Chem. 264: 6863-6869.

Scallen, T.J., Arebalo, R.E., Tormanen, C.D. & Hardgrave, J.E. (1982) The effect of short-term fasting on rat liver microsomal 3-hydroxy-3-methylglutaryl coenzyme A reductase. Fed. Proc., Fed. Am. Soc. Exp. Biol. 41: 1399.

Schafer, W.R., Kim, R., Sterne, R., Thorner, J., Kim, S.H. & Rine, J. (1989) Genetic and pharmacological suppression of oncogenic mutations in RAS genes of yeast and humans. Science 245: 379-385.

Schmidt, R.A., Schneider, C.J. & Glomset, J.A. (1984) Evidence for post-translational incorporation of a product of mevalonic acid into Swiss 3T3 cell proteins. J. Biol. Chem. 259: 10175-10180.

Shao, M.S.J. & Lei, K.Y. (1980) Conversion of [2-^{14}C]mevalonate into cholesterol, lanosterol and squalene in copper-deficient rats. J. Nutr. 110: 859-867.

Shapiro, D.J. & Rodwell, V.W. (1971) Regulation of hepatic 3-hydroxy-3-methylglutaryl coenzyme A reductase and cholesterol synthesis. J. Biol. Chem. 246: 3210-3216.

Shapiro, D.J., Nordstrom, J.L., Mitschelen, J.J., Rodwell, V.W. & Schimke, R.T. Biochim. Biophys. Acta 370: 369-377.

Siperstein, M.D. & Fagan, V.M. (1966) Feedback control of mevalonate synthesis by dietary cholesterol. J. Biol. Chem. 241: 602-609.

Siperstein, M.D. Regulation of cholesterol biosynthesis in normal and malignant tissues. In: Current Topics in Cellular Regulation, Vol. 2. Ed. B.L. Horecker and E. R. Stadtman. Academic Press, New York, pp. 65-100, 1970.

Skalnik, D.G., Narita, H., Kent, C. & Simoni, R.D. (1988) The membrane domain of 3-hydroxy-3-methylgutaryl coenzyme A reductase confers endoplasmic reticulum localization and sterol regulated degradation onto ß-galactosidase. J. Biol. Chem. 263: 6836-6841.

Slakey, L.L., Craig, M.C., Beytia, E., Briedis, A., Felbruegge, D.H., Dugan, R.E., Qureshi, A.A., Subbarayan, C. & Porter, J.W. (1972) The effects of fasting, refeeding and time of day on the levels of enzymes effecting the conversion of ß-hydroxy-ß-methylglutaryl-coenzyme A to squalene. J. Biol. Chem. 247: 3014-3022.

Smith, J.R., Osborne, T.F., Brown, M.S., Goldstein, J.L. & Gil, G. (1988) Multiple sterol regulatory elements in promoter for hamster 3-hydroxy-3-methylglutaryl coenzyme A synthase. J. Biol. Chem. 263: 18480-18487.

Southern, E.M. (1975) Detection of specific sequences among DNA fragments separated by gel electrophoresis. J. Mol. Biol. 98: 503-517.

Spady, D.K. & Dietschy, J.M. (1983) Sterol synthesis in vivo in 18 tissues of the squirrel monkey, guinea pig, rabbit , hamster, and rat. J. Lipid Res. 24: 303-315.

Steel, R.G.D. & Torrie, J.H. (1960) Analysis of variance I. The one way classification. In Principles of Procedures for Statistics, pp. 99-128, McGraw-Hill Book Co., New York, N.Y.

Sudhof, T.C, Russell, D.W., Brown, M.S. & Goldstein, J.L. (1987a) 42 bp element from LDL receptor gene confers end-product repression by sterols when inserted into viral TK promoter. Cell 48: 1062-1069.

Sudhof, T.C., Goldstein, J.L., Brown, M.S. & Russell, D.W. (1985) The LDL receptor gene: a mosaic of exons shared with different proteins. Science 228: 815-822.

Sudhof, T.C., Van Der Westhuyzen, D.R., Goldstein, J.L., Brown, M.S. & Russell, D.W. (1987b) Three direct repeats and a TATA-like sequence are required for regulated expression of the human low density ipoprotein receptor gene. J. Biol. Chem. 262: 10773-10779.

Tanaka, R.D., Edwards, P.A., Lan, S.F., Knoppel, E.M. & Fogelman, A.M. (1982) The effects of cholestyramine and mevinolin on the diurnal cycle of rat hepatic 3-hydroxy-3-methylglutaryl coenzyme A reductase. J. Lipid Res. 23: 1026-1031.

Thomas, P.S. (1980) Hybridization of denatured RNA and small DNA fragments transferred to nitrocellulose. Proc. Natl. Acad. Sci. 77: 5201-5205.

Turley, S.D & Dietschy, J.M. (1988) The metabolism and excretion of cholesterol by the liver. In The Liver: Biology and Pathobiology. 2nd Ed. Arias, I.M., Jakoby, W.B., Popper, H., Schachter, D. & Shafritz, D.A., editors. Raven Press, Ltd., New York. 617-641.

Walsh-Hentges, L.S. & Martin, R.J. (1987) Serum and lipoprotein lipids of fetal pigs and their dams during gestation as compared with man. Biol. Neonate. 52: 127-134.

White, L.W. & Rudney, H. (1970) Regulation of 3-hydroxy-3-methylglutarate and mevalonate biosynthesis by rat liver homogenates. Effects of fasting, cholesterol feeding, and triton administration. Biochemistry 9: 2725-2730.

Williams, R.S., Marshall, P.C., Lott, I.T. & Caviness, U.S.,Jr. (1978) The cellular pathology of Menkes' steely hair syndrome. Neurology 28: 575-583.

Wrobel, J., Boguslawski, W., Michalska, L. & Niemiro, R. (1973) Developmental changes in sterol biosynthesis from acetate and mevalonate in rat liver. Int. J. Biochem. 4: 565-568.

Yamamoto, T., Davis, G.C., Brown, M.S., Schneider, W.J., Casey, M.L., Goldstein, J.L. & Russell, D.W. (1984) The human LDL receptor: a cysteine-rich protein with multiple Alu sequences in its mRNA. Cell 39: 27-38.

Ylostalo, P., Kirkinen, P., Heikkinen, J., Maentausta, O. & Jarvinen, P.A. (1982) Gall bladder volume and serum bile acids in cholestasis of pregnancy. Br. J. Obstet. Gynaecol. 89: 59-61.

Yount, N.Y., T.P. Carr, Lei, K.Y. & McNamara, D.J. (1991) Incorporation of tritiated water into sterols in copper-deficient rats. Biochim. Biophys. Acta. 1082: 79-84.

Yount, N.Y. & McNamara, D.J. (1991) Dietary regulation of maternal and fetal cholesterol metabolism in the guinea pig. Biochim. Biophys. Acta. (in press).

Yount, N.Y., McNamara, D.J., Al-Othman, A.A. & Lei, K.Y. (1990) The effect of copper deficiency on rat hepatic 3-hydroxy-3-methylglutaryl coenzyme A reductase activity. J. Nutr. Biochem. 1: 21-27.

Zannis, V.I., Kurnit, D.M. & Breslow, J.L. (1982) Hepatic apo-A-I and apo-E and intestinal apo-A-I are synthesized in precursor isoprotein forms by organ cultures of human fetal tissues. J. Biol. Chem. 257: 536-544.